Materials **2014**, *7*, 673-726; doi:10.3390/ma7020673

OPEN ACCESS

materials

ISSN 1996-1944

www.mdpi.com/journal/materials

Review

Organic-Inorganic Hybrid Polymers as Adsorbents for Removal of Heavy Metal Ions from Solutions: A Review

Babak Samiey [1,*,†], Chil-Hung Cheng [2,*,†] and Jiangning Wu [2,*,†]

[1] Department of Chemistry, Faculty of Science, Lorestan University, Khoramabad 68137-17133, Iran

[2] Department of Chemical Engineering, Ryerson University, Toronto, ON M5B 2K3, Canada

† These authors contributed equally to this work.

* Authors to whom correspondence should be addressed; E-Mails: babsamiey@yahoo.com (B.S.); chilhung.cheng@ryerson.ca (C.-H.C.); j3wu@ryerson.ca (J.W.); Tel.: +98-0661-2202782 (B.S.); +1-416-979-5000 (ext. 2131) (C.-H.C.); +1-416-979-5000 (ext. 6549) (J.W.).

Received: 25 November 2013; in revised form: 6 January 2014 / Accepted: 10 January 2014 / Published: 27 January 2014

Abstract: Over the past decades, organic-inorganic hybrid polymers have been applied in different fields, including the adsorption of pollutants from wastewater and solid-state separations. In this review, firstly, these compounds are classified. These compounds are prepared by sol-gel method, self-assembly process (mesopores), assembling of nanobuilding blocks (e.g., layered or core-shell compounds) and as interpenetrating networks and hierarchically structures. Lastly, the adsorption characteristics of heavy metals of these materials, including different kinds of functional groups, selectivity of them for heavy metals, effect of pH and synthesis conditions on adsorption capacity, are studied.

Keywords: organic-inorganic hybrid polymer; heavy metal ion; wastewater treatment; adsorption; sol-gel method; self-assembly process; nanobuilding blocks; interpenetrating networks

1. Introduction

A wide variety of toxic inorganic and organic chemicals are discharged into the environment as industrial wastes, causing serious water, air, and soil pollution. Water pollution caused by toxic heavy metal ions has become a serious environmental problem. Heavy metals (such as Pt, Pd, Ag, Cu, Cd,

Pb, Hg, Ni, Co, Zn, *etc*.) are natural constituents of the earth crust and present in the environment as a result of weathering and erosion of parent rocks [1]. In addition to natural sources, they are introduced in ecosystems through wastewaters originating from anthropogenic sources such as chemical manufacturing, metal finishing, welding, alloys manufacturing, painting, mining, extractive metallurgy, plating, tannery and battery industry and using metal-containing fertilizers and pesticides [2].

These toxic metal ions, even at low concentrations, have deteriorated water resources and drinking water and easily accumulated in the human body throughout the food chain, causing a variety of diseases and disorders [3]. So, it is necessary to remove these metal ions from industrial effluents for their subsequent safe disposal.

The removal of heavy metal ions from wastewaters has been a subject of extensive industrial research. At the same time, some of them (e.g., Pt and Au) are precious and can be recycled and reused for extensive applications [4,5]. The recovery of heavy or valuable metals from water or wastewaters can often result in considerable cost savings and have both ecological and economic benefits.

Different methods, such as precipitation [6], solvent extraction [7] chemical and electrochemical techniques [8], ion-exchange methods [9] ultrafiltration [10] and reverse osmosis [11,12], flotation [13] and coagulation [14] have been developed for the removal of toxic metal ions from industrial effluents and wastewaters. However, most of these processes are unacceptable, owing to the disposal of sludge, their high cost, low efficiency and inapplicability to a wide range of pollutants [15].

Adsorption is a well-known separation method and recognized as one of efficient and economic methods for water decontamination applications. In addition, owing to the reversible nature of most adsorption processes, the adsorbents can be regenerated by suitable desorption processes for multiple uses [16], and many desorption processes are of low maintenance cost, high efficiency, and ease of operation [17].

However, the major problem in this field is to select novel types of adsorbents. A number of adsorbents such as activated carbon [18], zeolites [19,20], clays [21,22] and agricultural residues [23–25] have been used for the removal of heavy metal ions. However, the major disadvantages of these adsorbents are their low adsorption capacities, their relatively weak interactions with metallic ions and difficulties of separation and regeneration of some of them from water. Ion-exchange resins can remove metal ions substantially; however, they have low selectivities and show a high degree of swelling combined with poor mechanical stability [26].

To overcome these limitations, more recently, promising organic-inorganic hybrid polymers have been used for the removal of toxic species from wastewater [27–35]. In these compounds, the functional variation of organic materials is combined with advantages of a thermally stable and robust inorganic substrate, resulting in strong binding affinities toward selected metal ions and relatively high metal ion adsorption capacities. Functionalized hybrid polymeric materials as adsorbent are regarded as one of the most effective techniques because metal ions can be chemically bonded by the organic-inorganic polymer hybrids. These kinds of materials often present the best properties of each of its components in a synergic way and have high performances of physical, chemical and mechanical properties [36].

Organic-inorganic hybrid polymeric materials are currently intensely studied [37] for their efficient applications. The intrinsic multifunctional character of these materials makes them potentially useful in multiple fields. Different forms of organic-inorganic hybrids have been intensively studied due to their

interesting properties resulting in a number of applications such as electroanalytical applications [38], their extensive applications as membranes for ultra-and nanofiltration [39,40], superhydrophobic surfaces [41,42], highly transparent films [43,44], pH sensitive composites [45], solar cells [46,47], electrolyte [48], molecular shuttles [49], semiconductors [50], gas separation [51,52], catalysts [53], biosensors [54], drug delivery systems [55], coatings for corrosion protection [56], adsorbents of toxic compounds [27–35], Fire retardant polymers [57], biomaterials for osteo-reconstructive surgery [58], materials for telecommunications or information displays [59], *etc*.

This review describes classifications and synthesis methods of organic-inorganic hybrid polymers and particular attention will be focused on application of them for the adsorption of heavy metals from water as well as their performances and mechanisms.

2. Classification and Synthesis of Organic-Inorganic Hybrid Polymers

Organic-inorganic hybrid polymers are classes of materials whose structure includes both organic and inorganic units that interact with each other at the molecular level. These materials are divided into two classes on the basis of interaction between organic and inorganic components. In class I, organic and inorganic are embedded and there are weak interactions, such as hydrogen bonding, van der Waals, π–π or weak electrostatic interactions between them and in class II, these two components are bonded together through strong covalent or coordinative bonds [37]. Organic-inorganic hybrid polymers are obtained through (1) sol-gel process; (2) self-assembly process; (3) assembling or dispersion of nanobuilding blocks; (4) hierarchical structures [37] and interpenetrating networks [60].

2.1. Sol-Gel Process

In 1846, Ebelmanl and Graham reported that the hydrolysis of tetraethylorthosilicate (TEOS), under acidic conditions produced SiO_2 in the form of fibres [61,62]. In 1950s, Brady *et al*. [63] produced a number of phenylsilsesquioxane-alkylsilsesquioxane copolymers that were the first successful commercial organic-inorganic hybrid polymers. The sol-gel process is a cheap and low-temperature method for producing transparent and homogenous solid materials with high purity from small molecules and for controlling the chemical composition of products. Compounds produced by the sol-gel process have many applications in superhydrophobic surfaces [41] (shown in Scheme 1), electrolyte [48], biosensors [54], corrosion protection [56], *etc*.

This process is carried out in water and organic solvents and its precursors are usually metal halides [64] (in organic solvents) and metal alkoxides such as $Si(OR)_4$, $SiR'(OR)_3$, $Ti(OR)_4$, *etc*. [41,65–67] (Scheme 1). As seen in Scheme 2 [68], these materials are subject to a series of hydrolysis (or non-hydrolytic process in organic solvents) and condensation reactions that through nucleophilic substitution mechanisms result in sol formation. Sol is a colloidal solution in which individual particles interact weakly with each other and due to cross-linking reactions, converts into an integrated network (wet gel). This structure with further drying processes converts to gel.

In spite of silicon alkoxides, hydrolysis reactions of other metal alkoxides in water are too fast. The hydrolysis reaction of silicon alkoxides, is typically acid- or base-catalyzed [69]. As reported [70], silica networks formed under acid-catalyzed conditions are dense and those of formed in the presence of base are porous and loose.

Scheme 1. Schematic superhydrophobic surfaces prepared through the sol-gel derived organic-inorganic hybrid emulsion. Reprinted with permission from [41]. Copyright 2011 Elsevier.

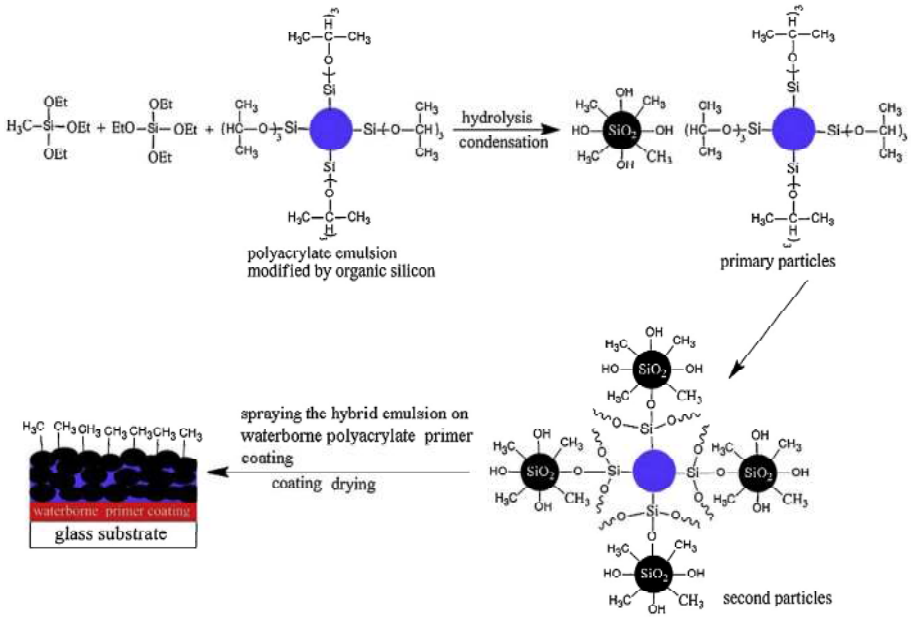

Scheme 2. Description of technologies and products of the sol-gel process [68].

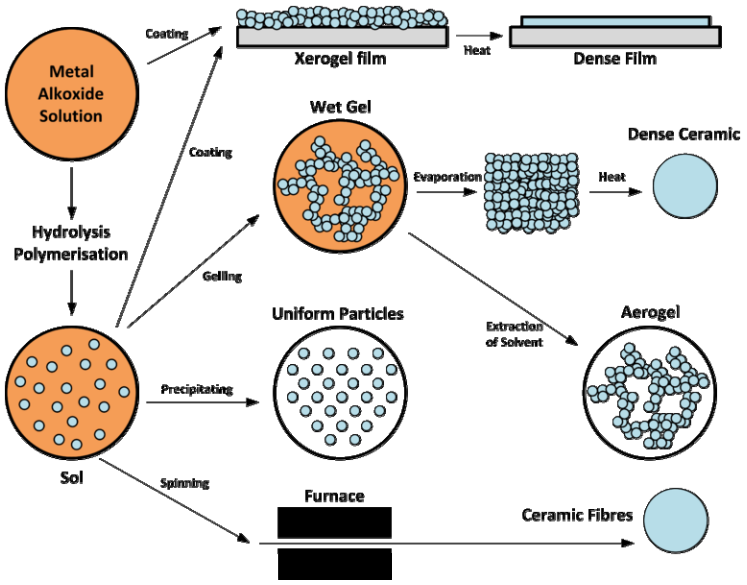

A suitable way for modifications of properties of materials obtained from this method is the introduction of organic groups (R) into their structure [71]. For example, the Si–C bond does not hydrolyze in most sol-gel processes and organic groups can be incorporated covalently into the network of inorganic gel using silsesquioxanes [$(R–SiO_{1.5})_n$ (n = even number)], such as $R'(OR)_2Si–R–Si(OR)_3$ compounds or derivatives of tetrafunctional silicon alkoxide [organically modified silicates (ORMOSILs)], such as TEOS, $R'Si(OR)_3$, *etc*. [71]. If an organic group remains stable and does not hydrolyze during sol-gel processes (e.g., alkyl groups) it is defined as a network modifier. On the other hand, if it can react with another monomers or with itself (e.g., $–CH=CH_2$) it is named as a network builder. Moreover, if it is a reactive functional group, such as $–NH_2$, it is specified

as a network functionalizer [72] (Scheme 3). These materials belong to class II interactions of organic-inorganic hybrid polymers.

Scheme 3. Organically functionalized trialkoxysilanes, R′Si(OR)$_3$, used as (**a**) modifier; (**b**) builder and (**c**) functionalizer of silica-based network through the sol-gel process. Reproduced with permission from [72]. Copyright 2006 WILEY-VCH Verlag GmbH.

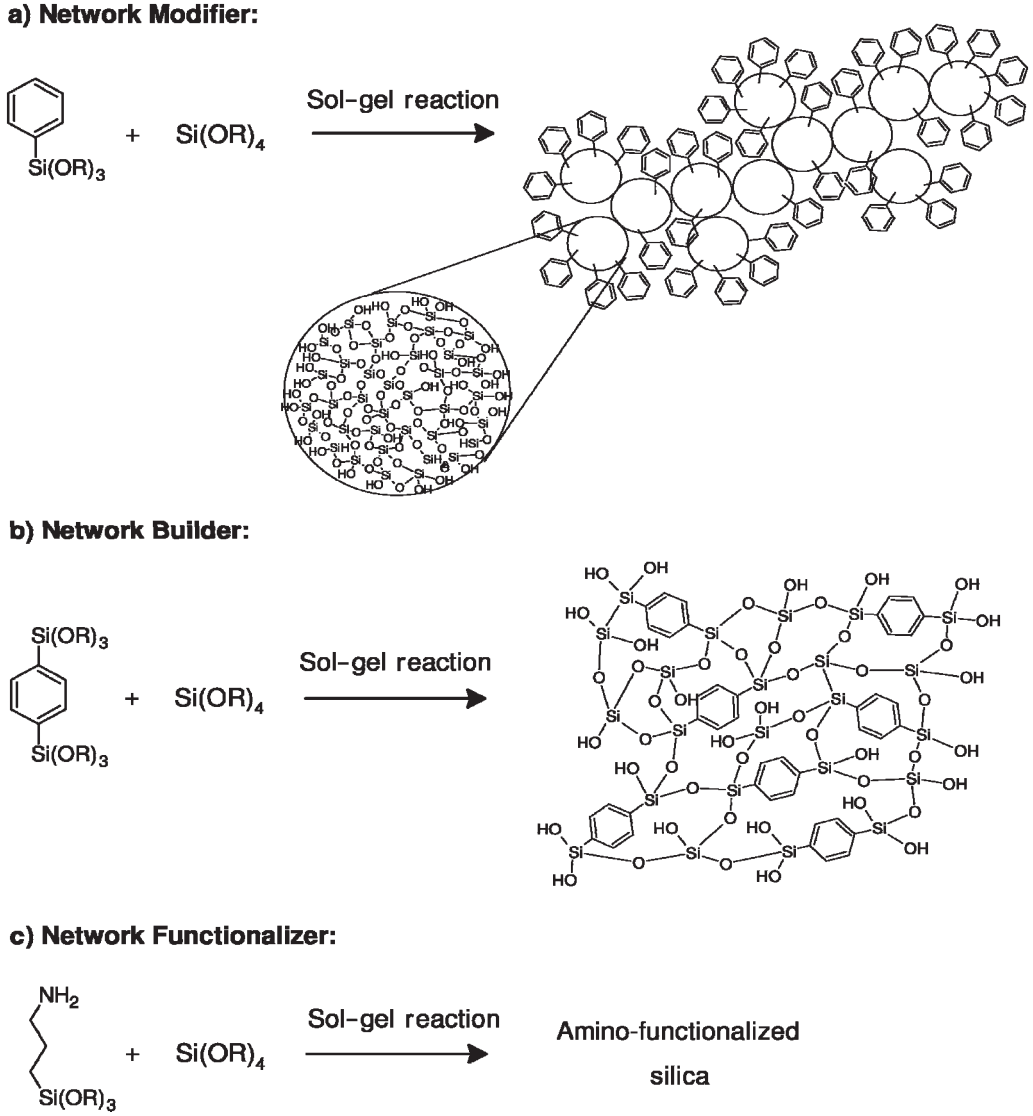

Another example of using sol-gel processes is the synthesis of microporous zeolites (or molecular sieves). These materials are framework aluminosilicate and have a three-dimensional structure with high internal surface area and an ordered crystalline structure [73]. Zeolites with high silica contents are synthesized in the presence of bulky organic alkylammonium cations known as structure-directing agents or templates [74].

Synthetic zeolites are microporous (diameter of their pores < 2 nm) and have many applications such as membranes, catalysts, catalyst supports, gas storage, *etc*. [73]. In recent years, great efforts have been made on the direct preparation of hybrid organic-inorganic zeolites [75,76]. The incorporation of organic moieties within the pores or in the framework of microporous zeolites has developed their catalytic activity [77], molecular sieving property [78] and adsorption capacity [79].

2.2. Self-Assembly Process

In 1992, researchers of Mobil Oil Company discovered a new type of mesoporous silicas, so-called M41S [80,81]. M41S family includes hexagonal MCM–41, cubic MCM–48, and lamellar MCM–50 [82] (Figure 1). MCM is an abbreviation of "Mobil Crystalline Materials".

Notwithstanding their amorphorous pore walls, these organic-inorganic hybrid compounds exhibit a long-range ordered array of uniform and controllable mesopores with sizes ranging between 2–10 nm [82]. Mesostructure compounds have high specific surface areas (greater than 1000 m^2/g) [82] and the pore size of these materials enables them to adsorb much larger molecules than is possible for zeolites. These compounds are used for catalysis [83], gas adsorption [84], *etc*. M41S type compounds were synthesized using a silica source (e.g., TEOS) in the presence of long-chain alkyltrimethylammonium halide surfactants as templates or structure-directing agents [80]. These compounds formed through a base-catalysed hydrolytic sol-gel process. Mesostructures can be synthesized using different ionic or non-ionic surfactants or water-soluble polymers as templates [85,86]. Other types of ordered mesoporous silicas are Santa Barbara Amorphous (SBA) (e.g., SBA–15 [87]), Michigan State University (MSU) (e.g., MSU–2 [88]), folded sheets mechanism (FSM) (e.g., FSM–16 [89]), *etc*., respectively.

Figure 1. Representation of mesoporous M41S compounds including (**a**) MCM–41; (**b**) MCM–48 and (**c**) MCM–50. Reproduced with permission from [82]. Copyright 1999 WILEY-VCH Verlag GmbH.

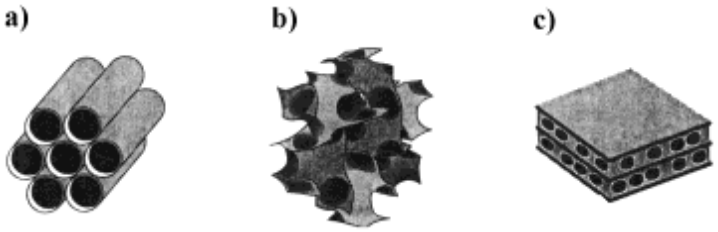

In recent years, attempts of scientists resulted in syntheses of non-silica mesoporous metal oxides such as TiO_2, ZrO_2, Al_2O_3, Nb_2O_5, SnO_2, mixed oxides such as $SiAlO_{3.5}$, $SiTiO_4$, carbon nanocage, mesoporous carbon nitride, *etc*. [90]. The formation of mesoporous materials is depicted schematically in Figure 2, based on "liquid crystal templating" mechanism [91]. Through route (a) at surfactant concentrations above its critical micelle concentration (CMC), the self-assembly of precursor molecules on the space between micellar rods of lyotropic liquid crystal phase and creates walls between them. Through route (b) at surfactant concentrations below CMC, the mesostructure is formed as a cooperative self-assembly of the precursor and surfactant molecules [82,91].

To prevent phase separation, there should be attractive interactions between inorganic precursors and template molecules. Depending on reaction conditions, such as pH and chemicals, e.g., inorganic precursors and templates, six routes have been suggested for syntheses of ordered mesoporous compounds [92]. These routes include (a) S^+I^-; (b) $S^+X^-I^+$; (c) $S^-M^+I^-$; (d) S^-I^+; (e) S^0I^0 or N^0I^0 and (f) $S^0(XI)^0$ where S is the surfactant, I is the inorganic phase and X^- is a mediator anionic species (usually a halide), M^+ is a mediator cation, S^0 is a neutral amine and N^0 is a long-chain non-ionic template. Interactions between the charged inorganic phase and the head group of surfactants in

routes (a–d) are mainly electrostatic forces; while those between neutral inorganic species and non-electrolyte template molecules are hydrogen bonds in routes (e) and (f) [92,93] (Figure 3). It is necessary to say that the inorganic precursor is neutral at its isoelectric point (e.g., at pH~2 for silica [94]) and has negative and positive electric charge at pH above and below this point, respectively.

Figure 2. Synthesis of mesoporous compounds in the presence of template through (**A**) liquid-crystal template or (**B**) cooperative liquid-crystal mechanisms. Reprinted with permission from [91]. Copyright 2002 American Chemical Society.

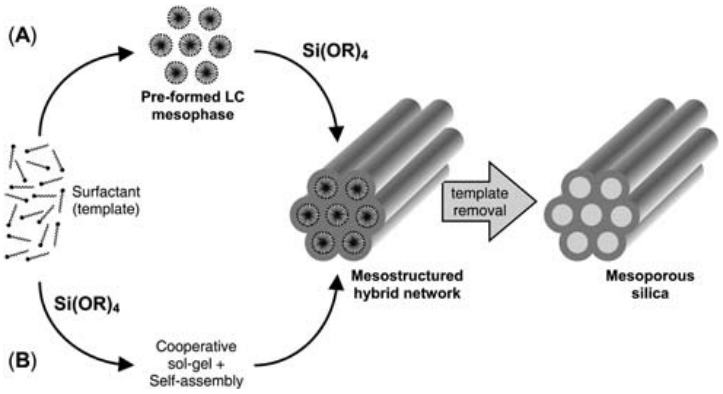

Figure 3. Different kinds of interactions between inorganic species and surfactant head groups through electrostatic interactions in (**a**) and (**c**) basic, (**b**) acidic and (**d**) neutral media or via hydrogen bonds between (**e**) unchared species or (**f**) ion pairs. Reproduced with permission from [93]. Copyright 2006 WILEY-VCH Verlag GmbH.

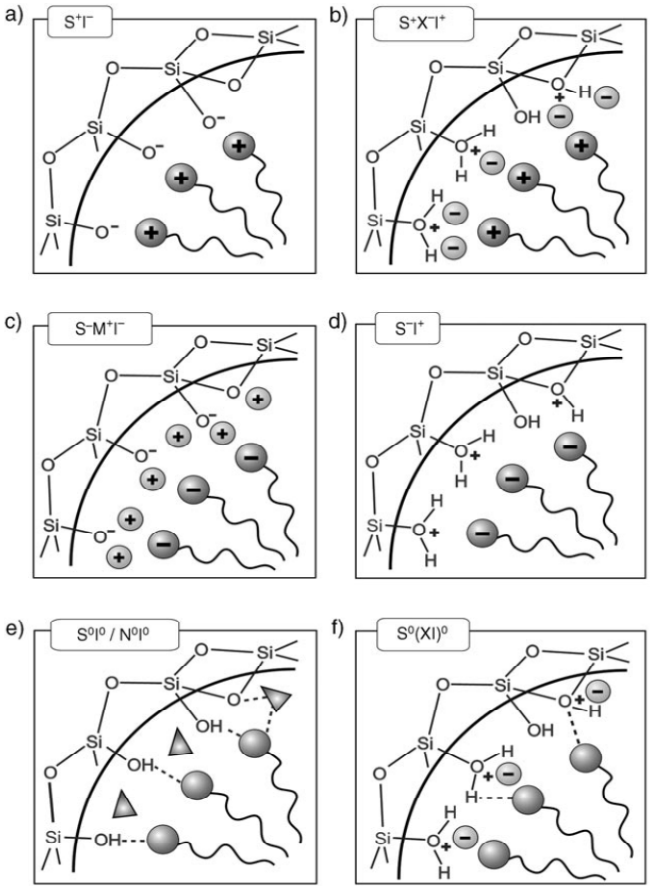

In recent years, mesoporous silicas have been used as supports for preparations of organic-inorganic hybrid polymers and have many applications in lasers [95], drug delivery [96], pollutant adsorption [36], *etc*. In these compounds, different organic functional groups are located on the robust, thermally stable and porous inorganic substrate.

As illustrated in Figure 4, these organosilica compounds are prepared through (a) grafting or post-synthetic functionalisation; (b) co-condensation or one-pot synthesis and (c) synthesis of periodic mesoporous organosilicas (PMOs) [93,97,98]. In grafting processes, an organosilica is synthesized through condensation reaction between Si–OH groups of the pore walls of mesoporous silica and appropriate reagents such as, chlorosilanes (e.g., $ClSiR_3$), alkoxyorganosilanes [e.g., $RSi(OR')_3$] *etc*. In the co-condensation method, an organosilica compound is prepared in one step through co-condensation reactions of tetraalkoxysilanes (e.g., TEOS) and an appropriate reagent (e.g., terminal trialkoxyorganosilanes) in the presence of a template. Syntheses of PMOs are carried out through the hydrolysis and condensation of bridged organosilane precursors of the type $(R'O)_3$ Si–R–$Si(OR')_3$ in the presence of a structure-directing agent. In this method, R organic group are incorporated uniformly and periodically in the pore walls of resulted organosilica [93,98].

Figure 4. Different methods for the synthesis of organic-inorganic hybrid mesoporous silica: 1. Grafting, 2. Co-condensation or in situ grafting and 3. Periodic mesoporous silica. Reproduced wity permissiom from [93]. Copyright 2006 WILEY-VCH Verlag GmbH.

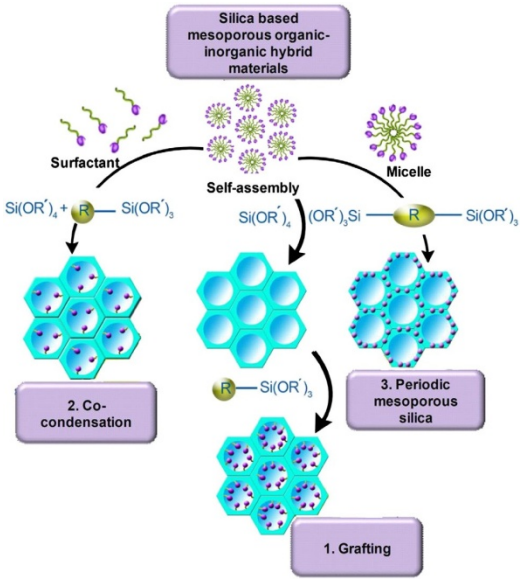

2.3. Assembling or Dispersion of Nanobuilding Blocks (NBBs)

The interest in nanoscale materials originates from this fact that their properties are a function of their size, composition, and structural order. Here, a series of compounds called as nanobuilding blocks (NBBs) are used for preparing organic-inorganic hybrid polymers. NBBs are capped with polymerizable ligands or connected through organic spacers, e.g., telechelic molecules or functional dendrimers [37]. These compounds maintain their integrity and fulfill certain (chemical or physical) functions in the final material. NBBs are classified as (1) clusters; (2) organically *in situ*- or post-functionalized nanoparticles; (3) layered compounds and (4) core-shell nanocompounds [37,99].

2.3.1. Clusters

Metallic clusters (e.g., polyoxometalates) are an ensemble of bound atoms and contain a group of two or more metal atoms that bind together by direct Metal-Metal bonding. Clusters are connected either (1) by the polymerization of their ligands (e.g., allyl) and are called cross-linked clusters or (2) by coordinative bonds between coordinating groups of organic ligands (called as a linker or spacer) to each metal center (called as a connector) of clusters [100,101]. In the latter case, a linker is a bi-, tri- or tetradentate organic ligand (e.g., 1,4-benzenedicarboxylate) with an organic spacer between coordinating groups [102]. For example, a one-dimensional polymer is built when a metal cluster links to just one coordinating group of two bidentate organic linkers and through them links to other metal clusters. Coordination of more than two coordinating groups to each metal center, optionally through tri- or tetradentate linkers, results in two- or three-dimensional polymers [100]. The three-dimensional polymers are called metal-organic frameworks (MOFs) and their metal centers are bridged in three dimensions (Supporting information Figure S1). MOFs along with cross-linked clusters are major types of cluster-based organic-inorganic hybrid polymers [103,104].

2.3.2. Organically *in Situ*- or Post-Functionalized Nanoparticles

In this method reactive organic groups are bound to the surface of inorganic moiety by strong ionic or covalent interactions. These organic groups are either grafted to preformed nanoparticles (called as post-functionalization) [105] or are incorporated during the synthesis of nanoparticles (called as *in-situ*-functionalization) [106]. This method is used for metal oxides (e.g., TiO_2 [107]), chalcogenides (e.g., CdSe [108]), metallic nanoparticles (e.g., Au [109]) and polyoxometalates (e.g., γ-$[SiW_{10}O_{36}]^{8-}$ [110]), *etc*.

2.3.3. Layered Compounds

To improve the physical properties of polymers, inorganic compounds physically are dispersed in them (as fillers) in various forms such as platelets, spheres, fibers, *etc*. If the size of discrete inorganic components is in the range of 1–100 nm, the resulted organic-inorganic compound is called a nanocomposite [111]. Organic-inorganic hybrid nanocomposites are either as interpenetrating networks which will be explained in Section 2.4 [99] or layered inorganic components embedded into the organic matrix.

Layered compounds are regular stacks of two-dimensional inorganic constituent. These compounds such as clay, are used as fillers in organic-inorganic hybrid composites. Some examples of nanocomposites are polyaniline-montmorillonite [112], polyaniline–V_2O_5 [113], polyvinyl alcohol-layered double hydroxide (LDH) [114], poly-N-vinyl carbazole-graphene oxide [115], *etc*. These compounds are incorporated in organic polymers as (a) a phase-separated structure in which the polymer can not intercalate within the inorganic layers and the inorganic component is dispersed as aggregates or particles within the polymer matrix; (b) an intercalated structure in which one or more polymer chains are inserted into the galleries (space between layers) of inorganic components and subsequently increase the interlayer spacing and (c) an exfoliated structure in which the insertion of polymer chains between inorganic sheets delaminates the layered compound [116] (Figure 5).

Polymers can be intercalated to layered compounds by (1) solution; (2) melting polymers and (3) in situ polymerization of intercalated monomers [99]. However, some compounds (e.g., EDTA and malate) intercalate layer compounds [117,118] are purly nanocomposites and not organic-inorganic hybrid polymers.

Figure 5. Schematic representation of different kinds of composites produced from interaction of layer compound with polymers: (**a**) phase separated; (**b**) intercalated and (**c**) exfoliated structures. Reprinted with permission from [116]. Copyright 2000 Elsevier.

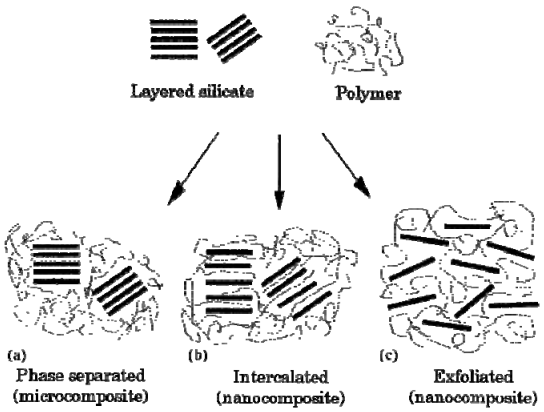

2.3.4. Core-Shell Nanocomposites

Core-shell nanocomposites (CSNs) consist of a core region covered by a shell domain (Figure 6). A series of CSNs are polymer-coated inorganic compounds [119–121]. The encapsulation of an inorganic particles in a polymer shell are carried out through (1) the adsorption of monomers on the surface of inorganic moiety followed by their polymerization in the adsorbed layer [122,123] and (2) interaction of inorganic particle with preformed polymer as in situ growing inorganic components in a polymer matrix [124]. CSNs are also shown as core@shell. Some kinds of CSNs are completely inorganic in nature (e.g., CdS@TiO_2 [125]).

Figure 6. TEM of polystyrene-coated Fe_2O_3 particles. The polymer coatings are seen as a shell around the Fe_2O_3 cores. Reprinted with permission from [122]. Copyright 2003 American Chemical Society.

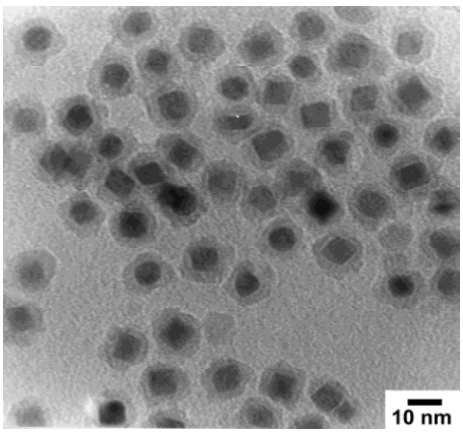

2.3.5. Hierarchical Structures

A hierarchy is a feature of self-assembly, where primary building blocks associate into more complex structures which are integrated into the next size level in the hierarchy. Self-assembly is emerging as an elegant, "bottom-up" method for the construction of nanostructured materials and is distinct from the template-directed assembly [126]. The feature of an integrated chemical, biological, *etc*. system is the assembly of components into a specific architecture that performs a certain function. Many examples of hierarchical structural designs are seen in nature and are characteristic of many self-assembling biological structures (e.g., lobster cuticle [127] and tendon [128]) (Figure 7).

Figure 7. Hierarchical structure of lobster cuticle. Reproduced with permission from [127]. Copyright 2010 WILEY-VCH Verlag GmbH.

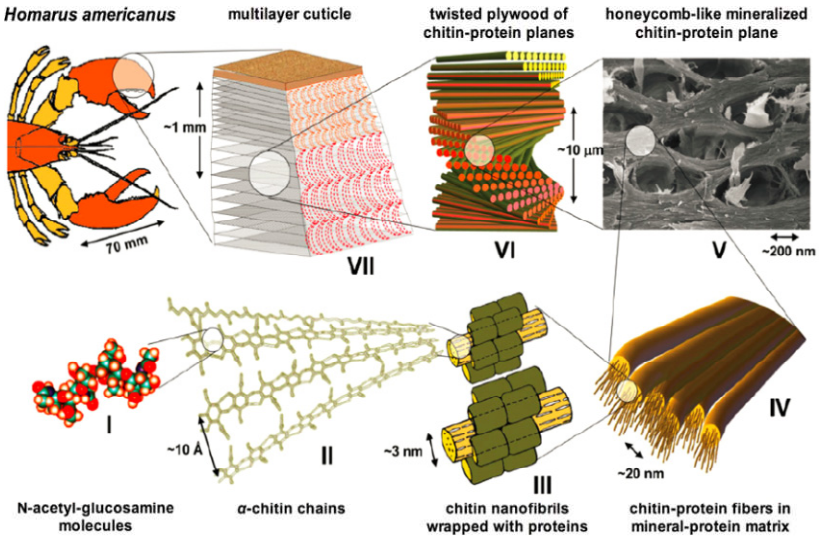

Also, the hierarchy has resulted in the discovery of versatile nanoparticles with many applications [129], synthetic bone implant materials [130], mesostructured solid electrolytes [131], TiO_2–graphene composite [132], *etc*. For example, the incorporation of interconnected macropores in mesoporous films of TiO_2–graphene composite (Supporting information Figure S2) augments the capacity of composite film for adsorption and photodegrading organic molecules and can be used for the treatment of waters.

2.4. Interpenetrating Networks (IPNs)

IPNs comprise organic and inorganic networks that are microscopically phase-separated. However, they seem uniform macroscopically and there are weak interactions between moieties of IPNs (class I interactions). These components are partially interlaced and, upon separating IPNs, chemical bonds are broken. IPNs are synthesized by (1) the formation of a secondary network in a primary one (a sequential two-step process); (2) the simultaneous formation of two networks and (3) IPN components connect to each other through covalent bonds in which the compound is named a dual organic-inorganic hybrid polymer (class II interactions) [99] (Figure 8). In the first method, IPNs are prepared by polymerization in a sol-gel network [133] or sol-gel process in the presence of preformed polymer [134]. In the third case, either bifunctional precursors are used or a preformed inorganic or

organic polymer are functionalized by the required functional groups for the formation of other types of networks [135].

But, when three-dimensional frameworks such as zeolites or mesoporous silicates, are used as inorganic components and polymer is formed without crosslinking, the polymer chains could be partially or completely removed from the product. In this case, the composite is called pseudo-interpenetrating polymer network (PIPN) [136,137].

At the end of this section, it is noteworthy that the inclusion of metals in organic-inorganic hybrid polymers occurs at the molecular scale and the incorporation of metal complexes and metallic ions in polymers by coordination interactions does not produce organic-inorganic hybrid polymers [99]. For example, metal-centered polymers [138] and products of coordination of metallic ions to the polymer backbone [139] and polymerization of metal-coordinated monomers [140] are called metal-containing polymers [99].

Figure 8. Schematic representation of IPNs (**a**) without chemical bonds between moieties and (**b**) dual hybrid network. Reprinted with permission from [99]. Copyright 2003 Elsevier.

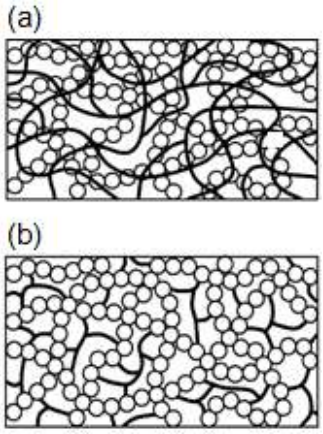

3. Removal of Heavy Metals by Organic-Inorganic Hybrid Polymers

Based on the classifications of these kinds of compounds in the previous section, by analysis some comprehensive references, we study their synthesis methods, structure and mechanisms of heavy metal adsorption from water or wastewater.

3.1. Adsorption of Heavy Metals Using Materials Synthesized from Sol-Gel Method

As extensive researches have been done on producing silica-based compounds by the sol-gel method, these kinds of materials are discussed here. These compounds can be synthesized either directly through polymerization reaction of their precursors [141] or grafting appropriate functional groups on parent materials formed from sol-gel method such as silica gel and some examples [142–167] are given in Table 1.

Zwitterionic hybrid polymers [142,143] were synthesized on the basis of ring-opening polymerization of pyromellitic acid dianhydride (PMDA) (a network builder) and phenylaminomethyl trimethoxysilane (PAMTMS), followed by the amination (Scheme 4).

Table 1. Chemicals used for synthesizing adsorbents by sol-gel method, adsorbed heavy metals, maximum adsorption capacity, pH and temperature for adsorption of heavy metals from waters.

Chemicals (interacting group)	Heavy metal [q_{max}, pH and t (°C)]	Isotherm	Reference
Pyromellitic acid dianhydride/phenylaminomethyl trimethoxysilane (–COOH)	Pb^{2+} (7.16 mmol/g, 5, room)	Langmuir	[142]
Pyromellitic acid dianhydride/phenylaminomethyl trimethoxysilane (–COOH)	Cu^{2+} (0.28 mmol/g, 4, room) Pb^{2+} (1.56 mmol/g, 5, room)	Langmuir Langmuir	[143]
3-Thiocyanatopropyltriethoxysilane/TEOS (–SH)	Cd^{2+} (87.7 mg/g, 5, 25)	Langmuir	[144]
3-[2-(2-Aminoethylamino)ethylamino]propyl-trimethoxysilane (Cd^{2+}– imprinted hybrid sorbent) (–NH_2)	Cd^{2+} (77.2 mg/g, 6, 25)	Langmuir	[145]
Cd^{2+}-imprinted mercapto-functionalized silica gel (–SH)	Cd^{2+} (83.89 mg/g, 6, 27)	Experimental	[146]
Non-imprinted mercapto-functionalized silica gel (–SH)	Cd^{2+} (35.91 mg/g, 6, 27)	Experimental	–
Fe^{3+}-imprinted cyanato-functionalized silica gel (–C≡N)	Fe^{3+} (35.6 mg/g, 3, 20)	Experimental	[147]
3-Glycidyloxypropyltrimethoxysilane/potassium tert-butoxide/titanium isopropoxide (oxygen atoms of adsorbent)	Pb^{2+} (181.2 mg/g, 5.5, room) Cu^{2+} (44.64 mg/g, 5.5, room) Cd^{2+} (35.84 mg/g, 5.5, room)	Langmuir Langmuir Langmuir	[148]
$Zr(OCH_2CH_2CH_3)_4$/3-mercapto-1-propanesulfonic acid (–SH)	Pb^{2+} (0.36 mmol/g, neutral, room) Hg^{2+} (0.87 mmol/g, neutral, room)	Experimental Experimental	[149]
$Ti(OCH_2CH_2CH_3)_4$/3-mercapto-1-propanesulfonic acid (–SH)	Pb^{2+} (1.24 mmol/g, neutral, room) Hg^{2+} (1.41 mmol/g, neutral, room)	Experimental Experimental	–
7-Amine-4-aza-heptyltrimethoxisilane/TEOS (amine group)	Pb^{2+} (36.64 mg/g, neutral, room)	Langmuir	[150]
10-Amine-4-aza-decyltrimethoxisilane/TEOS (amine group)	Pb^{2+} (30.27 mg/g, neutral, room)	Langmuir	–
3-Chloropropyltrimethoxysilane/TEOS (nitrogen center of sorbent)	Ni^{2+} (0.47 mmol/g, 4.5, room)	Langmuir	[151]
3-Aminopropyl triethoxysilane/TEOS (–NH_2)	Pb^{2+} (45.45 mg/g, 6, 25) Cu^{2+} (35.71 mg/g, 6, 25)	Langmuir Langmuir	[152] –
3-Chloropropyltrimethoxysilane/TEOS (nitrogen center of sorbent)	Mn^{2+} (0.35 mmol/g, 4.5, room)	Langmuir	–
Amino-terminated dendrimer-like PAMAM polymer/silica gel (amino content 1.91 mmol/g) (–NH– and –NH_2)	Cu^{2+} (78.7 mg/g, ethanolic, 25)	Langmuir	[153]
2-Aminoethyl-3-aminopropyltrimethoxysilane/ poly(dimethyl siloxane) (–NH/NH_2)	Cu^{2+} (1.2 mmol/g, ethanolic, 25) Ni^{2+} (0.37 mmol/g, ethanolic, 25) Fe^{3+} (1.3 mmol/g, ethanolic, 25)	Langmuir	[154]
Bis[3-(triethoxysilyl)propyl]disulfide/TEOS (–S–S–)	Cd^{2+} (26.8 mg/g, 6, 25) Pb^{2+} (56.7 mg/g, 6, 25) Cu^{2+} (13.3 mg/g, 6, 25)	Langmuir Langmuir Langmuir	[155]
Salen(NEt_2)$_2$/silica gel (–OH and –N(C_2H_5)$_2$)	Cu^{2+} (4.36 mg/g, 11, room) Mn^{2+} (2.34 mg/g, 11, room) Pb^{2+} (10.06 mg/g, 11, rom) Zn^{2+} (11.3 mg/g, 11, room)	Langmuir Langmuir Langmuir Langmuir	[156]
2-Acrylamido-2-methylpropanesulfonic acid/silica gel (–OH, –NH– and –SO_3H)	Cu^{2+} (0.66 mmol/g, ethanolic, 25)	Langmuir	[157]
Amino-terminated dendrimer-like polyamidoamine polymer/silica gel (–NH_2)	Pd^{2+} (0.7 mmol/g, neutral, room) Pt^{4+} (0.41 mmol/g, neutral, room) Au^{3+} (0.12 mmol/g, neutral, room)	Experimental Experimental Experimental	[158]
Polyethylene glycol/3-mercaptopropyl trimethoxysilane (–SH)	Cu^{2+} (0.4 mmol/g, 4, 40)	Langmuir	[159]
Polyvinilalcohol/3-(2-aminoethylamino)propyl trimethoxysilane (–NH/NH_2)	Pb^{2+} (67.6 mg/g, 5, 30)	Langmuir	[160]

Table 1. *Cont.*

Chemicals (interacting group)	Heavy metal (q_{max}, pH and t (°C))	Isotherm	Reference
Activated alumina/3-mercaptopropyl trimethoxysilane (–SH)	As(III) (9.28 mg/g, 7, room)	Experimental	[161]
N-[3-(trimethoxysilyl)propyl]-ethylenediamine/TEOS (–NH_2)	Pt^{2+} (139 mg/g, 3.05, 25)	Langmuir–Freundlich	[162]
Escherichia coli/TEOS (immobilized *E. coli* cells)	Cd^{2+} (79.9 mg/g, 5.7–6.2, 25)	Langmuir	[163]
N,N-(dipropylcarbamothioyl)thiophene-2-carboxamide/TEOS (–S–, C=O and amine groups)	Cd^{2+} (3.89 mg/g, 7, 30)	Langmuir	[164]
	Hg^{2+} (8.52 mmol/, neutral, 25)	Langmuir	
	Pb^{2+} (1.90 mmol/g, neutral, 25)	Langmuir	
SiNSSH/TEOS (via sulfur or nitrogen atoms of sorbent)	Cu^{2+} (1.66 mmol/g, neutral, 25)	Langmuir	[165]
	Ni^{2+} (1.44 mmol/g, neutral, 25)	Langmuir	
	Co^{2+} (1.26 mmol/g, neutral, 25)	Langmuir	
	Ni^{2+} (31.29 mg/g, 4.5, 25)	Langmuir	
3-Aminopropyltriethoxysilane/TEOS (–NH_2)	Cd^{2+} (40.73 mg/g, 4.5, 25)	Langmuir	[166]
	Pb^{2+} (96.79 mg/g, 4.5, 25)	Langmuir	
	Co^{2+} (0.32 mmol/g, 4.5, 25)	Experimental	
3-Chloropropyltrimethoxysilane/aniline/TEOS (–NH–)	Zn^{2+} (0.34 mmol/g, 4.5, 25)	Experimental	[167]
	Cd^{2+} (0.12 mmol/g, 4.5, 25)	Experimental	

Ionic groups of opposite charges on the polymer chain (quaternary amines and carboxylic groups) allowed their electrostatic interactions with heavy metals. TGA analysis showed a higher PDMA content of prepared samples, increased their thermal degradation temperature [143].

Scheme 4. The preparation steps of zwitterionic hybrid polymers. Reprinted with permission from [142]. Copyright 2010 Elsevier.

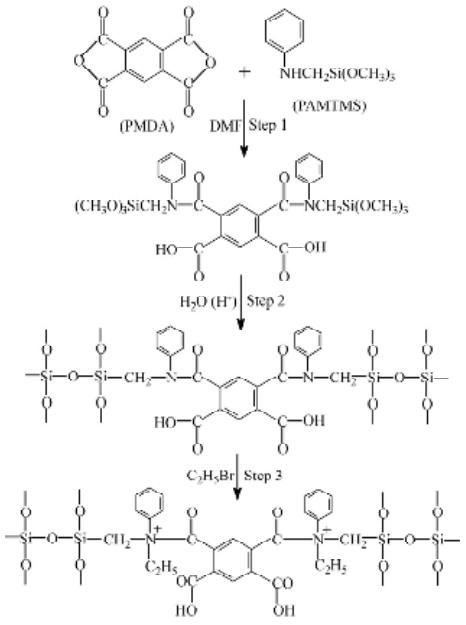

Kinetics experiments showed about 80% of Pb^{2+} and Cu^{2+} ions were adsorbed after approximately 3 h. Kinetics and thermodynamics measurements of Cu^{2+} and Pb^{2+} were carried out at pH = 4 and 5, respectively in which these metal ions exist mainly as their free forms.

Some researchers prepared imprinted ionic polymers (IIPs) for adsorption of metal ions [144–147]. IIPs were prepared by either the functionalization of a support surface (e.g., silica gel) using an organic chelating group and subsequently imprinted with metal ions as a template or by the co-condensation of monomers containing functional groups (in the presence of metal ions) and then co-condensation of them by sol-gel processes and finally releasing metal ion from the prepared compound. For example, thiocyanato- [144] and amino-functionalized [145] monomers were used to synthesize Cd^{2+}-imprinted polymers. These compounds showed high adsorption capacity and high selectivity toward templating ions.

SEM images of Cd^{2+}-imprinted and non-imprinted amino-functionalized hybrid polymers show that the former exhibits the porous feature [145]. The amino-functionalized Cd^{2+}-imprinted adsorbent [145] had rough surface and smaller size and thus larger surface area (152 m^2/g), compared to its non-imprinted form (101 m^2/g). Optimum pHs for the adsorption of Cd^{2+} were in the range of 4–8 where adsorption sites were deporotonated and Cd^{2+} ions were not hydroxilated. Kinetics experiments showed that the saturation of these sites was after about 20 min. The q_{max} (maximum adsorption capacity) value for the adsorption of Cd^{2+} on adsorbent was 77.2 mg/g. An IIP synthesized using mercapto-functionalized monomers [146] was applied for the separation of Cd^{2+} from Ni^{2+}, Cu^{2+} and Zn^{2+} that have similar ionic radii. The *relative selective factor values* of Cd^{2+}/Ni^{2+}, Cd^{2+}/Cu^{2+} and Cd^{2+}/Zn^{2+} (imprinted relative to non-imprinted) were 41.687, 65.617 and 66.937, respectively. The q_{max} values for the adsorption of Cd^{2+} on Cd^{2+}-imprinted and non-imprinted adsorbents were 83.89 and 35.91mg/g, respectively which were due to larger surface area of Cd^{2+}-imprinted adsorbent and its selectivity toward Cd^{2+}.

For a Fe^{3+}-imprinted adsorbent [147] prepared by grafting silica gel with cyanato functional groups, the q_{max}, optimum pH, and the time for the equilibrium binding of Fe^{3+} on the Fe^{3+}-imprinted adsorbent were 35.6 mg/g, 3 and 20 min, respectively. The selective coefficient values of Fe^{3+}/Co^{2+}, Fe^{3+}/Pb^{2+}, Fe^{3+}/Cd^{2+} and Fe^{3+}/Ni^{2+} of the Fe^{3+}-imprinted adsorbent were 11.95, 50.71, 16.96 and 8.56 times greater than those of a non-imprinted adsorbent, respectively. Due to the high affinity of these functional groups for Fe^{3+} and Cd^{2+}, the adsorption rate in these kinds of adsorbents is rapid. As reported by a number of authors [144−147], they washed the used imprinted adsorbents with 3 M HCl and reused the regenerated adsorbent repeatedly without significant loss of adsorption capacity.

Some researchers are interested in synthesizing silicon and metal containing compounds [148,149] which one of them is poly-GPTS/Ti(O)OH [148]. Poly-GPTS is prepared from the hydrolysis of 3-glycidyloxypropyltrimethoxysilane (GPTS) and poly-GPTS/Ti(O)OH from the hydrolysis of poly-GPTS and titanium isopropoxide, respecyively (Scheme 5).

Scheme 5. Silicon and titanium-contained adsorbent. Reprinted with permission from [148]. Copyright 2013 Taylor and Francis.

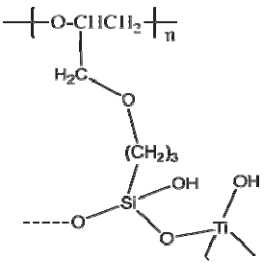

According to the kinetics experiments, the adsorption equilibrium was attained after about 10 min. Their experiments showed that at pH ≈ 5.5, Pb^{2+}, Cu^{2+} and Cd^{2+} interact with oxygen atoms of –OH groups of these adsorbents. Authors believed that due to stronger interactions between metal ions and –OH groups of poly-GPTS/Ti(O)OH, the q_{max} values for the adsorption of Pb^{2+}, Cu^{2+} and Cd^{2+} on poly-GPTS/Ti(O)OH (199, 42.79 and 39.41 mg/g, respectively) were bigger than those of poly-GPTS.

Another example of metal containing compounds is a series of macroporous thiol-functionalized titania and zirconia frameworks with propyl-siloxane, ethyl-sulfonate and propyl-sulfonate linkages [149] (Figure 9). The q_{max} values for the adsorption of Pb^{2+} and Hg^{2+} were in the ranges of 0.27–0.82 and 0.33–1.41 mmol/g, respectively.

Figure 9. (**a**) Scheme of macroporous thiol-titania material with propyl-siloxane linkages and (**b**) its SEM image. Reproduced with permission from [149]. Copyright 2002 The Royal Society of Chemistry.

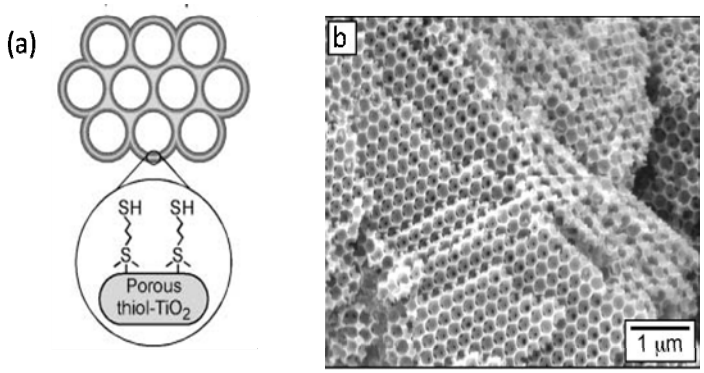

The ratio of adsorbed moles of Hg^{2+} and Pb^{2+} per mole of –SH groups (or their adsorption efficiency) were in the ranges of 0.19–0.82 and 0.21–0.72, respectively. This showed that the inner surface of these compounds were not completely accessible for these metal ions and had a smaller q_{max} value for Pb^{2+} compared to that of Poly-GPTS.

Xerogels [150,151] and aerogels [152] have been used for the adsorption of heavy metals [150,151]. Lima *et al*. [150] used mesoporous 7-amine-4-azahepthylsilica and 10-amine-4-azadecylsilica xerogels (abbreviated as AAH–Si and AAD–Si, respectively) for the adsorption of Pb^{2+} on which silica gels were functionalized with $–(CH_2)_3–NH–(CH_2)_3–NH_2$ and $–(CH_2)_3–NH–(CH_2)_6–NH_2$ groups, respectively. AAH–Si and AAD–Si interacted with Pb^{2+} through their amine groups and q_{max} values for the adsorption of Pb^{2+} on AAH–Si and AAD–Si were 36.64 and 30.27 mg/g, respectively and the equilibrium time of process was about 120 min. The higher adsorption capacity of AAH–Si over AAD–Si was due to the ability of AAH–Si to form a stable six-member ring with Pb^{2+} whereas AAD–Si was expected to form a nine-member ring that shows a transannular strain. In another work, an aniline-functionalized silica xerogel [151] was used for adsorption of Ni^{2+} and Mn^{2+} at pH 4–5. The adsorption equilibrium was achieved after about 20 and 30 min for Ni^{2+} and Mn^{2+}, respectively. The enthalpies of adsorption, obtained from calorimetric measurements, showed that weak interactions occur between xerogel and metal ions. It implied that the steric hindrance of phenyl group limits the accessibility of amine groups towards metal ions. Similar to above-mentioned xerogels, an amino

propyl-modified aerogel used for adsorption of Pb^{2+} and Cd^{2+} [152]. However, in spite of xerogels, the equilibrium time was 24 h.

Some efforts were done for the separation of metal ions from ethanol [153,154]. Qu *et al*. [153] investigated it through functionalization of silica gel using a series of amino-terminated dendrimer-like polyamidoamine (PAMAM) polymers. This process was endothermic and the Cu^{2+} adsorption capacities of these compounds with different amino contents were in the range of 9.8–78.7 mg/g. Kinetic experiments showed its adsorption equilibrium time was about 10 h. Pissetti *et al*. [154] synthesized an ethylenediamine-modified poly(dimethylsiloxane) elastomeric network (Pen) for the adsorption of Cu^{2+}, Fe^{3+} and Ni^{2+} from ethanol. In these compounds, the ethylenediamine functional groups were located at the nodes of the networks constituted by silsesquioxane clusters. The nodes of the polymeric network were constituted of clusters rich in $CSi(OSi)_3$ units. The interacting groups of this polymer were amine groups too (Supporting information Figure S3). Also, characteristics of a number of adsorbents [155–167] prepared by sol-gel method, have been given in Table 1.

3.2. Adsorption of Heavy Metals on Organically-Functionalized Mesoporous Compounds

In this section, adsorption capacities and operation conditions of silica-based mesopores are studied. As referred in Section 2.2, these compounds are synthesized through grafting, co-condensation or in situ grafting of mesopores and by synthesis of periodic mesoporous silicas. Details of a number of examples [168–198] are given in Table 2. One characteristic of mesoporous compounds is their high surface area. For example, it was shown that [168] when under similar conditions SBA–16 mesoporous compound was used or preparation of organic-inorganic hybrid compounds, its q_{max} values for adsorption of Cu^{2+} and Co^{2+} were higher than those of adsorbent prepared by silica gel.

Table 2. Adsorbed heavy metals, maximum adsorption capacity, pH and temperature for adsorption of heavy metals by mesoporous compounds.

Adsorbent (interacting group)	Heavy metal (q_{max}, pH and t (°C))	Isotherm	Reference
SBA-16 modified with n-propyl-salicylaldimine ($–NH_2$)	Cu^{2+} (58 mg/g, 4, room)	Experimental	[168]
	Co^{2+} (16 mg/g, 4, room)	Experimental	
SBA-16 modified with n-propyl-salicylaldimine and salicylaldehyde (–N=)	Cu^{2+} (15.2 mg/g, 4, room)	Experimental	–
	Co^{2+} (4.5 mg/g, 4, room)	Experimental	
SiO_2 modified with n-propyl-salicylaldimine ($–NH_2$)	Cu^{2+} (45.2 mg/g, 4, room)	Experimental	–
	Co^{2+} (11.2 mg/g, 4, room)	Experimental	
SiO_2 modified with n-propyl-salicylaldimine and salicylaldehyde (–N=)	Cu^{2+} (10.2 mg/g, 4, room)	Experimental	–
	Co^{2+} (3.6 mg/g, 4, room)	Experimental	
3-Aminopropyl-functionalized MCM-41 (ammonium group)	Arsenate (64.4 mg/g, 3–4,room)	Experimental	[169]
	Chromate (52.9 mg/g, 7–8,room)	Experimental	
3-Aminopropyl-functionalized SBA-1 (ammonium group)	Arsenate (94.2 mg/g, 3–4,room)	Experimental	–
	Chromate (132.7 mg/g, 7–8,room)	Experimental	
$H_2N–(CH_2)_2–NH–(CH_2)_3$–functionalized SBA-15 ($–NH_2$ and –NH–)	Cu^{2+} (0.83 mmol/g, neutral, 25)	Langmuir	[170]
3-Aminopropyl-functionalized SBA–15–N–C–H ($–NH_2$)	Cu^{2+} (0.39 mmol/g, neutral, 25)	Langmuir	–
3-Aminopropyl-functionalized SBA–15–N–E ($–NH_2$)	Cu^{2+} (0.35 mmol/g, neutral, 25)	Langmuir	–
3-Aminopropyl-functionalized SBA–15–N–C ($–NH_2$)	Cu^{2+} (0.24 mmol/g, neutral, 25)	Langmuir	–

Table 2. *Cont.*

Adsorbent (interacting group)	Heavy metal (q_{max}, pH and t (°C))	Isotherm	Reference
3-(2-Aminoethylamino) propyltrimethoxysilane modified ordered mesoporous silica	As(V) (10.3 mg/g, 7, room)	Experimental	[171]
N-propyl aniline-functionalized MCM-41 (–NH–)	Arsenate (0.85 mmol/g, 4.2, room)	Experimental	[172]
	Hg^{2+} (0.92 mmol/g, 3.5, room)	Experimental	
	Pb^{2+} (0.78 mmol/g, 5.8, room)	Experimental	
H_2N–functionalized SBA-15 ($–NH_2$)	Cu^{2+} (1.28 mg/g, neutral, room)	Experimental	[173]
	Pb^{2+} (1.31 mg/g, neutral, room)	Experimental	
	Cd^{2+} (1.35 mg/g, neutral, room)	Experimental	
Imidazole-functionalized SBA-15 (N atoms of imidazole)	Pd^{2+} (0.091 mmol/g, 4, room)	Experimental	[174]
	Pt^{2+} (0.091 mmol/g, 4, room)	Experimental	
SBA-15 modified with 3-aminopropyl-triethoxysilane and salicylaldehyde (–N= and $–O^-$ groups)	Cu^{2+} (46 mg/g, 4.8, room)	Experimental	[175]
	Ni^{2+} (22 mg/g, 4.8, room)	Experimental	
	Co^{2+} (19 mg/g, 4.8, room)	Experimental	
	Zn^{2+} (26 mg/g, 4.8, room)	Experimental	
Amino-functionalized mesoporous silica ($–NH_2$ and –OH)	Ni^{2+} (2.48 mmol/g, 8.5, 25)	Sips	[176]
2-Mercaptopyrimidine-functionalized SBA-15 (N and S atoms)	Cd^{2+} (0.99 mmol/g, 6, 25)	Experimental	[177]
3-Aminopropyl-functionalized MCM-41 ($–NH_2$)	Au^{3+} (0.4 mmol/g, 2.5, room)	Experimental	[178]
NH(propyl)-functionalized MCM-41 (–NH–)	Au^{3+} (0.33 mmol/g, 2.5, room)	Experimental	–
$N(propyl)_2$-functionalized MCM-41 (N atom of amine group)	Au^{3+} (0.2 mmol/g, 2.5, room)	Experimental	–
Chemically modified MCM-41 (–NH– and $–NH_2$)	Hg^{2+} (0.7 mmol/g, 5, 25)	Langmuir	[179]
3-Aminopropyl-functionalized MCM-41 ($–NH_2$)	Ag^+ (0.62 mmol/g, 5, 22)	Experimental	[180]
	Cu^{2+} (0.84 mmol/g, 5, 22)	Experimental	
3-Mercaptopropyl-functionalized MCM-41 (–SH)	Ag^+ (0.97 mmol/g, 5, 22)	Experimental	–
	Cu^{2+} (0.02 mmol/g, 5, 22)	Experimental	
3-Mercaptopropyl-functionalized SBA-16 (–SH)	Cu^{2+} (36.42 mg/g, 5.5, 25)	Langmuir	[181]
3-Aminopropyl-modified SBA-15 ($–NH_2$)	Cu^{2+} (73.5 mg/g, 6.3, 25)	Langmuir	[182]
SBB or *N*-((trimethoxysilyl)propyl)-*N*,*N*,*N*-tri-*n*-butylammonium chloride-functionalized SBA-15 (quaternary ammonium)	ReO_4^- (1.85 mmol/g, 6.4, room)	Experimental	[183]
3-Aminopropyl and 3-mercaptopropyl bi-functionalized mesoporous silica (–SH)	Hg^{2+} (1.51 mmol/g, neutral, room)	Experimental	[184]
Meso-structured silica modified with 3-mercaptopropyltrimethoxy silane and 9-(chloromethyl)anthracene (–SH)	Pb^{2+} (13.96 mg/g, neutral, 25)	Experimental	[185]
	Cu^{2+} (12.56 mg/g, neutral, 25)	Experimental	
	Hg^{2+} (12.09 mg/g, neutral, 25)	Experimental	
	Zn^{2+} (3.69 mg/g, neutral, 25)	Experimental	
3-Mercaptopropyl-functionalized SBA-15 (–SH)	Hg^{2+} (2.88 mmol/g, 4.5, 20)	Langmuir	[186]
Ordered mesoporous silica modified with 2,5-dimercapto-1,3,4-thiadiazole (–SH)	Hg^{2+} (1.7 g/g, neutral, room)	Experimental	[187]
1-Benzoyl-3-propylthiourea-functionalized MCM-41 (=N, =O, –NH– and $–NH_2$ groups)	Hg^{2+} (1 g/g, neutral, room)	Experimental	[188]
Disulfide-bridged periodical mesoporous organosilica (–S–S–)	Hg^{2+} (716 mg/g, 2, room)	Experimental	[189]
3-Mercaptopropyl-functionalized MCM-41 (–SH)	Hg^{2+} (0.59 mmol/g, neutral, room)	Experimental	[36]
3-Mercaptopropyl-functionalized HMS (–SH)	Hg^{2+} (1.5 mmol/g, neutral, room)	Experimental	–
Mesoporous thioether-functionalized polyvinylpyrrolidone (PVP)/SiO_2 composite (–S–)	Hg^{2+} (4.26 mmol/g, 2, room)	Experimental	[190]

Table 2. *Cont.*

Adsorbent (interacting group)	Heavy metal (q_{max}, pH and t (°C))	Isotherm	Reference
Disulfide-functionalized SBA-1 (–SH)	Hg^{2+} (849 mg/g, 2, room)	Experimental	[191]
3-(((5-ethoxybenzenethiol)imino)methyl)-salicylic acid immobilized onto mesoporous silica (–N= and –SH groups)	Pd^{2+} (164.2 mg/g, 3, room)	Langmuir	[192]
3-(3-(Methoxycarbonyl)benzylidene) hydrazinyl)benzoic acid immobilized onto mesoporous silica (C=O and –N=NH–)	Cu^{2+} (145.98 mg/g, 7, room)	Langmuir	[193]
3-(2-Aminoethylamino)propyl-functionalized mesoporous silica (–NH– and $–NH_2$)	Cu^{2+} (0.107 mmol/g, 3, room)	Experimental	[194]
3-Aminopropyl-functionalized MCM-41 ($–NH_2$)	Cd^{2+} (0.71 mmol/g, 5, 22) Ni^{2+} (0.69 mmol/g, 5, 22)	Experimental Experimental	[195]
Diamino-functionalized MCM-41	Co^{2+} (0.69 mmol/g, neutral, 25) Ni^{2+} (0.52 mmol/g, neutral, 25)	Experimental Experimental	[196]
Diamino-functionalized MCM-48	Co^{2+} (1 mmol/g, neutral, 25) Ni^{2+} (0.86 mmol/g, neutral, 25)	Experimental Experimental	–
Aminopropyl grafted SBA-15 modified with EDTA (–NH– and $–COO^-$)	Pb^{2+} (273.2 mg/g, 5, 25)	Langmuir	[197]
$CONH_2$-functionalized SBA-15 ($CONH_2$ group)	Cu^{2+} (1.4 mmol/g, 5, 298)	Langmuir	[198]

Another factor affecting the adsorption capacity of an adsorbent is the density of its functional groups [169,170]. Yoshitale *et al*. [169] studied and compared effects of functional group density on the adsorption of chromate and arsenate oxyanions and other heavy metals. The $H_2N–(CH_2)_3–$, $H_2N–(CH_2)_2–NH–(CH_2)_3–$ and $H_2N–(CH_2)_2–NH–(CH_2)_2–NH–(CH_2)_3–$ groups were grafted on the surface of MCM–41and SBA–1 to prepare their mono-, di- and triamino-functionalized derivatives, respectively [169]. These amino groups are abbreviated as N–, NN– and NNN–, respectively. They showed that the pore size and the surface area of these compounds decrease with the increase of their amine density and similar results have been reported for mono-, di- and triamino-functionalized SBA–15 [170]. Experimental results implied that the interaction between the amine groups and oxyanions was ionic and all amine groups can involve in the adsorption process. Thus, q_{max} values for the adsorption of CrO_4^- and $HAsO_4^{2-}$ increase from mono- to triamino-functionalized derivatives of both MCM–41 and SBA–1 (Figure 10) [169]. As reported [169,171,172], amino groups under acidic conditions had much higher q_{max} for the adsorption of arsenate. At the adsorption saturation, the stoichiometries of oxyanions to N atoms were 0.5 for all adsorbents derived from SBA–1, whereas they were 0.25–0.35 for MCM–41 derivatives [169]. This was due to, on SBA–1, all amino heads were randomly distributed and acted as adsorption sites but, on MCM–41, they formed domains on MCM–41.

Arencibia *et al*. [170] compared effect of synthesis condition on the adsorption of a number of metallic ions by monoamino-functionalized SBA–15 prepared by calcination, extraction and further hydration of calcined silica. They showed that q_{max} values of these adsorbents for Ni^{2+}, Cu^{2+}, Zn^{2+}, Cd^{2+} and Pb^{2+} were different from each other and there was no relation between the pore size and surface area of mesopores with their q_{max} values for the adsorption of metallic ions from solutions. Also, different functional groups on SBA–15 can adsorb different metal cations [173–177].

Figure 10. Adsorption isotherms of (**a**) arsenate and (**b**) chromate on mono-, di- and triamino-functionalized MCM–41 which are shown with N–MCM–41, NN–MCM–41 and NNN–MCM–41, respectively. Reprinted with permission from [169]. Copyright 2002 American Chemical Society.

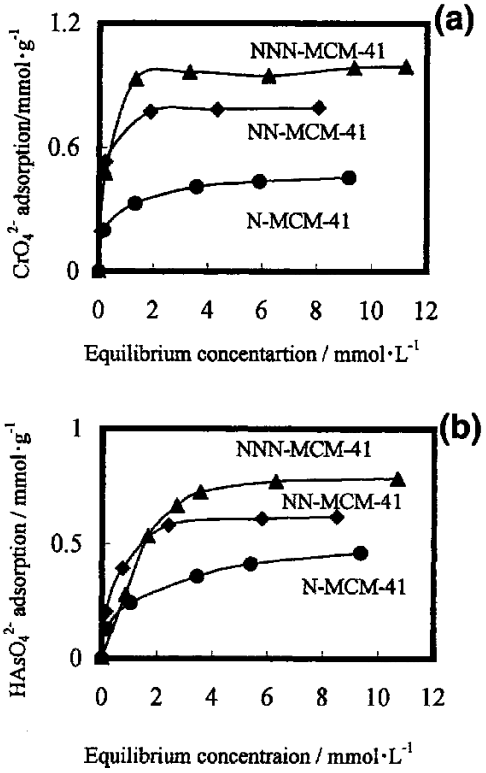

In some works, amino-functionalized MCM–41 mesopores were used for adsorption of heavy metal cations [178–180]. Yeoung *et al.* [178] studied the steric hindrance effect on the adsorption of Au^{3+}, Cu^{2+} and Ni^{2+} on $NH_2CH_2CH_2CH_2$–, $CH_3CH_2CH_2NHCH_2CH_2CH_2$– and $(CH_3CH_2CH_2)_2NCH_2CH_2CH_2$–functionalized MCM–41 which their abbreviated names are NH_2–MCM–41, NHR–MCM–41 and NR_2–MCM–41, respectively. The results showed that only Au^{3+} (from the mixture of these ions) was selectively adsorbed on these compounds, resulted from interactions of Au^{3+} ions with lone pair electrons of N atom of amine groups. They observed that the adsorption capacity of Au^{3+} decreased from NH_2–MCM–41 to NR_2–MCM–41 which was due to the increase in steric hindrance of these spacious groups on the lone-pair electrons of N atoms. Authors showed that Au^{3+} was adsorbed on NH_2–MCM–41 with the amine loading ratios higher than 0.6 mmol/g. This was because, at low amine loading ratios (<0.6), strong H-bonding between silanol and amine groups prevented interactions of amine groups with Au^{3+} ions whereas at the amine loading ratio higher than 0.6 amine groups formed patches of amino-derived areas and this destroys H-bonding between silanol and amine groups which was revealed at the peak shifting of around 1300 cm^{-1} in the FT-IR spectra (Figure 11). The used NH_2–MCM–41 was washed by 5 M HCl and all the adsorbed gold ions were recovered and the regenerated adsorbent retained its adsorption capacity after repeating usages.

Figure 11. FTIR spectrum of NH_2–MCM–41 with different NH_2 loadings. The insert figure displays the peak shift caused by the interaction between the amino and surface silanol groups. Reprinted with permission from [178]. Copyright 2006 American Chemical Society.

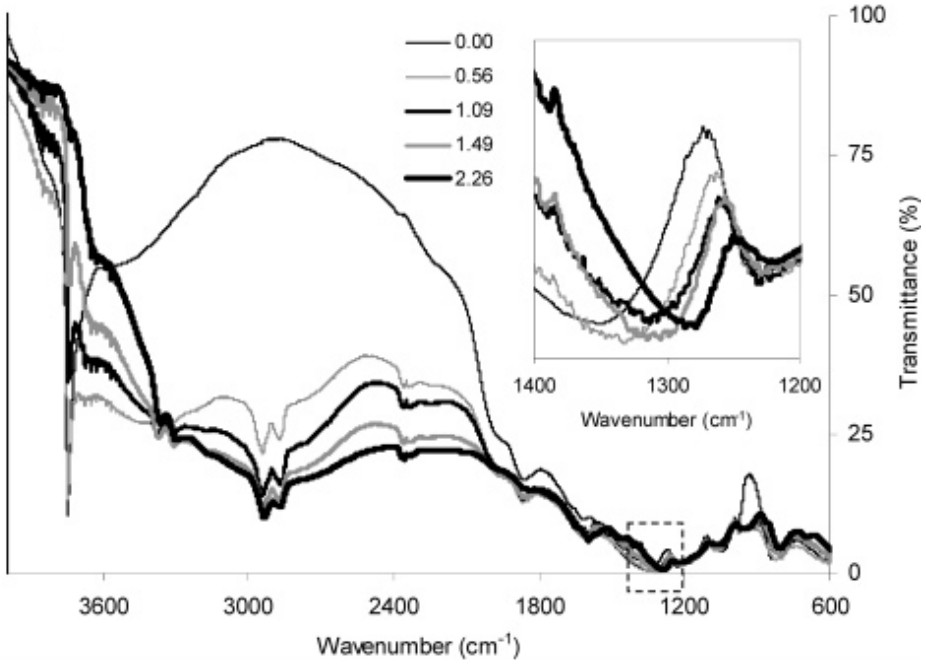

In another work, researchers changed contents of functional groups and used different ratios of 3-mercaptopropyl triethoxysilane (TMMPS) and TEOS to synthesize thiol-functionalized SBA–16 (SH–SBA–16) samples [181]. With the increase in the sulfur content of samples, –SH groups on the surface partially blocked the adsorption of nitrogen molecules and decrease their surface areas and pore sizes and the adsorption capacity of SH–SBA–16 samples increases. The used SH–SBA–16 sample for the adsorption of Cu^{2+} was recovered by 1 M HCl and after the seventh stripping cycle, its adsorption capacity was 90.5% of its initial value.

The adsorption of Cu^{2+} on aminopropyl-substituted SBA–15 (SBA–15–N) and a temperature-aged sample (SBA–15–N–T) was studied by Soler–Illia *et al*. [182]. It was observed that upon the addition of functional groups, the surface area of SBA–15–N and SBA–15–N–T decrease compared to SBA–15. Experiments showed that the q_{max} value for the adsorption of Cu^{2+} on SBA–15–N was bigger than that of SBA–15–N–T which was due to the rearrangement of inorganic network in SBA–15–N–T. Due to the thermal treatment of SBA–15–N intensive H-bond interactions between its amino groups and the surface silanols disrupted and this improved the accessibility of amino groups on the pore surface.

Dai *et al*. [183] studied effect of hydrophobicity of functional groups on their adsorption capacity. HMS, SBA–15 and PME (PMO material bridged with ethylene groups) functionalized with *N*-((trimethoxysilyl)propyl)-*N*,*N*,*N*-tri-*n*-butylammonium (TSPBC) and *N*-((trimethoxysilyl)propyl)-*N*,*N*,*N*-trimethylammonium (TSPMC) ions were used for the adsorption of hydrophobic ReO_4^- ions [183]. The results showed that TSPBC-functionalized HMS, SBA–15 and PME had bigger q_{max} values for the adsorption of ReO_4^- than those functionalized with TSPMC. This was due to the higher hydrophobic character of butyl groups compared to methyl groups that enhanced the adsorption of

ReO_4^- ions. When a cationic surfactant (here CTAC) was used for synthesizing mesopores (called as MEB sample), its chloride ions attached to the protonated silanol groups and anion-exchange sites and hindered the adsorption of ReO_4^- ions. To avoid high chloride content in these mesopores, authors used TSPBC and a neutral surfactant (rather than CTAC) to synthesize mesoporous compound (called as NMEB) that increased greatly its q_{max} for the adsorption of ReO_4^- ions compared to MEB. In another work, a bifunctional HMS, prepared by mercaptopropyl and aminopropyl groups, was used for the adsorption of Hg^{2+}, Cu^{2+} and Cd^{2+} [184]. Heavy Metal ions were adsorbed by –SH heads of mercaptopropyl groups. Due to higher affinity between –SH group and different mechanisms of its adsorption, the Hg^{2+} adsorption and its adsorption selectivity increased greatly compared to Cu^{2+} and Cd^{2+} (Figure 12). Hg^{2+} can be adsorbed on the inner surface of pores whereas Cu^{2+} and Cd^{2+} were adsorbed on the outer surface of adsorbent or near the pore openings. As reported [36,180,185–187], −SH groups of organically-functionalized mesopores have a great q_{max} for adsorption of Hg^{2+}. An example of a compound with two functional groups is 1-benzoyl-3-propylthiourea-functionalized MCM–41 (MCM–41 BTU) which was synthesized through a two-step modification process [188] to better control removal of Hg^{2+} and to prevent unnecessary pore blocking. In the first step they prepared 3-aminopropyl-MCM–41 (MCM–41 NH_2) and in the second step, they prepared MCM–41 BTU using MCM–41 NH_2. Their surface area and pore size were decreased as in order as MCM–41 > MCM–41 NH_2 > MCM–41 BTU.

The concentration of 1-benzoyl-3-propylthiourea and (unreacted) aminopropyl groups on the surface of MCM–41 BTU were 1.5 and 0.65 mmol/g, respectively (Figure 13). The adsorption isotherm of Hg^{2+} on MCM–41 BTU had two regions (Figure 13). In the first region, Hg^{2+} strongly were adsorbed on 3-aminopropyl residuals (K_1 = 1.41 × 10^5 M^{-1} and q_{max} = 1.55 mmol/g) and then in the second region the ions were adsorbed on the 1-benzoyl-3-propylthiourea residuals (K_2 = 1.08 × 10^2 M^{-1} and q_{max} = 3.48 mmol/g).

Figure 12. Difference between adsorption mechanism of Hg^{2+} and other metallic ions. Reprinted with permission from [184]. Copyright 2001 Elsevier.

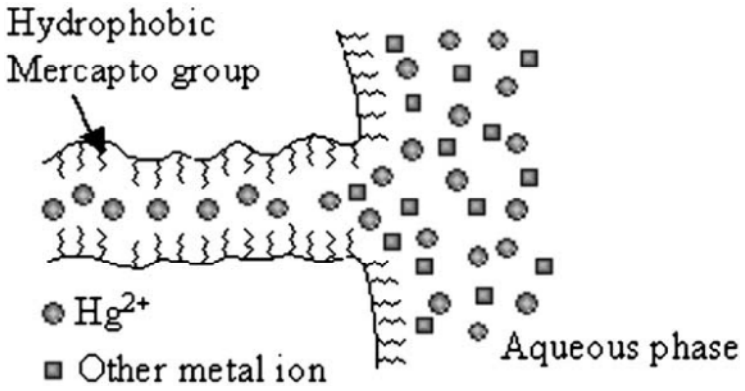

Figure 13. (**a**) Functional groups of MCM–41BTU and (**b**) adsorption isotherm for adsorption of Hg^{2+} on MCM–41 BTU. The initial sharp part of adsorption isotherm is related to adsorption by 3-aminopropyl residuals. Reprinted with permission from [188]. Copyright 2003 Springer Science and Business Media.

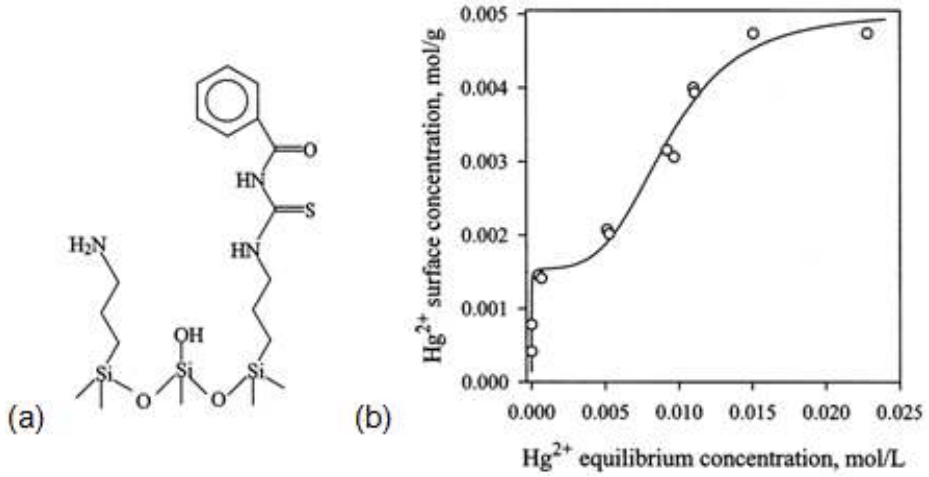

Zhao *et al*. [189] synthesized a number of two-dimensional disulfide-bridged periodical mesoporous organosilicas (PMO) with high sulfide contents for the adsorption of Hg^{2+}. They used bis(triethoxysilylpropyl) disulfide (BTSPDS) and TEOS as precursors and also applied $Zn(NO_3)_2$ in a number of syntheses. XRD patterns demonstrate that in the presence of Zn^{2+} highly ordered hexagonal disulfide-bridged PMO composites were obtained. Eventually, Zn^{2+} ions were etched off in a strong acid solution. XRD patterns of the Zn^{2+} treated compounds showed their high hydrothermal stability which was enhanced with the increase in their BTSPDS/TEOS ratios. Hg^{2+} ions interacted with sulfur atoms of –S–S– bridges of adsorbents. Adsorption capacities of these compounds for Hg^{2+}, similar to those of tetrasulfide-functionalized polyvinylpyrrolidone (PVP)/SiO_2 composite mesopores [190] or disulfide-functionalized SBA–1 [191], were high and increased with increase in their BTSPDS content [189]. This shows that double sulfide functioalized mesopores are emerging candidates for adsorption of Hg^{2+}.

Also, other kinds of mesoporous compounds with various functional groups were used for adsorption of heavy metals [192–198]. Yeung *et al*. [195] increased selectivity of an aminopropyl-grafted MCM–41 (NH_2–MCM–41) for the adsorption of Ni^{2+} and Cd^{2+} through chelation of these ions. The isoelectric point of NH_2–MCM–41 was 3.2. Below this pH, the adsorbent did not adsorb Ni^{2+} and Cd^{2+} and at pH = 5, its q_{max} values of Cd^{2+} and Ni^{2+} were 0.71 and 0.69 mmol/g, respectively. In binary mixtures of Ni^{2+} and Cd^{2+} at pH > 3.2, the q_{max} values of NH_2–MCM–41 for Ni^{2+} and Cd^{2+} were 0.60 and 0.16 mmol/g, respectively. The authors tuned the selectivity of adsorbent by an appropriate chelate, EDTA. EDTA selectively bound to Ni^{2+} (as $NiEDTA^{2-}$ complex) and changed its adsorption selectivity toward Cd^{2+}. Authors tried to separate these ions by adding EDTA and adjusting the pH of solution. At pH = 2, only Ni^{2+} ions (as $NiEDTA^{2-}$) were adsorbed by $–NH_3^+$ headgroups in mesopores and, at pH = 5, only Cd^{2+} ions were adsorbed by $–NH_2$ groups of adsorbent (Supporting information Figure S4).

The $H_2N(CH_2)_2NH(CH_2)_3$–functionalized MCM–41 and MCM–48 (abbreviated as NN–MCM–41 and NN–MCM–48) [196] were used for the adsorption of Fe^{3+}, Cu^{2+}, Co^{2+} and Ni^{2+}. Then, the authors

applied the used mesopores for the adsorption of arsenate. The Fe^{3+}, Cu^{2+} and Co^{2+} ions bound to ethylenediamine (en) headgroups of mesoperes as $Fe(en)_2$, $Cu(en)_2$ and Co(en) whereas Ni^{2+} interacted with surface silanol groups. The adsorption capacities of NN–MCM–48 for these metal ions were much larger than those of NN–MCM–41. Also, it was shown that Cl^- and SO_4^{2-} anions inhibited arsenate adsorption on these kinds of adsorbents by different extents.

3.3. Adsorption of Heavy Metals on Composites of Layered Compounds with Organic Polymers

As pointed in Section 2.3.3, these kinds of compounds are prepared as phase separated, intercalated and exfoliated structures [118]. Here, we study a number of works carried out regarding their abilities for the adsorption of heavy metals. Some examples [199–232] are summarized in Table 3.

Chitosan is a natural polycationic biopolymer that can chelate with heavy metals by its amino and hydroxyl groups and its nanocomposites with clays and zeolites are used for adsorption of heavy metals. However, it has a low surface area, with weak chemical and mechanical properties. Thus, physical and chemical modifications are necessary to overcome these limitations. On the other hand, the clay has a lamellar structure with negatively charged surface that interacts with polycationic chitosan. There is high possibility that one or both surfaces of the clay layers can be modified by chitosan. Chitosan-functionalized closite 10A [199], bentonite [200], perlite [201–204], clinoptilolite [205], alumina [206,207], montmerilonite [208,209] and calcium alginate [210] were used for the adsorption of heavy metals from water. In these compounds, functional groups of chitosan ($–NH_2$ and –OH) interact with heavy metals, in spite of cellulose/hydyoxyapatite in which negative sites of hydroxylapatite are interacting sites of nanocomposite [211]. XRD showed the interlayer spacing of chitosan-functionalized bilayer compounds increases, which showed a complete [199] or partial exfoliated [209] surface morphology. Electrostatic interaction between chitosan and negatively-charged surface of layer compounds such as closite A [199], perlite [203,204] and, alumina [206,207] resulted in the formation of nanocomposites. As an example for the adsorption of heavy metals by these kinds of compounds, authors studied the adsorption of Cr(VI) polyanions by closite 10 A/chitosan nanocomposite (CCN) (Figure 14) [199]. The TEM image demonstrated the formation of exfoliated surface morphology. The zeta potential of CCN surface at pH below eight was positive because the amine groups of chitosan were protonated at pH below eight and Cr(VI) ions existed as $Cr_2O_7^{2-}$, CrO_4^{2-} and $HCrO_4^-$ polyanions at pH range of 2–6. Thus, The optimum pH for the adsorption process was found to be 3. Similarly, interactions of nanocomposites of chitosan with perlite [201], alumina [206,207], montmorillonite [208], with Cr(VI) oxyanion or chitosan-clay with selenate [209] occur via their protonated amino groups. As reported [200,202–205,210] chitosan-layered nanocomposites interaction with metal cations occurs through –OH and $–NH_2$ groups of chitosan. The q_{max} values of these adsorbents completely depend on the used layered compounds, Table 3. The used CCN was regenerated by washing with 0.01 N H_2SO_4 and, after four cycles, its adsorption capacity was 78.47% of its initial value [199].

In another work, Wan *et al*. [212] used chitosan/bentonite and crosslinked chitosan immobilized on bentonite as adsorbent for Cu^{2+}. Crosslinking agents are used to amend mechanical and chemical properties of the adsorbents.

Figure 14. (**a**) Schematic structure of chitosan and clay hybrid and (**b**) mechanism of interaction of closite 10 A/chitosan nanocomposite (CCN) with Cr(VI). Reprinted with permission from [199]. Copyright 2011 Elsevier.

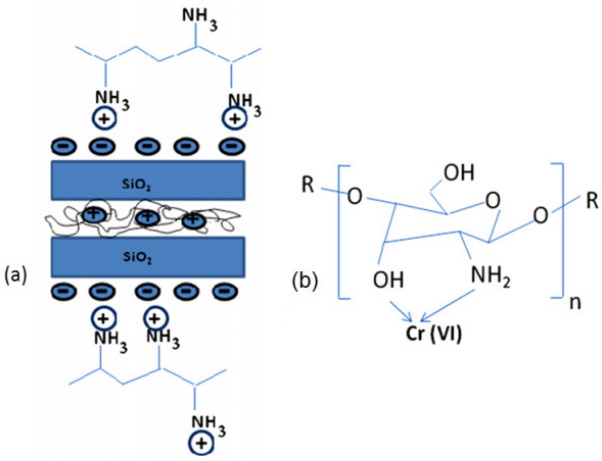

Table 3. Adsorbed heavy metals, maximum adsorption capacity, pH and temperature for adsorption of heavy metals by organic polymer/layered compound hybrids.

Adsorbent (interacting group)	Heavy metal (q_{max}, pH and t (°C))	Isotherm	Reference
Chitosan/cloisite 10 A (protonated –NH_2)	Cr(VI) (357.14 mg/g, 3, 35)	Langmuir	[199]
Chitosan/bentonite (ion exchange property of bentonite and –OH and –NH_2 groups of chitosan)	Pb^{2+} (15 mg/g, 4, 25)	Langmuir	[200]
	Cu^{2+} (12.6 mg/g, 4, 25)	Langmuir	
	Ni^{2+} (6.1 mg/g, 4, 25)	Langmuir	
Chitosan/perlite (protonated –NH_2)	Cr(VI) (153.8 mg/g, 4, 25)	Experimental	[201]
Chitosan/perlite (–NH_2 and –OH)	Cu^{2+} (196.08 mg/g, 5, room)	Langmuir	[202]
	Ni^{2+} (114.95 mg/g, 5, room)	Langmuir	
Chitosan/perlite (–NH_2)	Cd^{2+} (178.6 mg/g, 6, 25)	Experimental	[203]
Chitosan/perlite (–NH_2 and –OH)	Cu^{2+} (1.59 mmol/g, 4.5, 25)	Langmuir	[204]
Chitosan/clinoptilolite (–NH_2)	Cu^{2+} (11.32 mmol/g, 5, 25)	Langmuir	[205]
	Co^{2+} (7.94 mmol/g, 5, 25)	Langmuir	
	Ni^{2+} (4.21 mmol/g, 5, 25)	Langmuir	
Chitosan/alumina (protonated amino groups)	Cr(VI) (9.71 mg/g, 4, 40)	Langmuir	[206]
Chitosan/alumina (protonated –NH_2)	Cr(VI) (153.85 mg/g, 4, 25)	Langmuir	[207]
Chitosan/montmorillonite (protonated –NH_2)	Cr(VI) (40.65 mg/g, 4, 35)	Langmuir	[208]
Chitosan/montmorillonite (protonated –NH_2 group of chitosan)	Selenate (18.4 mg/g, 4, room)	Langmuir	[209]
Chitosan/calcium alginate (–NH_2 and –OH)	Ni^{2+} (222.2 mg/g, 5, room)	Langmuir	[210]
Cellulose/hydroxyapatite (ion exchange property of hydroxyapatite)	Pb^{2+} (16.32 mg/g, neutral, 25)	Langmuir	[211]
Chitosan/bentonite (–NH_2)	Cu^{2+} (9.85 mg/g, 4, 25)	Langmuir	[212]
Epichlorohydrin-crosslinked chitosan/bentonite (–NH_2)	Cu^{2+} (11.75 mg/g, 4, 25)	Langmuir	–
Ethylene glycol diglycidyl ether-crosslinked chitosan/bentonite (–NH_2)	Cu^{2+} (10.52 mg/g, 4, 25)	Langmuir	–
Glutaraldehyde-crosslinked chitosan/bentonite (–NH_2)	Cu^{2+} (4.17 mg/g, 4, 25)	Langmuir	–
Chitosan-*g*-poly(acrylic acid)/attapulgite/sodium humate ($–COO^-$, –COOH, –NH_2 and $–O^-$)	Pb^{2+} (809.5 mg/g, 5.5, 35)	Langmuir	[213]
Chitosan-*g*-poly(acrylic acid)/attapulgite ($–COO^-$)	Cu^{2+} (303.03 mg/g, 5.5, 30)	Langmuir	[214]
Chitosan-*g*-poly(acrylic acid)/attapulgite (–COOH, –NH_2 and –OH)	Hg^{2+} (785.2 mg/g, 5, 30)	Langmuir	[215]
Poly(methacrylic acid) grafted chitosan/bentonite (–COOH)	U(VI) (117.2 mg/g, 5.5, 30)	Langmuir	[216]

Table 3. *Cont.*

Adsorbent (interacting group)	Heavy metal (q_{max}, pH and t (°C))	Isotherm	Reference
Poly-methacrylic acid grafted chitosan/bentonite (amino and hydroxyl groups of chitosan)	Hg^{2+} (125 mg/g, 6, room)	Langmuir	[217]
	Pb^{2+} (111 mg/g, 6, room)	Langmuir	
	Cd^{2+} (83 mg/g, 6, room)	Langmuir	
Chitosan-*g*-poly(acrylic acid)/vermiculite (–COOH, $–NH_2$ and –OH)	Pb^{2+} (3.08 mmol/g, neutral, 30)	Langmuir	[218]
	Cd^{2+} (2.94 mmol/g, neutral, 30)	Langmuir	
Humic acid-immobilized-amine modified polyacrylamide/bentonite (–COOH)	Cu^{2+} (106.2 mg/g, 5, 30)	Langmuir	[219]
	Zn^{2+} (96.1 mg/g, 9, 30)	Langmuir	
	Co^{2+} (52.9 mg/g, 8, 30)	Langmuir	
Polyethylenimine800/magnetite-montmorillonite (protonated $–NH_2$)	Cr(VI) (8.77 mg/g, 3, 25)	Langmuir	[220]
Polyacrylic acid crossliked by N,N´-methylenebisacrylamide/montmorillonite (–CONH– and –COOH)	Ni^{2+} (270.3 mg/g, neutral, 25)	Langmuir	[221]
	Pb^{2+} (1666.7 mg/g, neutral, 25)	Langmuir	
Poly[N-(4-vinylbenzyl)-N-methyl-D-glucamine]/montmorillonite (protonated tertiary amine)	As(V) (72.26 mg/g, 6, 30)	Langmuir	[222]
	As(V) (72.99 mg/g, 6, 40)	Langmuir	
	As(V) (82.64 mg/g, 6, 50)	Langmuir	
Polyacrylamide/bentonite ($–NH_2$)	Cu^{2+} (32.81 mg/g, 6.2, 20)	Langmuir	[223]
Polyacrylamide-bentonite composite (negatively charged sites of bentonite)	Pb^{2+} (0.16 mmol/g, 4.5–5, room)	Langmuir	[224]
Phytic acid-modified polyacrylamide-bentonite composite (negatively charged sites of bentonite)	Pb^{2+} (0.18 mmol/g, 4.5–5, room)	Langmuir	–
Polyaniline/attapulgite (–NH– and –N=)	Hg^{2+} (909.1 mg/g, 6, 25)	Langmuir	[225]
Polyacrylamide/attapulgite ($–NH_2$)	Hg^{2+} (192.5 mg/g, 4.4, 30)	Langmuir	[226]
Polyvinyl alcohol/attapulgite (–OH)	Pb^{2+} (169.5 mg/g, 5, 30)	Langmuir	[227]
Acrylamide-2-acrylamido-sodium 2-methylpropane sulfonate copolymer/clay ($–SO_3^-$)	Cu^{2+} (1.07 mmol/g, 4.5, 25)	Experimental	[228]
	Cd^{2+} (1.28 mmol/g, 4.5, 25)	Experimental	
	Pb^{2+} (1.03 mmol/g, 4.5, 25)	Experimental	
Poly(methoxyethyl)acrylamide/clay (–NH–)	Pb^{2+} (0.385 mmol/g, 5, 30)	Langmuir	[229]
3-Aminopropyltriethoxysilane/sepiolite ($–NH_2$)	Fe^{2+} (0.44 mmol/g, 3, 25)	Langmuir	[230]
	Cu^{2+} (0.14 mmol/g, 4, 25)	Langmuir	
Triethoxy-3-(2-imidazolin-1-yl)propylsilane/sepiolite (negatively charged sites of sepiolite and N atoms of imidazolin)	Mn^{2+} (0.085 mmol/g, 4, 25)	Langmuir	[231]
	Cu^{2+} (0.13 mmol/g, 4, 25)	Langmuir	
	Fe^{3+} (0.05 mmol/g, 2.5, 25)	Langmuir	
	Zn^{2+} (0.035 mmol/g, 4, 25)	Langmuir	
	Co^{2+} (0.28 mmol/g, 4, 25)	Langmuir	
	Cd^{2+} (0.09 mmol/g, 4, 25)	Langmuir	
Iodine-modified chitosan/bentonite (I_2 and I^-)	Gas-phase Hg^0 at 110 °C	Experimental	[232]

Some researchers prepared nanocomposites using a natural carbohydrate (e.g., chitosan), a polymer and a layered compound [213–219]. Wang *et al*. [213] increased the number of compounds for synthesizing hybrid polymer and prepared chitosan-*g*-poly(acrylic acid)/attapulgite/sodium humate composite hydrogels for the adsorption of Pb^{2+}. In this adsorbent, $–NH_2$ groups of chitosan (CSA), –COOH and $–COO^-$ groups of polyacrylic acid (PAA), $–COO^-$ and $Ph–CO^-$ groups of sodium humate (SH) and Si–OH groups of attapulgite (APT) adsorbed Pb^{2+} ions. Depending on the used quantity of the above constituents, the adsorption capacity of hybrid polymer for Pb^{2+} was in the range of 702.35 to 843.86 mg/g.

Chitosan-*g*-poly(acrylic acid)/attapulgite (CTS–*g*–PAA/APT) composites were used for the fast adsorption of Cu^{2+} [214]. Results showed that attapulgite (APT) really reacted with the CTS–*g*–PAA polymer (Supporting information Figure S5). Adsorption experiments were carried out at pH = 5.5. It was fast and more than 90% of Cu^{2+} was adsorbed after about 15 min. FTIR spectra of CTS–*g*–PAA/APT compound before and after the adsorption of Cu^{2+} showed that $–NH_2$, –OH groups of chitosan and –COOH groups of PAA in the composites interacted with Cu^{2+}. This compound had a high q_{max} (785.2 mg/g) for the adsorption of Hg^{2+} [215], as well.

Poly(methacrylic acid)-grafted chitosan/bentonite (CTS–g–PMAA/Bent) composite (Supporting information Figure S6) was synthesized for the adsorption of U(VI) [216]. They used *N*,*N*′-methylenebisacrylamide as a crosslinking agent. XRD patterns showed that bentonite was exfoliated during the formation of composite. The adsorption process was carried out at pH = 5.5 in which the CTS–g–PMAA/Bent surface charge was negative and $UO_2(OH)^+$ was the predominant species. XPS spectra showed that $–COO^-$ groups of composite interacted with UO_2^{2+}. Similarly, methacrylic acid grafted chitosan/bentonite [217], Chitosan-*g*-poly(acrylic acid)/vermiculite [218] and humic acid-immobilized-amine modified polyacrylamide immobilized on bentonite [219] were used for the adsorbtion of a number of heavy metal cations.

In another groups of organically-functioalized layered compounds, synthetic polymers were used as organic moiety. Fe_3O_4 nanoparticles coated with polyethylenimine (PEI) polymer were intercalated between sodium rich montmorillonite (MMT) layers [220] under acidic conditions (pH = 2) and used it as a magnetic sorbent for the adsorption of Cr(VI). At pH = 2, amine groups of PEI were protonated and intercalated between MMT platelets by cationic exchange (Scheme 6). Two different molecular weights of PEI were investigated (*x* = 800 or 25,000 g/mol). The TEM images of Fe_3O_4–PEI*x*–MMT compound showed MMT existed as individual exfoliated platelets and intercalation tactoids composed by a few sheets (Figure 15).

Scheme 6. Schematic representation of Fe_3O_4–PEI*x*–MMT formation. Reprinted with permission from [220]. Copyright 2012 Elsevier.

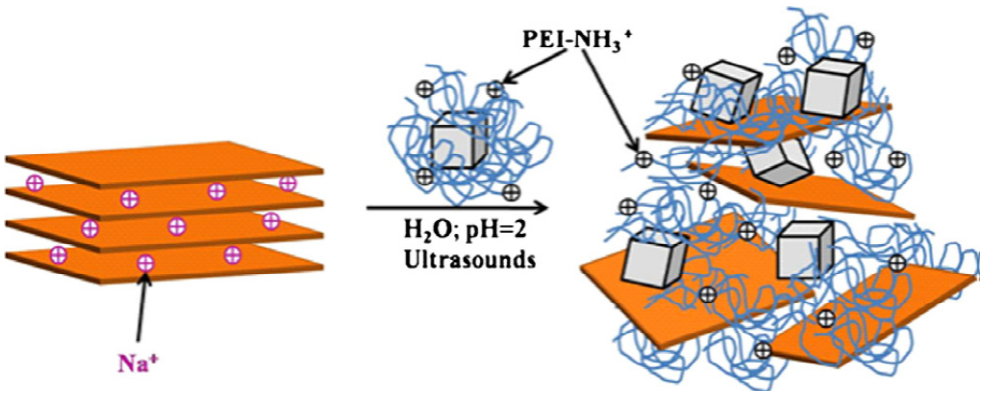

Figure 15. TEM images of (**a**) Fe_3O_4–PEI800–MMT and (**b**) Fe_3O_4–PEI2500–MMT hybrid materials. Reprinted with permission from [220]. Copyright 2012 Elsevier.

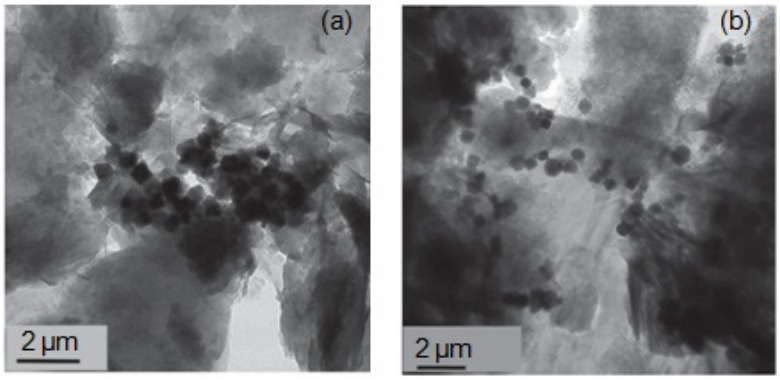

A better dispersion of magnetites was obtained in Fe_3O_4–PEI2500–MMT. The pH of zero point of charge of magnetite was 8.3 and the amine groups of PEI were protonated at pH below 10.4 and adsorbed Cr(VI) polyanions (CrO_4^{2-}, $HCrO_4^-$ and $Cr_2O_7^{2-}$) through electrostatic interactions. In pH lower than 2, Cr(VI) ions were mainly as H_2CrO_4 and the adsorption decreased. Experiments showed that they can be used for a wide pH range and the optimum pH for the adsorption process was 6. The q_{max} values of Fe_3O_4–PEI800–MMT and Fe_3O_4–PEI25000–MMT compounds were 8.77 and 7.69 mg/g, respectively.

A novel superabsorbent composite was synthesized by copolymerization reaction of partially neutralized acrylic acid (AA) on bentonite micropowder using *N*,*N*′-methylenebisacrylamide as a crosslinker [221]. The superabsorbent composite (SAC) was characterized by Fourier transform infrared spectroscopy (FTIR), thermogravimetric analysis (TGA) and scanning electron microscopy (SEM). The q_{max} values for adsorption of Pb^{2+}, Ni^{2+}, Cd^{2+} were 1666.67, 270.27, 416.67 and 222.22 mg/g respectively, Scheme 7.

Scheme 7. Adsorption isotherms of Pb^{2+}, Ni^{2+}, Cd^{2+} and Cu^{2+}. Reprinted with permission from [221]. Copyright 2009 Elsevier.

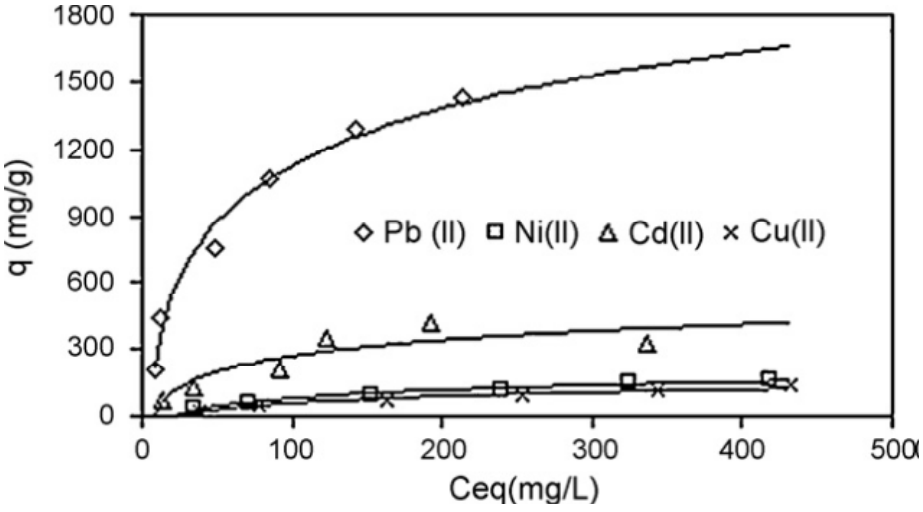

Organic-modified montmorillonite coated by *N*-(4-vinylbenzyl)-*N*-methyl-*D*-glucamine polymer was studied in the presence of a crosslinking reagent for the adsorption of arsenate [222]. XRD

patterns showed that the intercalation process was not complete. Also, TEM images confirmed the dispersion of montmorillonite within matrix. Adsorption experiments were carried out at pH = 6 and As(V) polyanions (as $H_2AsO_4^-$) interacted with ammonium groups of adsorbent and its q_{max} was 72.99 mg/g.

Bentonite (BENT) embedded in polyacrylamide (PAAm) composite was used [223] for the removal of Cu^{2+} from water. XRD patterns of BENT and BENT–PAAm (Figure 16) shows that acrylamide polymerization destroyed BENT structure and resulted in the crystal confusion. Results showed that the optimum pH for the adsorption of Cu^{2+} was 6.2. Increasing pH, increased the negatively charged or deprotonated amines and SiOH groups of BENT–PAAm and also increased the hydrolysis of Cu(II).

Below pH = 6.5, Cu(II) is mainly as Cu^{2+} (Supporting information Figure S7). In pHs of 5 and 6.2, q_{max} values of BENT–PAAm were bigger than those of BENT which was due to the presence of amine groups of PAAm. On the other hand, it was reported that negatively charged sites of bentonite in BENT–PAAm composite adsorbed Pb^{2+} [224]. In this compound, polyacrylamide chains just increase thermal and mechanical stabilities of the nanocomposite and its q_{max} for the adsorption of Pb^{2+} is less than that of pure bentonite.

Polyaniline/attapulgite (PANI/ATP) composite was used achieving a high adsorption of mercury [225]. X-ray photoelectron spectroscopy showed that after the adsorption of Hg^{2+} on PANI/ATP, its amine (–NH–) content reduced from 6.97 to 4.55 atom% and its imine (–NH^+–) content also diminished from 4.54 to 0.96 atom%. This showed that Hg^{2+} was adsorbed on both amine and imine functional groups. The optimum pH for the adsorption process was 6 and its q_{max} values at ionic strengths of 0.01, 0.1 and 1M were 909.1, 813.1 and 781.3 mg/g, respectively. As reported before [226], polyacrylamide/attapulgite adsorbed Hg^{2+} via its $–NH_2$ functional groups and its q_{max} value was 192.5 mg/g. It was observed that Cl^- decreased drastically its adsorption capacity of Hg^{2+} via forming $HgCl_4^{2-}$ compound. The adsorption capacity of PANI/ATP was preserved at 93% by the fifth cycle. Also, as seen in Table 3, –OH, $–SO_3^-$ and –NH– groups of organic moiety in polyvinyl alcohol/attapulgite [227], acrylamide-2-acrylamido-sodium 2-methylpropane sulfonate/clay [228] and poly(methoxyethyl)acrylamide/clay [229], respectively had a relatively high affinity for adsorption of Pb^{2+}.

Figure 16. XRD patterns of Bentonite (BENT) and BENT–PAAm. Reprinted with permission from [223]. Copyright 2010 Elsevier.

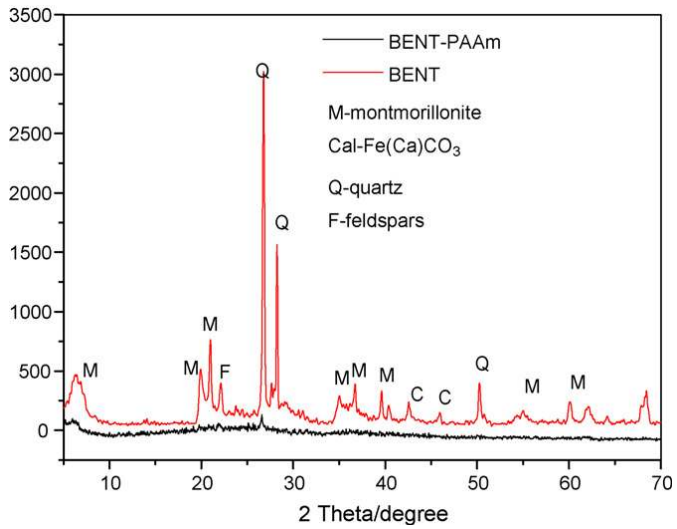

3.4. Adsorption of Heavy Metals on Organic-Inorganic Core-Shell Nanocomposites (CSNs)

CSNs have different applications and were studied briefly in Section 2.3.4. Here, we discuss the role of these compounds in the adsorption of metal ions. A number of examples [233–252] have been given in Table 4.

Table 4. Adsorbed heavy metals, maximum adsorption capacity, pH and temperature for adsorption of heavy metals by organic-inorganic core/shell and hierarchically structured nanocomposites.

Adsorbent (interacting group)	Heavy metal (q_{max}, pH and t (°C))	Isotherm	Reference
Core/shell nanocomposites			
SiO_2/salicyclic acid functionalized polystyrene (O atom of –COOH and N atom of –N=N–)	Cu^{2+} (1.29 mmol/g, 5, room)	Langmuir	[233]
	Ag^{+} (1.85 mmol/g, 5, room)	Langmuir	
	Au^{3+} (1.61 mmol/g, 2.7, room)	Langmuir	
SiO_2/amino functionalized polystyrene (–NH_2)	Cu^{2+} (0.17 mmol/g, neutral, room)	Experimental	[234]
	Ag^{+} (0.47 mmol/g, neutral, room)	Experimental	
	Au^{3+} (0.59 mmol/g, neutral, room)	Experimental	
SiO_2/imidazole-functionalized polystyrene (–N=N– and imidazole)	Au^{3+} (1.7 mmol/g, 2.7, room)	Langmuir	[235]
SiO_2/aniline formaldehyde condensate (–NH_2)	Cu^{2+} (76.33 mg/g, 5.4–5.7, room)	Langmuir	[236]
SiO_2/polyacrylamide (–NH_2)	Hg^{2+} (26.5 mg/g, acidic, 40)	Experimental	[237]
SiO_2/*Chetoceros* sp microalgae	Pb^{2+} (0.19 mmol/g, 5, 27)	Langmuir	[238]
SiO_2/chitosan imprinted by sucrose (amino groups)	Cu^{2+} (3.2 mg/g, 6, 25)	Langmuir	[239]
SiO_2/chitosan imprinted by polyethylene glycol 4000 (amino groups)	Cu^{2+} (9.1 mg/g, 6, 25)	Langmuir	–
SiO_2/chitosan imprinted by sucrose and polyethylene glycol 4000 (amino groups)	Cu^{2+} (10.5 mg/g, 6, 25)	Langmuir	–
SiO_2/Cd^{2+}-imprinted chitosan (amino groups)	Cd^{2+} (1.14 mmol/g, 6, room)	Experimental	[240]
SiO_2/chitosan (amino groups)	Cd^{2+} (0.58 mmol/g, 6, room)	–	–
SiO_2/chitosan (–NH_2 and –OH)	Cu^{2+} (0.2 mmol/g, 5.5, 25)	Experimental	[241]
SiO_2/chitosan (amino groups)	Ni^{2+} (182 mg/g, 7, 25)	Langmuir	[242]
SiO_2(CO_2H)/chitosan (amino groups)	Ni^{2+} (210 mg/g, 7, 25)	Langmuir	–
Fe_3O_4/poly(3,4-ethylenedioxythiophene) (–O–)	Ag^{+} (27.96 mmol/g, neutral, room)	Experimental	[243]
	Hg^{2+} (16.02 mmol/g, neutral, room)	Experimental	
	Pb^{2+} (14.99 mmol/g, neutral, room)	Experimental	
γ-Fe_2O_3/polyrhodanine (oxygen, nitrogen and sulfur atoms of polyrhodanine)	Hg^{2+} (179 mg/g, 4, 25)	Langmuir	[244]
Fe_3O_4 nanoparticle/chitosan (amino groups)	Cu^{2+} (21.5 mg/g, 5, 27)	Langmuir	[245]
Fe_3O_4 nanoparticle/chitosan (amino groups)	Au^{3+} (59.52 mg/g, 2, 25)	Langmuir	[246]
Fe_3O_4 nanoparticle/thiol-functionalized mesoporous microsphere (–SH)	Hg^{2+} (185.19 mg/g, 5, 20)	Langmuir	[247]
	Pb^{2+} (114.7 mg/g, 5, 20)	Langmuir	
Chitosan/zerovalent iron nanoparticles (complexation between Fe and Arsenic)	As^{3+} (94 mg/g, 7, 25)	Langmuir	[248]
	Arsenate (119 mg/g, 7, 25)	Langmuir	
Polystyrene/nano-Fe_3O_4 (Fe_3O_4)	Arsenate (139.3 mg/g, 6, 25)	Langmuir	[249]
Nanosized hydrous MnO_2/porous polystyrene cation exchanger resin (–SO_3^-, –Mn(OH) and –$Mn(OH)_2$ groups)	Cd^{2+} (1.96 mmol/g, 4.7, 25)	Langmuir	[250]
	Zn^{2+} (1.67 mmol/g, 4.7, 25)	Langmuir	

Table 4. *Cont.*

Adsorbent (interacting group)	Heavy metal (q_{max}, pH and t (°C))	Isotherm	Reference
Hierarchically structured nanocomposites			
Fe_3O_4/SiO_2/poly(1,2-diaminobenzene) (–NH_2, –NH– and –N=)	As^{3+} (84.5 mg/g, 6, 25)	Langmuir	[251]
	Cr^{3+} (77 mg/g, 5.3, 25)	Langmuir	
	Cu^{2+} (65 mg/g, 6, 25)	Langmuir	
SiO_2/Fe_3O_4/ion-imprinted polymer (–NH –CH_2 –CH_2 –NH_2)	Pb^{2+} (19.61 mg/g, 7.5, room)	Langmuir	[252]
SiO_2/Fe_3O_4/non-imprinted polymer (–NH –CH_2 –CH_2 –NH_2)	Pb^{2+} (6.57 mg/g, 7.5, room)	Experimental	–
Polyaniline nanorods on graphene oxide nanosheets (amine group)	Cr(VI) (1149.4 mg/g, 3, 25)	Langmuir	[253]
Silica/polystyrene (–SH)	Cu^{2+} (11.33 mg/g, 5, 15)	Langmuir	[254]
$CaCO_3$-pepsin ($CaCO_3$ and adsorption occurs through formation of $PbCO_3$ and $CuCO_3$)	Pb^{2+} (1167 mg/g, neutral, room)	Experimental	[255]
	Cu^{2+} (611 mg/g, neutral, room)	Experimental	
$CaCO_3$-maltose ($CaCO_3$ and adsorption occurs through formation of $PbCO_3$, $CuCO_3$, $NiCO_3$ and $CdCO_3$)	Pb^{2+} (3242.48 mg/g, 7, 25)	Langmuir	[256]
	Cd^{2+} (487.8 mg/g, 7, 25)	Langmuir	
	Cu^{2+} (628.93 mg/g, 7, 25)	Langmuir	
	Ni^{2+} (769.23 mg/g, 7, 25)	Langmuir	

Silica gel is a commonly used supporting material in inorganic-organic hybrid materials due to its environmental and economic factors and high thermal and mechanical stabilities [233–241]. Polystyrene diazo-coupled with salicyclic acid [233] (SG–PS–azo–SA) and encapsulated silica gel by polystyrene containing amino groups (SG–PS–NH_2) [234] (Scheme 8) were used for the removal of a number of heavy metals.

Scheme 8. Structures of (**a**) SG–PS–NH_2 and (**b**) SG–PS–azo–SA. Reprinted with permission from [233]. Copyright 2010 Springer Science and Business Media.

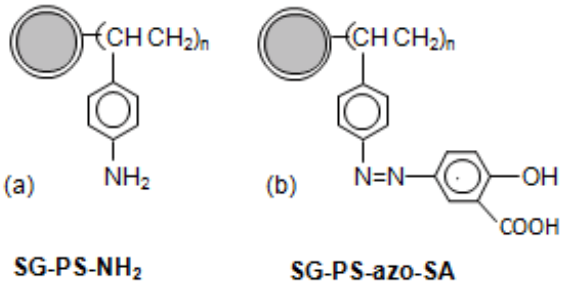

Thermogravimetric analysis of SG–PS–NH_2 and SG–PS–azo–SA showed that the respective organic layer had a high thermal stability. Also, the values of BET surface area, pore volume and pore size decreased greatly from silica gel to SG–PS–NH_2 to SG–PS–azo–SA. SEM images of silica gel, SG–PS–NH_2 and SG–PS–azo–SA indicated that the spherical shape and sizes of these three samples were similar (Supporting information Figure S8), proving that the microspheres of silica gel had good mechanical stability during the process of reaction. The q_{max} values of SG–PS–NH_2 for Cu^{2+}, Ag^{+} and Au^{3+} were 0.17, 0.47 and 0.59 mmol/g [234] and those of SG–PS–azo–SA were 1.29, 1.85 and 1.61 mmol/g, respectively [233]. Amine groups of SG–PS–NH_2 and –N=N– and salicyclic acid groups of SG–PS–azo–SA are their interacting groups.

On the other hand, adsorption capacities of organic functional groups change considerably depending on the nature of inorganic moiety. For example, q_{max} value of polyacrylamide in SiO_2/polyacrylamide [237] for Hg^{2+} was much less than that of polyacrylamide/attapulgite [226].

Some authors have used natural carbohydrate and biomass as shell of their adsorbents. Immobilization of biomass (*Chetoceros* sp microalgae) on a SiO_2 core resulted in an adsorbent for adsorption of Pb^{2+} [238]. Chitosan-grafted silica gel imprinted by sucrose and polyethylene glycol 4000 (PEG 4000) was used for the adsorption of Cu^{2+} [239]. This method has been used for direct preparation of porous sorbent with low mass transfer resistance, available functional ligand and excellent mechanical resistance [240]. Sucrose and PEG 4000 interacted with chitosan via hydrogen bonds and extraction of them, by breakage of H-bonds, resulted in a porous structure. The optimum pH for the adsorption of Cu^{2+} on this adsorbent was 6. At this pH, copper was mostly as Cu^{2+} form and most of amine groups of chitosan (its interacting group) were as $–NH_2$. TG/DSC analyses showed that the thermal stability of grafted chitosan was higher than pure chitosan (Supporting information Figure S9). The XRD patterns show no peak for crystallization regions of chitosan in non-supported hybrid material compared to those of pure chitosan which might be ascribed to the demolition of its crystallinity (Figure 17). The q_{max} values of Cu^{2+} adsorption for the adsorbent imprinted with sucrose and PEG 4000, PEG 4000, sucrose and non-imprinted adsorbent [241] were 10.5, 9.1, 3.2 and 0.2 mmol/g, respectively.

Figure 17. XRD patterns of (**a**) pure chitosan and (**b**) chitosan in non-supported hybrid material. Reprinted with permission from [239]. Copyright 2007 Elsevier.

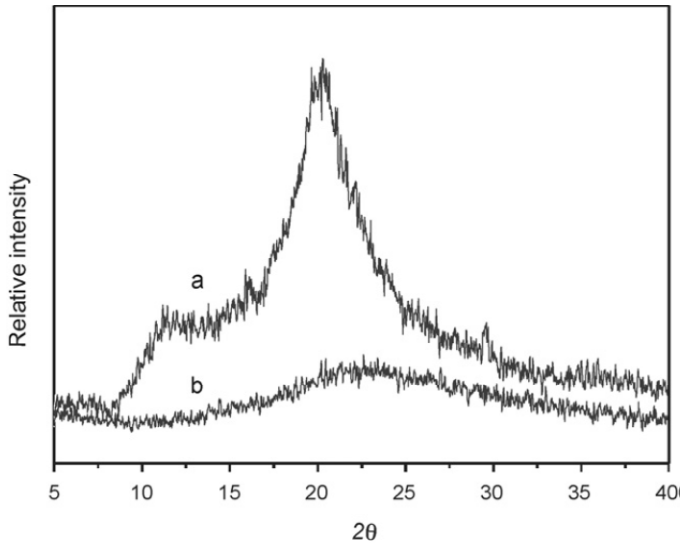

The used adsorbent was washed by 0.1 M HCl and the capacity of the regenerated sorbent through five cycles was detected to be 94% of the fresh one and equilibration time in the case of sucrose and PEG 4000 was 25 min. Also, q_{max} value of $SiO_2(CO_2H)$/chitosan for adsorption of Ni^{2+} was higher than that of SiO_2/chitosan [241] which shows effect of support on the adsorption property of adsorbent [242]. Another material that was used frequently in core-shell nanocomposites was Fe_3O_4 magnetic nanoparticle [243–248]. These kinds of compounds can be separated with the help of an external magnetic force. In a number of works, organic polymers were used as shell for Fe_3O_4 core [243,244]. Jang *et al*. [243] encapsulated Fe_3O_4 by poly(3,4-ethylenedioxythiophene) (PEDOT) and used the

produced compound (Fe_3O_4–PEDOT) for the removal of metal ions (Scheme 9). PEDOT has an excellent environmental stability and can interact with positively charged metal ions through its sulfur atom. The PEDOT shell has a lower surface energy than the core of magnetic nanoparticles, thus Fe_3O_4–PEDOT nanoparticles show amended stability and dispersibility in aqueous solutions, compared to pristine Fe_3O_4 nanoparticles. Adsorption experiments showed that adsorption capacities of Fe_3O_4–PEDOT nanoparticles were: $Ag^+ > Hg^{2+} > Pb^{2+}$. It was regenerated by acid treatment and the recovered adsorbent by ten cycles showed no loss in its adsorption capacity.

Scheme 9. Synthesis steps of Fe_3O_4–PEDOT nanoparticles by seeded polymerization mediated with acidic etching. Reproduced with permission from [243]. Copyright 2007 The Royal Society of Chemistry.

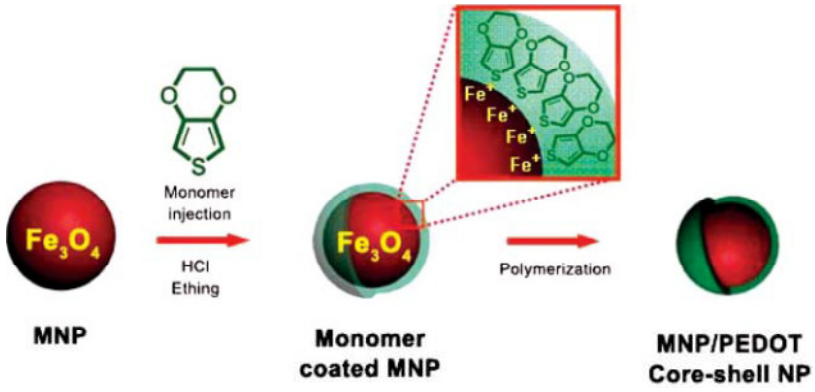

Chitosan-bound Fe_3O_4 magnetic nanoparticle has been used for the adsorption of Cu^{2+} and Au(III) ions [245,246]. TEM images showed that Fe_3O_4 and chitosan-bound Fe_3O_4 nanoparticles had a similar particle size of 13.5 nm and were monodisperse [245]. This revealed the reaction between Fe_3O_4 and chitosan occured only on the surface of Fe_3O_4. Also, XRD patterns showed that the binding of chitosan to the surface of Fe_3O_4 did not result in the phase change of Fe_3O_4. Experiments showed that the pH of isoelectric point of chitosan-bound Fe_3O_4 nanoparticles was 5.9 and the optimum pH for the adsorption of Cu^{2+} ions was in the range of 2–5 [245] and that of Au(III) negatively-charged complex was 2 [246]. The q_{max} values for Cu^{2+} and Au(III) were 21.5 [245] and 59.52 mg/g [246], respectively. In a different study, Tao *et al*. [247] used thiol-functionalized magnetic mesoporous microsphere (TMMM) for adsorption of Hg^{2+} and Pb^{2+}. The Fe_3O_4 nanoparticles were used as a core and coated with two silica layers, a tightly crossed silica thin layer and a mesoporous silica shell. The thiol moiety had a strong affinity towards these metal ions. The porous structure of the silica shell brought large surface area and provided the opportunity to graft organic moiety for adsorption of metal ions. q_{max} value of Hg^{2+} was 185.19 mg/g at 20 °C and decreased in the presence of Ca^{2+}, Mg^{2+} and Na^+ ions.

In some works, organic moieties (chitosan [248] and polystyrene [249]) were used as core. Polystyrene-supported Fe_3O_4 nanoparticles (PS–Fe_3O_4 NPs) was used for the adsorption of arsenate oxyanion [249]. Zeta potential measurements showed the polystyrene (PS) latex was negatively charged in a wide pH range and Fe_3O_4 nanoparticles were positively charged in acidic or neutral solutions. This was the driving force for the acervation of Fe_3O_4 nanoparticles on PS and the formation of PS-Fe_3O_4 NPs. At pH of 6, As(V) was as $HAsO_4^{2-}$ and PS–Fe_3O_4 NPs had the maximum adsorption capacity for its adsorption. TEM images showed that the diameter of fresh Fe_3O_4 spherical beads

(due to aggregation) were in the range of 350–400 nm, but there was not observed coalescence between PS–Fe_3O_4 NPs. Due to these, the q_{max} value for the adsorption of arsenate on PS–Fe_3O_4 was 139.3 mg/g whereas that of Fe_3O_4 was 78.4 mg/g. The used PS-Fe_3O_4 NP was recovered by 0.1 M NaOH and its recycling efficiency after the sixth cycle was 89.6%.

Lv *et al*. [250] synthesized nanosized hydrous MnO_2 encapsulated within porous polystyrene cation exchanger as adsorbent for heavy metals. The $-SO_3^-$ groups of polymeric matrix and –MnOH and $-Mn(OH)_2$ groups of MnO_2 interacted with Zn^{2+} and Cd^{2+}. In the presence of Ca^{2+}, due to its electrostatic interaction with $-SO_3^-$ groups, q_{max} values of nanocomposite for adsorption with Zn^{2+} and Cd^{2+} were decreased greatly.

Some researchers have used two inorganic compounds (e.g., SiO_2 and Fe_3O_4) as the core [251,252]. Firstly, they prepared Fe_3O_4 on which a layer of SiO_2 was synthesized, and then carried out the polymerization on the surface of SiO_2. Song *et al*. [251] synthesized Fe_3O_4–SiO_2–poly(1,2-diaminobenzene) sub-micron particle (FSP) for the removal of Cr(III), As(III) and Cu(II). Zhang *et al*. [252] used 3-(2-aminoethylamino)propyltrimethoxysilane (AAPTS) as the functional monomer and Pb^{2+} as the template to prepare an ion-imprinted polymer (Fe_3O_4@SiO_2@IIP) for the separation of Pb^{2+} ion from water (Scheme 10).

Scheme 10. Schematic structures of (**a**) FSP (Reprinted with Permission from [251]. Copyright 2012 Elsevier) and (**b**) template in Fe_3O_4@SiO_2@IIP (Reprinted with permission from [252]. Copyright 2011 Elsevier).

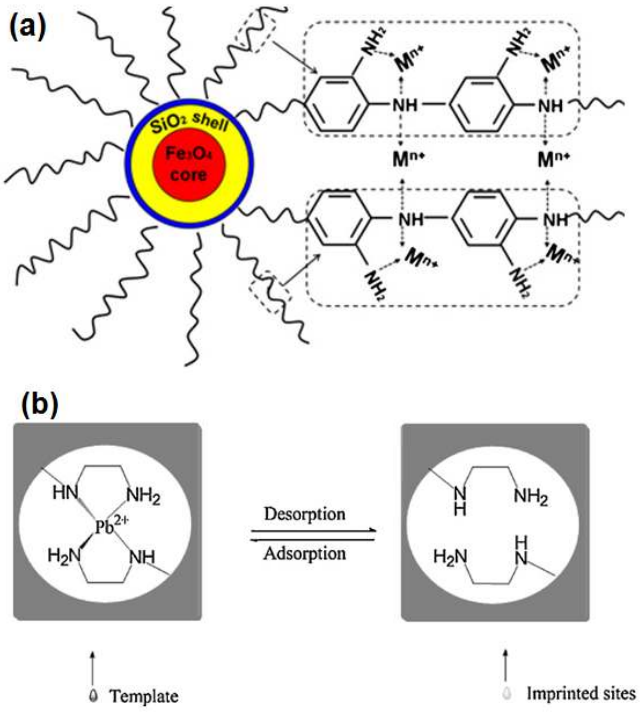

XRD patterns showed that peaks of Fe_3O_4 of the core-shell compounds were similar to those of naked Fe_3O_4 nanoparticles and the surface modification of Fe_3O_4 did not result in its phase change. In both adsorbents, amine groups interacted with metal ions. Experiments using Fe_3O_4@SiO_2@IIP at pH = 7.5 showed that in the presence of Cu^{2+}, Zn^{2+}, Cd^{2+} and Hg^{2+}, the relative selectivity factor values of Pb^{2+}/Cu^{2+}, Pb^{2+}/Zn^{2+}, Pb^{2+}/Cd^{2+} and Pb^{2+}/Hg^{2+} were 7.41, 6.76, 3.75 and 6.39, respectively [252].

However, when authors used a non-imprinted polymer to synthesize this core-shell polymer (Fe_3O_4@SiO_2@NIP), values of the above-mentioned relative selectivity factor were about 1 and this adsorbent was not selective toward Pb^{2+}.

As we saw in this section, synthesing core-shell nanocomposites does not result in the phase change of its inorganic moiety. In some cases, more than one inorganic compound was used as the core. Functional groups of the shell have a major role in the adsorption of heavy metal ions and core-shell nanocomposites had good mechanical stability and organic moiety of these compounds had higher thermal stability than that of its pure form.

3.5. Adsorption of Heavy Metals on Organic-Inorganic Hierarchically Structured Materials

Hierarchically structured compounds were explained briefly in Section 2.3.5. Li *et al*. [253] synthesized a hierarchical nanocomposite by the polymerization of aniline arrays on the surface of grapheme oxide nanosheets and used it as a superadsorbent for the adsorption of Cr(VI) oxyanion from water (Figure 18 and Table 4). Aniline monomers (ANI) were adsorbed on the surface of graphene oxide (GO) through electrostatic interactions with its reactive oxygen-containing functional groups and further the polymerization of ANIs resulted in the formation of aligned polyaniline (PANI) nanorods on the surface of GO (PANI/GO).

Figure 18. Mechanism of formation of polyaniline (PANI) nanorods on the surface of graphene oxide (GO) (PANI/GO) hierarchical nanocomposites. Reproduced with permission from [253]. Copyright 2013 The Royal Society of Chemistry.

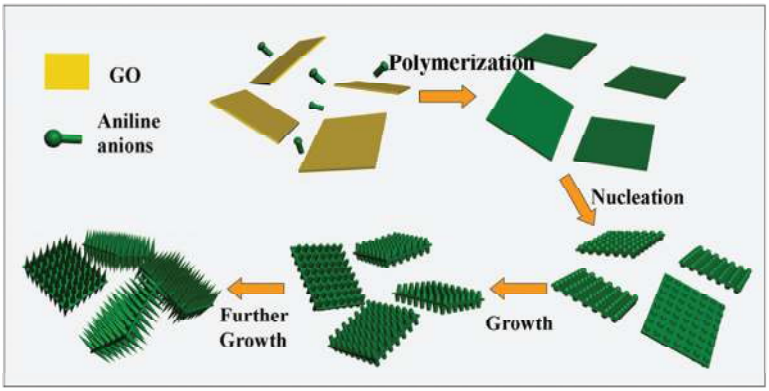

XRD patterns showed that the interplanar distance of GO nanosheets was 0.88 nm (as agglomerated) and PANI/GO demonstrated characteristic peaks of PANI (Supporting information Figure S10). These evidence proved that GO and PANI/GO were as agglomerated and separated nanosheets, respectively. Adsorption experiments were carried out at pH = 2 in which Cr(VI) adapting the form of $HCrO_4^-$ interacted with the protonated nitrogen atoms of PANI in pure PANI and PANI/GO. Pure PANI was simply aggregated and its surface area was smaller than PANI/GO and the q_{max} values of PANI and PANI/GO were 490.2 and 1149.4 mg/g, respectively.

In a novel work, Li *et al*. [254] fabricated polystyrene (PS) nanofibrous mats by an electrospinning method and used as a skeleton for thiol-functionalized mesoporous silica compound (Figure 19 and Table 4). In this hierarchical structure the PS nanofibers had macroporous structures (diameters of 3–10 μm) and were randomly distributed in the membrane (Supporting information Figure S11). The

optimum pH for the adsorption of Cu^{2+} was about 5 and its q_{max} value was 11.33 mg/g. Cu^{2+} ions were adsorbed by –SH groups within mesopores. The amount of thiol groups in the adsorbent was 0.32 mmol/g and the adsorption efficiency (Cu^{2+}/SH molar ratio) of adsorbent was about 80%. After the recovery of adsorbent by 0.5 M HCl, its adsorption capacity of Cu^{2+} was basically maintained after five cycles.

In another different works with hierarchical structure compounds, Ma *et al*. synthesized $CaCO_3$–pepsin [255] and $CaCO_3$–maltose [256] and used them as adsorbents. Here, structure and adsorption characteristics of $CaCO_3$–pepsin [255] are studied (Figure 20). Pepsin is an enzyme which is made up of 327 amino acids. SEM images showed that $CaCO_3$–pepsin consisted of a large number of tetrahedral micro-aggregates that were composed of smaller tetrahedral building nano-blocks (Supporting information Figure S12).

XRD, SEM and IR results showed that $CaCO_3$ and pepsin interacted through both coordination of Ca^{2+} and pepsin and interactions between the surface of $CaCO_3$ nanocrystals and –OH and –CO groups of pepsin.

Figure 19. Schematic illustration of preparing thiol-functionalized membranes using electrospun nanofibrous mats as the skeleton. Reproduced with permission from [254]. Copyright 2012 The Royal Society of Chemistry.

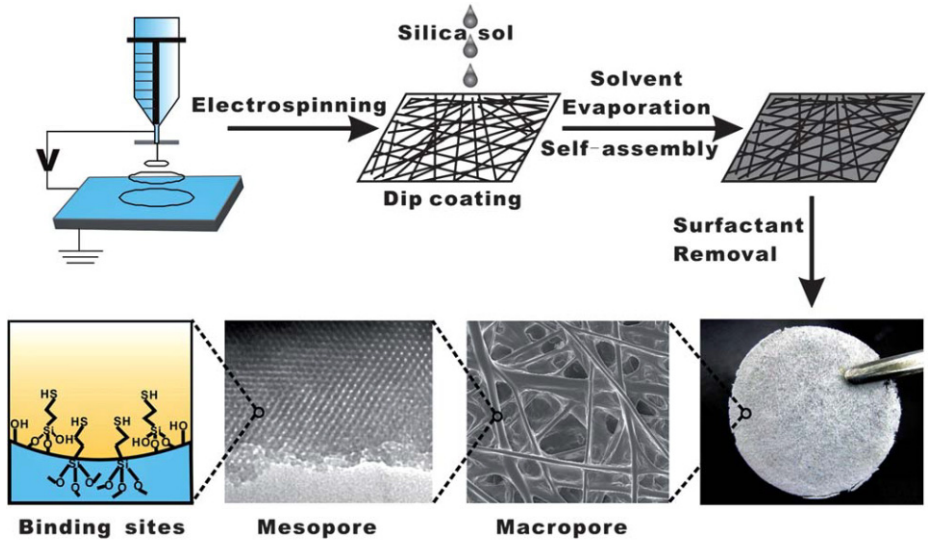

Adsorption experiments were carried out in neutral pH and the adsorption capacity of $CaCO_3$–pepsin for Pb^{2+} and Cu^{2+} were 1167 and 611 mg/g, respectively and the removal of Pb^{2+} was very rapid (about 20 min). Solubility product of $PbCO_3$ and $CuCO_3$ are less than $CaCO_3$ and thus Cu^{2+} and Pb^{2+} precipitate as their carbonates.

On the other hand, adsorption capacities of $CaCO_3$–maltose [256], another hierarchical structure superadsorbent, for Pb^{2+}, Ni^{2+}, Cu^{2+} and Cd^{2+} (as metal carbonate) were 3242.48, 769.23, 628.93 and 487.8 mg/g, respectively whereas adsorption capacity of $CaCO_3$ for Pb^{2+} is 62.5 mg/g and this showed clearly synergic effects between organic and inorganic moieties in these compounds. As we saw, the organic-inorganic hierarchically structured compounds are superadsorbent.

Figure 20. Mechanism of the formation of hierarchical structures of $CaCO_3$–pepsin from amorpuus precursors. Reprinted with permission from [255]. Copyright 2012 Elsevier.

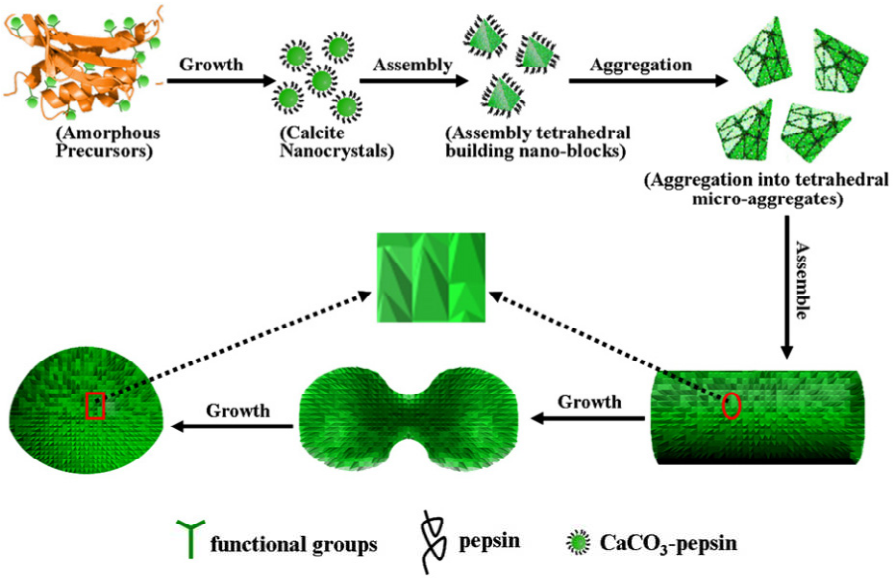

3.6. Characteristics of Organic-Inorganic Hybrid Polymers

To study Sections 3.1–3.5, the characteristics of different kinds of organic-inorganic hybrid polymers were as follows: (1) Some functional groups of these adsorbents are –SH, –COOH, amines and –S–S–, –OH, $–SO_3^-$ and ion exchange sites of hybrid polymer; (2) adsorption processes mostly obey the Langmuir isotherm that shows the adsorption is monolayer and there is a uniform distribution of sites on the surface of adsorbents; (3) the adsorption capacity of each certain organic functional group changes depending on its content [181,214], the used organic compound, inorganic support [166,195], crosslinking agent [212], aggregation of nanoparticles [253] and the used synthesis method [182,189]; (4) in some cases, organic compounds are used only for increasing thermal and mechanical stability of adsorbents and without adsorbing heavy metal ions [224]; (5) mesoprous compounds, due to their porous structures have a rather higher adsorption capacities compared to those of organically-functionalized layered, core-shell compounds and products of sol-gel method; (6) heavy metals as cations and oxyanions are adsorbed via electrostatic interactions and the increase in the hydrophobicity of functional groups of adsorbent (e.g., $–N(C_2H_5)_2$ [156] or from $–NH_2$ to –NH(propyl) to $–N(propyl)_2$ [178]) decreases their adsorption capacity for metal cations and increases their q_{max} values (e.g., from trimethylammonium to tri-*n*-butylammonium functional groups) for the adsorption of some hydrophobic oxyanions [183]; (7) In the most cases, for example [141–147,216,221,225,241,243,249,252], the used adsorbents are recovered by acid treatment and in the cases that acid dissolves the adsorbent [199], they have used another washing solutions; (8) some ions may react with metallic ions, e.g., $Cl^–$ with Hg^{2+} [226], and inhibit their adsorption; (9) some ions, e.g., $Cl^–$ [183], $SO_4^{2–}$ [196] or metallic cations [252], may react with functional groups of hybrid adsorbents and decrease their adsorption capacity for heavy metal ions; (10) steric hindrance on functional group decreases its adsorption capacity [151]; (11) in most cases, adsorption capacities of organic-inorganic hybrid polymers are bigger than those of their organic or inorganic constituents; (12) most of heavy metals were adsorbed in the pH range 4–7. With the increase in alkalinity of

solution, heavy metal ions convert to metal hydroxides and this decreases their affinity for interaction with binding sites of adsorbents [224] and in highly acidic solutions, H^+ ions compete with metal ions for adsorption on the adsorbent surface [212]; (13) increasing the content of functional groups increases the adsorption capacity of these kinds of hybrid polymers although it decreases their pore size and surface area [153,169,170]; and (14) adsorption capacities of hierarchically structure compounds are much greater than the other kinds of discussed organic-inorganic hybrid polymers and in the future they can be used as superadsorbents for the adsorption of heavy metals.

4. Conclusions and Outlook

Organic-inorganic hybrid polymers are obtained through sol-gel processes, self-assembly processes, assembling or dispersion of nanobuilding blocks, hierarchical structures and interpenetrating networks. In these compounds, the functional variation of organic materials combines with the benefits of a sturdy and thermally stable inorganic substrate. These materials have strong binding affinities toward selected metal ions (as cations or oxyanions) and relatively high metal ion adsorption capacities and can be used for wastewater treatment and solid-state separation of heavy metals. They are modified by suitable functional groups for high efficiency adsorption of heavy metal ions under the used experimental conditions. Techniques such as XRD and SEM show that in hybrid polymers, the structure of organic and inorganic moieties change and synergy effects between them increase their adsorption capacities, compared to their individual pristine organic or inorganic moieties. Heavy metal selective adsorbents can be prepared by methods such as cation-IIP. Although adsorbents similar to activated carbon are used routinely for their low cost and high adsorption capacity, different combinations of organic and inorganic moieties provide us a large number of selections of hybrid adsorbents that can be used under different experimental conditions, are reusable and can be prepared for selective adsorption of heavy metals and in some cases act as superadsorbents. For synthesis of these compounds, environmentally friendly compounds such as chitosan, humic acid, cellulose and bentonite are used and their partial leaching during adsorption processes has no negative impact on the environment.

Conflicts of Interest

The authors declare no conflict of interest.

References

1. Bohn, H.L.; McNeal, B.L.; O'Connor, G.A. *Soil Chemistry*; John Wiely: New York, NY, USA, 1985.
2. Bradl, H.B. *Heavy Metals in the Environment: Origin, Interaction and Remediation*; Elsevier: Amsterdam, The Netherlands, 2005.
3. Fergusson, J.E. *The Heavy Elements: Chemistry, Environmental Impact and Health Effects*; Pergamon Press: Exeter, UK, 1990.

4. Jha, M.K.; Lee, J.-C.; Kim, M.-S.; Jeong, J.; Kim, B.-S.; Kumar, V. Hydrometallurgical recovery/recycling of platinum by the leaching of spent catalysts: A review. *Hydrometallurgy* **2013**, *133*, 23–32.
5. Syed, S. Recovery of gold from secondary sources—A review. *Hydrometallurgy* **2012**, *115–116*, 30–51.
6. Esalah, O.J.; Weber, M.E.; Vera, J.H. Removal of lead, cadmium and zinc from aqueous solutions by precipitation with sodium di-(n-octyl) phosphinate. *Can. J. Chem. Eng.* **2000**, *78*, 948–954.
7. Lertlapwasin, R.; Bhawawet, N.; Imyim, A.; Fuangswasdi, S. Ionic liquid extraction of heavy metal ions by 2-aminothiophenol in 1-butyl-3-methylimidazolium hexafluorophosphate and their association constants. *Sep. Purif. Technol.* **2010**, *72*, 70–76.
8. Emamjomeh, M.M.; Sivakumar, M. Review of pollutants removed by electrocoagulation and electrocoagulation/flotation processes. *J. Environ. Manag.* **2009**, *90*, 1663–1679.
9. Mahmoud, A.; Hoadley, A.F. An evaluation of a hybrid ion exchange electrodialysis process in the recovery of heavy metals from simulated dilute industrial wastewater. *Water Res.* **2012**, *46*, 3364–3376.
10. Yurloval, L.; Kryvoruchko, A.; Kornilovich, B. Removal of Ni (II) ions from wastewater by micellar-enhanced ultrafiltration. *Desalination* **2002**, *144*, 255–260.
11. Greenlee, L.F.; Lawler, D.F.; Freeman, B.D.; Marrot, B.; Moulin, P. Reverse osmosis desalination: Water sources, technology, and today's challenges. *Water Res.* **2009**, *43*, 2317–2348.
12. Benit, Y.; Ruiz, M.L. Reverse osmosis applied to metal finishing wastewater. *Desalination* **2002**, *142*, 229–234.
13. Rubio, J.; Souza, M.L.; Smith, R.W. Overview of flotation as a wastewater treatment technique. *Miner. Eng.* **2002**, *15*, 139–155.
14. Ghurye, G.; Clifford, D.; Tripp, A. Iron coagulation and direct microfiltration to remove arsenic from groundwater. *AWWA* **2004**, *96*, 143–152.
15. Barakat, M.A. New trends in removing heavy metals from industrial wastewater. *Arab. J. Chem.* **2011**, *4*, 361–377.
16. Pan, B.J.; Pan, B.C.; Zhang, M.W.; Lv, L.; Zhang, Q.X.; Zheng, S.R. Development of polymeric and polymer-based hybrid adsorbents for pollutants removal from waters. *Chem. Eng. J.* **2009**, *151*, 19–29.
17. Mishra, S.P.; Singh, V.K.; Tiwari, D. Radiotracer technique in adsorption study. 14. Efficient removal of mercury from aqueous solutions by hydrous zirconium oxide. *Appl. Radiat. Isot.* **1996**, *47*, 15–21.
18. Uzun, I.; Güzel, F. Adsorption of some heavy metal ions from aqueous solution by activated carbon and comparison of percent adsorption results of activated carbon with those of some other adsorbents. *Turk. J. Chem.* **2000**, *24*, 291–297.
19. Biskup, B.; Subotic, B. Kinetic analysis of the exchange processes between sodium ions from zeolite A and cadmium, copper and nickel ions from solutions. *Sep. Purif. Technol.* **2004**, *37*, 17–31.
20. Cincotti, A.; Mameli, A.; Locci, A.M.; Orru, R.; Cao, G. Heavy metals uptake by Sardinian natural zeolites: Experiment and modeling. *Ind. Eng. Chem. Res.* **2006**, *45*, 1074–1084.

21. Gier, S.; Johns, W.D. Heavy metal-adsorption on micas and clay minerals studied by X–ray photoelectron spectroscopy. *Appl. Clay Sci.* **2000**, *16*, 289–299.
22. Koppelman, M.H.; Dillard, J.G. A study of the adsorption of Ni(II) and Cu(II) by clay minerals. *Clays Clay Miner.* **1977**, *25*, 457–462.
23. O'Connell, D.W.; Birkinshaw, C.; O'Dwyer, T.F. Heavy metal adsorbents prepared from the modification of cellulose: A review. *Bioresour. Technol.* **2008**, *99*, 6709–6724.
24. Dang, V.B.H.; Doan, H.D.; Dang-Vuc, T.; Lohi, A. Equilibrium and kinetics of biosorption of cadmium(II) and copper(II) ions by wheat straw. *Bioresour. Technol.* **2009**, *100*, 211–219.
25. Zewail, T.M.; El-Garf, S.A.M. Preparation of agriculture residue based adsorbents for heavy metal removal. *Desalin. Water Treat.* **2010**, *22*, 363–370.
26. Nagarale, R.K.; Gohil, G.S.; Shahi, V.K. Recent developments on ion-exchange membranes and electro-membrane processes. *Adv. Colloid Interface Sci.* **2006**, *119*, 97–130.
27. Wang, L.; Wu, X.L.; Xu, W.-H.; Huang, X.-J.; Liu, J.-H.; Xu, A.-W. Stable organic-inorganic hybrid of polyaniline/α-zirconium phosphate for efficient removal of organic pollutants in water environment. *Appl. Mater. Interfaces* **2012**, *4*, 2686–2692.
28. Gao, B.; Gao, Y.; Li, Y. Preparation and chelation adsorption property of composite chelating material poly(amidoxime)/SiO_2 towards heavy metal ions. *Chem. Eng. J.* **2010**, *158*, 542–549.
29. Zaitseva, N.; Zaitsev, V.; Walcarius, A. Chromium(VI) removal via reduction–sorption on bi-functional silica adsorbents. *J. Hazard. Mater.* **2013**, *250–251*, 454–461.
30. Simsek, E.B.; Duranoglu, D.; Beker, U. Heavy metal adsorption by magnetic hybrid-sorbent: An experimental and theoretical approach. *Sep. Sci. Technol.* **2012**, *47*, 1334–1340.
31. Suchithra, P.S.; Vazhayal, L.; Mohamed, A.P.; Ananthakumar, S. Mesoporous organic-inorganic hybrid aerogels through ultrasonic assisted sol-gel intercalation of silica-PEG in bentonite for effective removal of dyes, volatile organic pollutants and petroleum products from aqueous solution. *Chem. Eng. J.* **2012**, *200–202*, 589–600.
32. Repo, E.; Warchoł, J.K.; Bhatnagar, A.; Sillanpää, M. Heavy metals adsorption by novel EDTA-modified chitosan-silica hybrid materials. *J. Colloid Interface Sci.* **2011**, *358*, 261–267.
33. Ge, P.; Li, F.; Zhang, B. Synthesis of modified mesoporous materials and comparative studies of removal of heavy metal from aqueous solutions. *Pol. J. Environ. Stud.* **2010**, *19*, 301–308.
34. Pang, Y.; Zeng, G.; Tang, L.; Zhang, Y.; Liu, Y.; Lei, X.; Li, Z.; Zhang, J.; Xie, G. PEI-grafted magnetic porous powder for highly effective adsorption of heavy metal ions. *Desalination* **2011**, *281*, 278–284.
35. Wang, L.; Zhang, J.; Wang, A. Fast removal of methylene blue from aqueous solution by adsorption onto chitosan-g-poly (acrylic acid)/attapulgite composite. *Desalination* **2011**, *266*, 33–39.
36. Mercier, L.; Pinnavaia, T.J. Heavy metal ion adsorbents formed by the grafting of a thiol functionality to mesoporous silica molecular sieves: Factors affecting Hg(II) uptake. *Environ. Sci. Technol.* **1998**, *32*, 2749–2754.
37. Sanchez, C.; Julián, B.; Belleville, P.; Popall, M. Applications of hybrid organic-inorganic nanocomposites. *J. Mater. Chem.* **2005**, *15*, 3559–3592.
38. Walcarius, A. Electrochemical applications of silica-based organic-inorganic hybrid materials. *Chem. Mater.* **2001**, *13*, 3351–3372.

39. Kim, D.-G.; Kang, H.; Han, S.; Lee, J.-C. Dual effective organic/inorganic hybrid star-shaped polymer coatings on ultrafiltration membrane for bio- and oil-fouling resistance. *Appl. Mater. Interfaces* **2012**, *4*, 5898–5906.
40. Paun, G.; Neagu, E.; Tache, A.; Radu, G.L.; Parvulescu, V. Application of the nanofiltration process for concentration of polyphenolic compounds from geranium robertianum and salvia officinalis extracts. *Chem. Biochem. Eng. Quart.* **2011**, *25*, 453–460.
41. Wen, X.F.; Wang, K.; Pi, P.-H.; Yang, J.-X.; Cai, Z.-Q.; Zhang, L.-J.; Qian, Y.; Yang, Z.-R.; Zheng, D.-F.; Cheng, J. Organic-inorganic hybrid superhydrophobic surfaces using methyltriethoxysilane and tetraethoxysilane sol-gel derived materials in emulsion. *Appl. Surf. Sci.* **2011**, *258*, 991–998.
42. Sparks, B.J.; Hoff, E.F.; Xiong, L.; Goetz, J.T.; Patton, D.L. Superhydrophobic hybrid inorganic-organic thiol-ene surfaces fabricated via spray-deposition and photopolymerization. *Appl. Mater. Interfaces* **2013**, *5*, 1811–1817.
43. Yu, Y.-Y.; Chen, W.-C. Transparent organic-inorganic hybrid thin films prepared from acrylic polymer and aqueous monodispersed colloidal silica. *Mater. Chem. Phys.* **2003**, *82*, 388–395.
44. Nagappan, S.; Choi, M.-C.; Sung, G.; Park, S.S.; Moorthy, M.S.; Chu, S.-W.; Lee, W.-K.; Ha, C.-S. Highly transparent, hydrophobic fluorinated polymethylsiloxane/silica organic-inorganic hybrids for anti-stain coating. *Macromol. Res.* **2013**, *21*, 669–680.
45. Rottman, C.; Grader, G.; de Hazan, Y.; Melchior, S.; Avnir, D. Surfactant-induced modification of dopants reactivity in sol-gel matrixes. *J. Am. Chem. Soc.* **1999**, *121*, 8533–8543.
46. Date, J.D.; Moet, L.; Koster, J.A.; de Boer, B.; Blom, P.W.M. Hybrid polymer solar cells from highly reactive diethylzinc: MDMO-PPV *versus* P3HT. *Chem. Mater.* **2007**, *19*, 5856–5861.
47. He, M.; Qiu, F.; Lin, Z. Toward high-performance organic-inorganic hybrid solar cells: Bringing conjugated polymers and inorganic nanocrystals in close contact. *J. Phys. Chem. Lett.* **2013**, *4*, 1788–1796.
48. Souza, F.L.; Bueno, P.R.; Longo, E.; Leite, E.R. Sol-gel nonhydrolytic synthesis of a hybrid organic-inorganic electrolyte for application in lithium-ion devices. *Solid State Ion.* **2004**, *66*, 83–88.
49. Lee, C.-F.; Leigh, D.A.; Pritchard, R.G.; Schultz, D.; Teat, S.J.; Timco, G.A.; Winpenny, R.E.P. Hybrid organic-inorganic rotaxanes and molecular shuttles. *Nature* **2009**, *458*, 314–318.
50. Singh, A.; Singh, N.P.; Singh, R.A. Biomimetic synthesis and characterization of semiconducting hybrid organic-inorganic composite materials based on polyaniline-polyethylene glycol-CdS system. *Bull. Mater. Sci.* **2011**, *34*, 1017–1026.
51. Collins, D.J.; Zhou, H.-C. Hydrogen storage in metal-organic frameworks. *J. Mater. Chem.* **2007**, *17*, 3154–3160.
52. Rowsell, J.L.C.; Millward, A.R.; Park, K.S.; Yaghi, O.M. Hydrogen sorption in functionalized metal-organic frameworks. *J. Am. Chem. Soc.* **2004**, *126*, 5666–5667.
53. Raj, G.; Swalus, C.; Guillet, A.; Devillers, M.; Nysten, B.; Gaigneaux, E.M. Supramolecular organization in organic-inorganic heterogeneous hybrid catalysts formed from polyoxometalate and poly(ampholyte) polymer. *Langmuir* **2013**, *29*, 4388–4395.

54. Fu, G.; Yue, X.; Dai, Z. Glucose biosensor based on covalent immobilization of enzyme in sol-gel composite film combined with Prussian blue/carbon nanotubes hybrid. *Biosens. Bioelectron.* **2011**, *26*, 3973–3976.
55. Gwak, G.H.; Paek, S.M.; Oh, J.M. Electrophoretic preparation of an organic-inorganic hybrid of layered metal hydroxide and hydrogel for a potential drug-delivery system. *Eur. J. Inorg. Chem.* **2012**, *2012*, 5269–5275.
56. Chou, T.P.; Chandrasekaran, C.; Cao, G.Z. Sol-gel-derived hybrid coatings for corrosion protection. *JSST* **2003**, *26*, 321–327.
57. Bourbigot, S.; Duquesne, S. Fire retardant polymers: Recent developments and opportunities. *J. Mater. Chem.* **2007**, *17*, 2283–2300.
58. Kim, S.S.; Ahn, K.M.; Park, M.S.; Lee, J.H.; Choi, C.Y.; Kim, B.S. A poly(lactic-co-glycolide)/ hydroxyapatite composite scaffold with enhanced osteoconductivity. *J. Biomed. Mater. Res. A* **2007**, *80A*, 206–215.
59. Kwon, Y.K.; Han, J.K.; Lee, J.M.; Ko, Y.S.; Oh, J.H.; Leeb, H.-S.; Lee, E.-H. Organic-inorganic hybrid materials for flexible optical waveguide applications. *J. Mater. Chem.* **2008**, *18*, 579–585.
60. Frisch, H.L.; Mark, J.E. Nanocomposites prepared by threading polymer chains through zeolites, mesoporous silica, or silicananotubes. *Chem. Mater.* **1996**, *8*, 1735–1738.
61. Hench, L.L.; West, J.K. The sol-gel process. *Chem. Rev.* **1990**, *90*, 33–72.
62. Sol-Gel. Available online: http://en.wikipedia.org/wiki/sol-gel (acessed on 10 December 2013).
63. Warrick, E. *Forty Years of Firsts a Recollection of Dow Corning Pioneer*; McGraw-Hill: New York, NY, USA, 1990.
64. Hay, J.N.; Raval, H.M. Synthesis of organic-inorganic hybrids via the non-hydrolytic sol-gel process. *Chem. Mater.* **2001**, *13*, 3396–3403.
65. Wen, J.; Wilkes, G.L. Organic/inorganic hybrid network materials by the sol-gel approach. *Chem. Mater.* **1996**, *8*, 1667–1681.
66. Chong, M.N.; Jin, B. Sol-gel synthesis of inorganic mesostructured composite photocatalyst for water purification: An insight into the synthesis fundamentals, reaction, and binding mechanisms. *Synth. React. Inorg. Met. Org. Chem.* **2012**, *42*, 68–75.
67. Arkles, B. Comercial applications of sol-gel-derived hybrid materials. *MRS Bull.* **2001**, *26*, 402–408.
68. Sol-Gel. Avaliable on line: http://en.wikipedia.org/wiki/Sol-gel (accessed on 10 December 2013).
69. Kessler, V.G.; Spijksma, G.I.; Seisenbaeva, G.A.; Hakansson, S.; Blank, D.H.A.; Bouwmeester, H.J.M. New insight in the role of modifying ligands in the sol-gel processing of metal alkoxide precursors: A possibility to approach new classes of materials. *J. Sol-Gel Sci. Technol.* **2006**, *40*, 163–179.
70. Xiao, Y.; Shen, J.; Xie, Z.; Zhou, B.; Wu, G. Microstructure control of nanoporous silica thin film prepared by sol-gel process. *J. Mater. Sci. Technol.* **2007**, *23*, 504–508.
71. Ogoshi, T.; Chujo, Y. Organic-inorganic polymer hybrids prepared by the sol-gel method. *Compos. Interfaces* **2005**, *11*, 539–566.
72. Loy, D.A. Sol-Gel Processing of Hybrid Organic-Inorganic Materials Based on Polysilsesquioxanes. In *Hybrid Materials: Synthesis, Characterization, and Applications*; Kickelbick, G., Ed.; Wiley-VCH: Weinheim, Germany, 2006.

73. *Zeolites: Synthesis, Chemistry, and Applications*; Andreyev, M.K., Zubkov, O., Eds.; Nova Science Publishers: New York, NY, USA, 2012.
74. Wright, P.A. *Microporous Framework Solids*; RSC Publishing: Cambridge, UK, 2008; p. 186.
75. Bellussi, G.; Millini, R.; Montanari, E.; Carati, A.; Rizzo, C.; Parker, W.O., Jr.; Cruciani, G.; de Angelis, A.; Bonoldi, L.; Zanardi, S. A highly crystalline microporous hybrid organic-inorganic aluminosilicate resembling the AFI-type zeolite. *Chem. Commun.* **2012**, *48*, 7356–7358.
76. Maeda, K.; Kiyozumi, Y.; Mizukami, F. Synthesis of the first microporous aluminum phosphonate with organic groups covalently bonded to the skeleton. *Angew. Chem. Int. Ed.* **1994**, *33*, 2335–2337.
77. Zhou, D.; Lu, X.; Xu, J.; Yu, A.; Li, J.; Deng, F.; Xia, Q. Dry gel conversion method for the synthesis of organic-inorganic hybrid MOR zeolites with modifiable catalytic activities. *Chem. Mater.* **2012**, *24*, 4160–4165.
78. Jones, C.W.; Tsuji, K.; Davis, M.E. Organic-functionalized molecular sieves as shape-selective catalysts. *Nature* **1998**, *393*, 52–54.
79. Inagaki, S.; Yokoi, T.; Kubota, Y.; Tatsumi, T. Unique adsorption properties of organic-inorganic hybrid zeolite IEZ-1 with dimethylsilylene moieties. *Chem. Commun.* **2007**, *48*, 5188–5190.
80. Kresge, C.T.; Leonowicz, M.E.; Roth, W.J.; Vartuli, J.C.; Beck, J.S. Ordered mesoporous molecular sieves synthesized by a liquid-crystal template mechanism. *Nature* **1992**, *359*, 710–712.
81. Beck, J.S.; Vartuli, J.C.; Roth, W.J.; Leonowicz, M.E.; Kresge, C.T.; Schmitt, K.D.; Chu, C.T.-W.; Olson, D.H.; Sheppard, E.W.; McCullen, S.B.; *et al*. A new family of mesoporous molecular sieves prepared with liquid crystal templates. *J. Am. Chem. Soc.* **1992**, *114*, 10834–10843.
82. Ying, J.Y.; Mehnert, C.P.; Wong, M.S. Synthesis and applications of supramolecular-templated mesoporous materials. *Angew. Chem. Int. Ed.* **1999**, *38*, 56–77.
83. Nohair, B.; MacQuarrie, S.; Crudden, C.M.; Kaliaguine, S. Functionalized mesostructured silicates as supports for palladium complexes: Synthesis and catalytic activity for the Suzuki-Miyaura coupling reaction. *J. Phys. Chem. C* **2008**, *112*, 6065–6072.
84. Serrano, D.P.; Calleja, G.; Botas, J.A.; Gutierrez, F.J. Adsorption and hydrophobic properties of mesostructured MCM–41 and SBA–15 materials for volatile organic compound removal. *Ind. Eng. Chem. Res.* **2004**, *43*, 7010–7018.
85. Zhao, D.; Huo, Q.; Feng, J.; Chmelka, B.F.; Stucky, G.D. Nonionic triblock and star diblock copolymer and oligomeric surfactant syntheses of highly ordered, hydrothermally stable, mesoporous silica structures. *J. Am. Chem. Soc.* **1998**, *120*, 6024–6036.
86. Chen, D.; Li, Z.; Wan, Y.; Tu, X.; Shi, Y.; Chen, Z.; Shen, W.; Yu, C.; Tu, B.; Zhao, D. Anionic surfactant induced mesophase transformation to synthesize highly ordered large-pore mesoporous silica structures. *J. Mater. Chem.* **2006**, *16*, 1511–1519.
87. Da'na, E.; Sayari, A. Adsorption of heavy metals on amine-functionalised SBA-15 prepared by co-condensation: Applications to real water samples. *Desalination* **2012**, *285*, 62–67.
88. Brown, J.; Richer, R.; Mercier, L. One-step synthesis of high capacity mesoporous Hg^{2+} adsorbents by non-ionic surfactant assembly. *Microporous Mesoporous Mater.* **2000**, *37*, 41–48.
89. Antochshuk, V.; Jaroniec, M. Adsorption, thermogravimetric, and NMR studies of FSM–16 material functionalized with alkylmonochlorosilanes. *J. Phys. Chem. B* **1999**, *103*, 6252–6261.

90. Ariga, K.; Vinu, A.; Yamauchi, Y.; Ji, Q.; Hill, J.P. Nanoarchitectonics for mesoporous materials. *Bull. Chem. Soc. Jpn.* **2012**, *85*, 1–32.
91. Soler-Illia, G.J.; Sanchez, C.; Lebeau, B.; Patarin, J. Chemical strategies to design textured materials: From microporous and mesoporous oxides to nanonetworks and hierarchical structures. *Chem. Rev.* **2002**, *102*, 4093–4138.
92. Huo, Q.; Margolese, D.I.; Ciesla, U.; Demuth, D.G.; Feng, P.; Gier, T.E.; Sieger, P.; Firouzi, A.; Chmelka, B.F.; Schüth, F.; *et al*. Organization of organic molecules with inorganic molecular species into nanocomposite biphase arrays. *Chem. Mater.* **1994**, *6*, 1176–1191.
93. Hoffmann, F.; Cornelius, M.; Morell, J.; Fröba, M. Silica-based mesoporous organic-inorganic hybrid materials. *Angew. Chem. Int. Ed.* **2006**, *45*, 3216–3251.
94. Muto, S.; Imai, H. Relationship between mesostructures and pH conditions for the formation of silica-cationic surfactant complexes. *Microporous Mesoporous Mater.* **2006**, *95*, 200–205.
95. Wirnsberger, G.; Yang, P.; Huang, H.C.; Scott, B.; Deng, T.; Whitesides, G.M.; Chmelka, B.F.; Stucky, G.D. Patterned block-copolymer-silica mesostructures as host media for the laser dye rhodamine 6G. *J. Phys. Chem. B* **2001**, *105*, 6307–6313.
96. Zhang, Q.; Liu, F.; Nguyen, K.T.; Ma, X.; Wang, X.; Xing, B.; Zhao, Y. Multifunctional mesoporous silica nanoparticles for cancer-targeted and controlled drug delivery. *Adv. Funct. Mater.* **2012**, *22*, 5144–5156.
97. Wight, A.P.; Davis, M.E. Design and preparation of organic-inorganic hybrid catalysts. *Chem. Rev.* **2002**, *102*, 3589–3614.
98. Pal, N.; Bhaumik, A. Soft templating strategies for the synthesis of mesoporous materials: Inorganic, organic-inorganic hybrid and purely organic solids. *Adv. Colloid Interface Sci.* **2013**, *189–190*, 21–41.
99. Kickelbick, G. Concepts for the incorporation of inorganic building blocks into organic polymers on a nanoscale. *Prog. Polym. Sci.* **2003**, *28*, 83–114.
100. Schubert, U. Cluster-based inorganic-organic hybrid materials. *Chem. Soc. Rev.* **2011**, *40*, 575–582.
101. Agustin, D.; Dallery, J.; Coelho, C.; Proust, A.; Thouvenot, R. Synthesis, characterization and study of the chromogenic properties of the hybrid polyoxometalates $[PW_{11}O_{39}(SiR)_2O]^{3-}$ (R = Et, $(CH_2)_nCH{=}CH_2$ (n = 0, 1, 4), $CH_2CH_2SiEt_3$, $CH_2CH_2SiMe_2Ph$). *J. Organomet. Chem.* **2007**, *692*, 746–754.
102. Li, H.; Eddaoudi, M.; O'Keeffe, M.; Yaghi, O.M. Design and synthesis of an exceptionally stable and highly porous metal-organic framework. *Nature* **1999**, *402*, 276–279.
103. Férey, G. Some suggested perspectives for multifunctional hybrid porous solids. *Dalton Trans.* **2009**, *2009*, 4400–4415.
104. Guillerm, V.; Gross, S.; Serre, C.; Devic, T.; Bauer, M.; Férey, G. A zirconium methacrylate oxocluster as precursor for the low-temperature synthesis of porous zirconium (IV) dicarboxylates. *Chem. Commun.* **2010**, *46*, 767–769.
105. Proust, A.; Matt, B.; Villanneau, R.; Guillemot, G.; Gouzerh, P.; Izzet, G. Functionalization and post-functionalization: A step towards polyoxometalate-based materials. *Chem. Soc. Rev.* **2012**, *41*, 7605–7622.

106. Niederberger, M.; Garnweitner, G.; Krumeich, F.; Nesper, R.; Cölfen, H.; Antonietti, M. Tailoring the surface and solubility properties of nanocrystalline titania by a nonaqueous *in-situ* functionalization process. *Chem. Mater.* **2004**, *16*, 1202–1208.
107. Dimitrijevic, N.M.; Saponjic, Z.V.; Rabatic, B.M.; Rajh, T. Assembly and charge transfer in hybrid TiO_2 architectures using biotin-avidin as a connector. *J. Am. Chem. Soc.* **2005**, *127*, 1344–1345.
108. Potapova, I.; Mruk, R.; Prehl, S.; Zentel, R.; Basche, T.; Mews, A. Semiconductor nanocrystals with multifunctional polymer ligands. *J. Am. Chem. Soc.* **2003**, *125*, 320–321.
109. Vitale, F.; Fratoddi, I.; Battocchio, C.; Piscopiello, E.; Tapfer, L.; Russo, M.V.; Polzonetti, G.; Giannini, C. Mono- and bi-functional arenethiols as surfactants for gold nanoparticles: Synthesis and characterization. *NRL* **2011**, *6*, doi:10.1186/1556-276X-6-103.
110. Schroden, R.C.; Blanford, C.F.; Melde, B.J.; Johnson, B.J.S.; Stein, A. Direct synthesis of ordered macroporous silica materials functionalized with polyoxometalate clusters. *Chem. Mater.* **2001**, *13*, 1074–1081.
111. Mittal, V. Polymer layered silicate nanocomposites: A review. *Materials* **2009**, *2*, 992–1057.
112. Soundararajah, Q.Y.; Karunaratne, B.S.B.; Rajapakse, R.M.G. Montmorillonite polyaniline nanocomposites: Preparation, characterization and investigation of mechanical properties. *Mater. Chem. Phys.* **2009**, *113*, 850–855.
113. Lira-Cantu, M.; Gomez-Romero, P. Synthesis and characterization of intercalate phases in the organic–inorganic polyaniline/V_2O_5 system. *J. Solid State Chem.* **1999**, *147*, 601–608.
114. Huang, S.; Yang, Z.; Zhu, H.; Ren, L.; Tjiu, W.W.; Liu, T. Poly(vinly alcohol)/nano-sized layered double hydroxides nanocomposite hydrogels prepared by cyclic freezing and thawing. *Macromol. Res.* **2012**, *20*, 568–577.
115. Santos, C.M.; Mangadlao, J.; Ahmed, F.; Leon, A.; Advincula, R.C.; Rodrigues, D.F. Graphene nanocomposite for biomedical applications: Fabrication, antimicrobial and cytotoxic investigations. *Nanotechnology* **2012**, *23*, 395101.
116. Alexandre, M.; Dubois, P. Polymer layered silicate nanocomposites: Preparation, properties and uses of a new class of materials. *Mater. Sci. Eng. R Rep.* **2000**, *28*, 1–63.
117. Kameda, T.; Takeuchi, H.; Yoshioka, T. Kinetics of uptake of Cu^{2+} and Cd^{2+} by Mg-Al layered double hydroxides intercalated with citrate, malate, and tartrate. *Colloids Surf. A Physicochem. Eng. Asp.* **2010**, *355*, 172–177.
118. Rojas, R.; Perez, M.R.; Erro, E.M.; Ortiz, P.I.; Ulibarri, M.A.; Giacomelli, C.E. EDTA modified LDHs as Cu^{2+} scavengers: Removal kinetics and sorbent stability. *J. Colloid Interface Sci.* **2009**, *331*, 425–431.
119. Gangopadhyay, R.; De, A. Conducting polymer nanocomposites: A brief overview. *Chem. Mater.* **2000**, *12*, 608–622.
120. Daigle, J.-C.; Claverie, J.P. A Simple method for forming hybrid core-shell nanoparticles suspended in water. *J. Nanomater.* **2008**, *2008*, 609184:1–609184:8.
121. Wei, S.; Wang, Q.; Zhu, J.; Sun, L.; Lin, H.; Guo, Z. Multifunctional composite core-shell nanoparticles. *Nanoscale* **2011**, *3*, 4474–4502.
122. Wang, Y.; Teng, X.; Wang, J.-S.; Yang, H. Solvent-free atom transfer radical polymerization in the synthesis of Fe2O3@polystyrene core-shell nanoparticles. *Nano Lett.* **2003**, *3*, 789–793.

123. Huang, C.L.; Matijevic, E. Coating of uniform inorganic particles with polymers. 3. Polypyrrole on different metal oxides. *J. Mater. Res.* **1995**, *10*, 1327–1336.
124. Payne, R.; Fritz, G.; Narmann, H. Investigation into the interactions of metals and metal ions in polymer matrixes. *Angew. Makromol. Chem.* **1986**, *144*, 51–72.
125. Liu, S.; Zhang, N.; Tang, Z.-R.; Xu, Y.-J. Synthesis of one-dimensional CdS@TiO_2 core-shell nanocomposites photocatalyst for selective redox: The dual role of TiO_2 shell. *ACS Appl. Mater. Interfaces* **2012**, *4*, 6378–6385.
126. Ozin, G.A.; Ho, K.; Lotsch, B.V.; Cademartiri, L.; Puzzo, D.P.; Scotognella, F.; Ghadimi, A.; Thomson, J. Nanofabrication by self- assembly. *Mater. Today* **2009**, *12*, 12–23.
127. Nikolov, S.; Petrov, M.; Lymperakis, L.; Friák, M.; Sachs, C.; Fabritius, H.-O.; Raabe, D.; Neugebauer, J. Revealing the design principles of high-performance biological composites using Ab initio and multiscale simulations: The example of lobster cuticle. *Adv. Mater.* **2010**, *22*, 519–526.
128. Fratzel, P. *Collagen: Structure and Mechanics*; Springer: New York, NY, USA, 2008.
129. Kharisov, B.I. A Review for synthesis of nanoflowers. *Recent Pat. Nanotechnol.* **2008**, *2*, 190–200.
130. Soten, I.; Ozin, G.A. Porous hydroxyapatite- dodecylphosphate composite film on titania-titanium substrate. *J. Mater. Chem.* **1999**, *9*, 703–710.
131. Dag, Ö.; Verma, A.; Ozin, G.A.; Kresge, C.T. Salted mesostructures: Salt-liquid crystal templating of lithium triflate-oligo(ethylene oxide) surfactant-mesoporous silica nanocomposite films and monoliths. *J. Mater. Chem.* **1999**, *9*, 1475–1482.
132. Du, J.; Lai, X.; Yang, N.; Zhai, J.; Kisailus, D.; Su, F.; Wang, D.; Jiang, L. Hierarchically ordered macro-mesoporous TiO_2-graphene composite films: Improved mass transfer, reduced charge recombination, and their enhanced photocatalytic activities. *ACS Nano* **2011**, *5*, 590–596.
133. Pope, E.J.A.; Asami, M.; Mackenzie, J.D. Transparent silica gel-PMMA composites. *J. Mater. Res.* **1989**, *4*, 1018–1026.
134. Deng, Q.; Moore, R.B.; Mauritz, K.A. Novel Nafion/ORMOSIL hybrids via in situ sol-gel reactions. 1. Probe of ORMOSIL phase nanostructures by infrared spectroscopy. *Chem. Mater.* **1995**, *7*, 2259–2268.
135. Hajji, P.; David, L.; Gerard, J.F.; Pascault, J.P.; Vigier, G. Synthesis, structure, and morphology of polymer-silica hybrid nanocomposites based on hydroxyethyl methacrylate. *J. Polym. Sci. B Polym. Phys.* **1999**, *37*, 3172–3187.
136. Frisch, H.L.; Xue, Y.-P.; Maaref, S.; Beaucage, G.; Pu, Z.; Mark, J. Pseudo interpenetrating polymer networks and interpenetrating polymer networks of zeolite 13 X and polystyrene and poly(ethyl acrylate). *Macrmol. Symp.* **1996**, *106*, 147–166.
137. Frisch, H.L.; Chen, Z.J.; Chen, X. Electrical conductivity of iodine doped pseudo interpenetrating polymer networks. *Macromol. Symp.* **1994**, *81*, 181–194.
138. Abd-El-Aziz, A.S.; Strohm, E.A. Transition metal-containing macromolecules: En route to new functional materials. *Polymer* **2012**, *53*, 4879–4921.
139. McCurdie, M.P.; Belfiore, L.A. Solid-state complexes of poly (L-histidine) with metal chlorides from the first row of the d-block. *J. Polym. Sci. Part B Polym. Phys.* **1999**, *37*, 301–309.
140. Hardy, C.G.; Ren, L.; Tamboue, T.C.; Tang, C. Side-chain ferrocene-containing (meth)acrylate polymers: Synthesis and properties. *J. Polym. Sci.* **2011**, *49*, 1409–1420.

141. Mori, H. Design and synthesis of functional silsesquioxane-based hybrids by hydrolytic condensation of bulky triethoxysilanes. *Int. J. Polym. Sci.* **2012**, *2012*, 173624:1–173624:17.
142. Liu, J.; Ma, Y.; Zhang, Y.; Shao, G. Novel negatively charged hybrids. 3. Removal of Pb^{2+} from aqueous solution using zwitterionic hybrid polymers as adsorbent. *J. Hazard. Mater.* **2010**, *173*, 438–444.
143. Liu, J.; Ma, Y.; Xu, T.; Shao, G. Preparation of zwitterionic hybrid polymer and its application for the removal of heavy metal ions from water. *J. Hazard. Mater.* **2010**, *178*, 1021–1029.
144. Wu, J.-B.; Zang, S.-Y.; Yi, Y.-L. Sol-gel derived ion imprinted thiocyanato-functionalized silica gel as selective adsorbent of cadmium(II). *J. Sol-Gel Sci. Technol.* **2013**, *66*, 434–442.
145. Wu, J.-B.; Yi, Y.-L. Removal of cadmium from aqueous solution by organic-inorganic hybrid sorbent combining sol-gel processing and imprinting technique. *Korean J. Chem. Eng.* **2013**, *30*, 1111–1118.
146. Buhani; Narsito; Nuryono; Kunarti, E.S. Production of metal ion imprinted polymer from mercapto-silica through sol-gel process as selective adsorbent of cadmium. *Desalination* **2010**, *251*, 83–89.
147. Fan, H.-T.; Sun, T. Selective removal of iron from aqueous solution using ion imprinted cyanato-functionalized silica gel sorbents. *Sep. Sci. Technol.* **2012**, *47*, 507–512.
148. Bozbas, S.K.; Ay, U.; Kayan, A. Novel inorganic-organic hybrid polymers to remove heavy metals from aqueous solution. *Desalin. Water Treat.* **2013**, *51*, 7208–7215.
149. Schroden, R.C.; Al-Daous, M.; Sokolov, S.; Melde, B.J.; Lytle, J.C.; Stein, A.; Carbajo, M.C.; Fernández, J.T.; Rodríguez, E.E. Hybrid macroporous materials for heavy metal ion adsorption. *J. Mater. Chem.* **2002**, *12*, 3261–3267.
150. Passos, C.G.; Lima, E.C.; Arenas, L.T.; Simon, N.M.; da Cunha, B.M.; Brasil, J.L.; Costa, T.M.H.; Benvenutti, E.V. Use of 7-amine-4-azahepthylsilica and 10-amine-4-azadecylsilica xerogels as adsorbent for Pb(II) kinetic and equilibrium study. *Colloids Surf. A* **2008**, *316*, 297–306.
151. Pavan, F.A.; Lima, I.S.; Benvenutti, E.V.; Gushikem, Y.; Airoldi, C. Hybrid aniline/silica xerogel cation adsorption and thermodynamics of interaction. *J. Colloid Interface Sci.* **2004**, *275*, 386–391.
152. Faghihian, H.; Nourmoradi, H.; Shokouhi, M. Performance of silica aerogels modifi ed with amino functional groups in Pb(II) and Cd(II) removal from aqueous solutions. *PJCHT* **2012**, *14*, 50–56.
153. Qu, R.; Sun, C.; Ma, F.; Cui, Z.; Zhang, Y.; Sun, X.; Ji, C.; Wang, C.; Yin, P. Adsorption kinetics and equilibrium of copper from ethanol fuel on silica-gel functionalized with amino-terminated dendrimer-like polyamidoamine polymers. *Fuel* **2012**, *92*, 204–210.
154. Pissetti, F.L.; Yoshida, I.V.P.; Gushikem, Y.; Kholin, Y.V. Metal ions adsorption from ethanol solutions on ethylenediamine-modified poly(dimethylsiloxane) elastomeric network. *Colloids Surf. A* **2008**, *328*, 21–27.
155. Fan, H.T.; Su, Z.J.; Fan, X.L.; Guo, M.M.; Wang, J.; Gao, S.; Sun, T. Sol-gel derived organic-inorganic hybrid sorbent for removal of Pb^{2+}, Cd^{2+} and Cu^{2+} from aqueous solution. *J. Sol-Gel Sci. Technol.* **2012**, *64*, 418–426.
156. Kim, Y.S.; In, G.; Choi, J.M. Solid phase extraction of trace Cu(II), Mn(II), Pb(II) and Zn(II) in water samples with pulverized silica-salen$(NEt_2)_2$. *Bull. Korean Chem. Soc.* **2006**, *27*, 1557–1561.

157. Hongjie, W.; Jin, K.; Huijuan, L.; Jiuhui, Q. Preparation of organically functionalized silica gel as adsorbent for copper ion adsorption. *J. Environ. Sci.* **2009**, *21*, 1473–1479.
158. Qu, R.; Niu, Y.; Sun, C.; Ji, C.; Wang, C.; Cheng, G. Syntheses, characterization, and adsorption properties for metal ions of silica-gel functionalized by ester- and amino-terminated dendrimer-like polyamidoamine polymer. *Microporous Mesoporous Mater.* **2006**, *97*, 58–65.
159. Zhang, Y.; Wang, X.; Liu, J.; Wu, L. Removal of copper (Cu^{2+}) from water using novel hybrid adsorbents: Kinetics and isotherms. *J. Chem. Eng. Data* **2013**, *58*, 1141–1150.
160. Prakash, S.; Kumar, M.; Tripathi, B.P.; Shahi, V.K. Sol-gel derived poly(vinylalcohol)-3-(2-aminoethylamino) propyl trimethoxysilane: Cross-linked organic-inorganic hybrid beads for the removal of Pb(II) from aqueous solution. *Chem. Eng. J.* **2010**, *162*, 28–36.
161. Hao, J.; Han, M.-J.; Meng, X. Preparation and evaluation of thiol-functionalized activated alumina for arsenite removal from water. *J. Hazard. Mater.* **2009**, *167*, 1215–1221.
162. Barczak, M.; Dobrowolski, R.; Dobrzyńska, J.; Zięba, E.; Dąbrowski, A. Amorphous and ordered organosilicas functionalized with amine groups as sorbents of platinum (II) ions. *Adsorption* **2013**, *19*, 733–744.
163. Chen, J.; Lin, Y.-S. Sol-gel-immobilized recombinant *E. coli* for biosorption of Cd^{2+}. *J. Chin. Inst. Chem. Eng.* **2007**, *38*, 235–243.
164. Mehmood, R.F.; Mehmood, F.; Akhtar, J.; Shah, S.S.; Khosa, M.A. Adsorption of Cd(II) by sol-gel silica doped with N (dipropylcarbamothioyl)thiophene-2-carboxamide. *J. Dispers. Sci. Technol.* **2013**, *34*, 153–160.
165. Prado, A.G.S.; Arakaki, L.N.H.; Airoldi, C. Adsorption and separation of cations on chemically modified silica gel synthesised via the sol-gel process. *J. Chem. Soc. Dalton Trans.* **2001**, 2206–2209.
166. Najafi, M.; Yousefi, Y.; Rafati, A.A. Synthesis, characterization and adsorption studies of several heavy metal ions on amino-functionalized silica nano hollow sphere and silica gel. *Sep. Purif. Technol.* **2012**, *85*, 193–205.
167. Pavan, F.A.; Costa, T.M.H.; Benvenutti, E.V. Adsorption of $CoCl_2$, $ZnCl_2$ and $CdCl_2$ on aniline/silica hybrid material obtained by sol-gel method. *Colloids Surf. A* **2003**, *226*, 95–100.
168. Parvulescu, V.; Mureseanu, M.; Reiss, A.; Ene, R.; Suh, S.-H. Metal-organic hybrids obtained by functionalization of mesoporous silica. *Rev. Roum. Chim.* **2010**, *55*, 1001–1008.
169. Yoshitake, H.; Yokoi, T.; Tatsumi, T. Adsorption of chromate and arsenate by amino-functionalized MCM–41 and SBA–1. *Chem. Mater.* **2002**, *14*, 4603–4610.
170. Aguado, J.; Arsuaga, J.M.; Arencibia, A.; Lindo, M.; Gascón, V. Aqueous heavy metals removal by adsorption on amine-functionalized mesoporous silica. *J. Hazard. Mater.* **2009**, *163*, 213–221.
171. Chen, D.; Huang, C.; He, M.; Hu, B. Separation and preconcentration of inorganic arsenic species in natural water samples with 3-(2-aminoethylamino) propyltrimethoxysilane modified ordered mesoporous silica micro-column and their determination by inductively coupled plasma optical emission spectrometry. *J. Hazard. Mater.* **2009**, *164*, 1146–1151.
172. Showkat, A.M.; Zhang, Y.-P.; Kim, M.S.; Gopalan, A.I.; Reddy, K.R.; Lee, K.-P. Analysis of heavy metal toxic ions by adsorption onto amino-functionalized ordered mesoporous silica. *Bull. Korean Chem. Soc.* **2007**, *28*, 1985–1992.

173. Zhang, D.; Li, J.H. Ordered SBA-15 mesoporous silica with high amino-functionalization for adsorption of heavy metal ions. *Chin. Sci. Bull.* **2013**, *58*, 879–883.
174. Kang, T.; Park, Y.; Choi, K.; Sang Leec, J.; Yi, J. Ordered mesoporous silica (SBA–15) derivatized with imidazole-containing functionalities as a selective adsorbent of precious metal ions. *J. Mater. Chem.* **2004**, *14*, 1043–1049.
175. Mureseanu, M.; Reiss, A.; Stefanescu, I.; David, E.; Parvulescu, V.; Renard, G.; Hulea, V. Modified SBA–15 mesoporous silica for heavy metal ions remediation. *Chemosphere* **2008**, *73*, 1499–1504.
176. Hao, S.; Hou, J. Adsorption of Ni^{2+} on aminofunctionalized mesoporous silica templated by an anionic surfactant route. *J. Mater. Res.* **2013**, *28*, 2325–2331.
177. Pérez-Quintanilla, D.; del Hierro, I.; Fajardo, M.; Sierra, I. Adsorption of cadmium(II) from aqueous media onto a mesoporous silica chemically modified with 2-mercaptopyrimidine. *J. Mater. Chem.* **2006**, *16*, 1757–1764.
178. Lam, K.F.; Yeung, K.L.; McKay, G. An investigation of gold adsorption from a binary mixture with selective mesoporous silica adsorbents. *J. Phys. Chem. B* **2006**, *110*, 2187–2194.
179. Puanngam, M.; Unob, F. Preparation and use of chemically modified MCM–41 and silica gel as selective adsorbents for Hg(II) ions. *J. Hazard. Mater.* **2008**, *154*, 578–587.
180. Lam, K.F.; Yeung, K.L.; McKay, G. A rational approach in the design of selective mesoporous adsorbents. *Langmuir* **2006**, *22*, 9632–9641.
181. Xue, X.; Li, F. Removal of Cu(II) from aqueous solution by adsorption onto functionalized SBA–16 mesoporous silica. *Microporous Mesoporous Mater.* **2008**, *116*, 116–122.
182. Lombardo, M.V.; Videla, M.; Calvo, A.; Requejo, F.G.; Soler-Illia, G.J.A.A. Aminopropyl-modified mesoporous silica SBA–15 as recovery agents of Cu(II)-sulfate solutions: Adsorption efficiency, functional stability and reusability aspects. *J. Hazard. Mater.* **2012**, *223–224*, 53–62.
183. Lee, B.; Bao, L.-L.; Im, H.-J.; Dai, S.; Hagaman, E.W.; Lin, J.S. Synthesis and characterization of organic-inorganic hybrid mesoporous anion–exchange resins for perrhenate (ReO_4^-) anion adsorption. *Langmuir* **2003**, *19*, 4246–4252.
184. Lee, B.; Kim, Y.; Lee, H.; Yi, J. Synthesis of functionalized porous silicas via templating method as heavy metal ion adsorbents: The introduction of surface hydrophilicity onto the surface of adsorbents. *Microporous Mesoporous Mater.* **2001**, *50*, 77–90.
185. Liu, Y.-C.; Liu, S.-T. A recyclable thiol-functionalized mesoporous silica for detection and removal of Cu(II) ions. *JCCS* **2010**, *57*, 946–949.
186. Aguado, J.; Arsuaga, J.M.; Arencibia, A. Adsorption of aqueous mercury(II) on propylthiol-functionalized mesoporous silica obtained by co-condensation. *Ind. Eng. Chem. Res.* **2005**, *44*, 3665–3671.
187. Olkhovyk, O.; Jarioniec, M. Ordered mesoporous silicas with 2,5-dimercapto-1,3,4-thiadiazole ligand: High capacity adsorbents for mercury ions. *Adsorption* **2005**, *11*, 205–214.
188. Antochshuck, V.; Olkhovyk, O.; Jaroniec, M.; Park, I.-S.; Ryoo, R. Benzoylthiourea-modified mesoporous silica for mercury(II) removal. *Langmuir* **2003**, *19*, 3031–3034.
189. Hao, N.; Han, L.; Yang, Y.; Wang, H.; Webley, P.A.; Zhao, D. A metal-ion-assisted assembly approach to synthesize disulfide-bridged periodical mesoporous organosilicas with high sulfide contents and efficient adsorption. *Appl. Surf. Sci.* **2010**, *256*, 5334–5342.

190. Teng, M.; Wang, H.; Li, F.; Zhang, B. Thioether-functionalized mesoporous fiber membranes: Sol-gel combined electrospun fabrication and their applications for Hg^{2+} removal. *J. Colloid Interface Sci.* **2011**, *355*, 23–28.
191. Chiu, P.-J.; Vetrivel, S.; Chiang, A.S.T.; Kao, H.-M. Synthesis and characterization of cubic periodic mesoporous organosilicas with a high loading of disulfide groups. *New J. Chem.* **2011**, *35*, 489–494.
192. Awual, M.R.; Yaita, T.; El-Safty, S.A.; Shiwaku, H.; Okamoto, Y.; Suzuki, S. Investigation of palladium(II) detection and recovery using ligand modified conjugate adsorbent. *Chem. Eng. J.* **2013**, *222*, 172–179.
193. Awual, M.R.; Yaita, T.; El-Safty, S.A.; Shiwaku, H.; Suzuki, S.; Okamoto, Y. Copper(II) ions capturing from water using ligand modified a new type mesoporous adsorbent. *Chem. Eng. J.* **2013**, *221*, 322–330.
194. Lee, H.; Yi, J. Removal of copper ions using functionalizaed mesoporous silica in aqueous solution. *Sep. Sci. Technol.* **2001**, *36*, 2433–2444.
195. Lam, K.F.; Yeung, K.; McKay, G. Efficient approach for Cd^{2+} and Ni^{2+} removal and recovery using mesoporous mdsorbent with tunable selectivity. *Environ. Sci. Technol.* **2007**, *41*, 3329–3334.
196. Yoshitake, H.; Yokoi, T.; Tatsumi, T. Adsorption behavior of arsenate at transition metal cations captured by amino-functionalized mesoporous silicas, *Chem. Mater.* **2003**, *15*, 1713–1721.
197. Huang, J.; Ye, M.; Qu, Y.; Chu, L.; Chen, R.; He, Q.; Xu, D. Pb (II) removal from aqueous media by EDTA-modified mesoporous silica SBA-15. *J. Colloid Interface Sci.* **2012**, *385*, 137–146.
198. Ge, P.; Li, F. Kinetics and thermodynamics of heavy metal Cu(II) adsorption on mesoporous silicates. *Pol. J. Environ. Stud.* **2011**, *20*, 339–344.
199. Pandey, S.; Mishra, S.B. Organic-inorganic hybrid of chitosan/organoclay bionanocomposites for hexavalent chromium uptake. *J. Colloid Interface Sci.* **2011**, *361*, 509–520.
200. Futalan, C.M.; Tsai, W.-C.; Lin, S.-S.; Hsien, K.-J.; Dalida, M.L.; Wan, M.-W. Copper, nickel and lead adsorption from aqueous solution using chitosan-immobilized on bentonite in a ternary system. *Sustain. Environ. Res.* **2012**, *22*, 345–355.
201. Hasan, S.; Krishnaiah, A.; Ghosh, T.K.; Viswanath, D.S.; Boddu, V.M.; Smith, E.D. Adsorption of chromium (VI) on chitosan-coated perlite. *Sep. Sci. Technol.* **2003**, *38*, 3775–3793.
202. Kalyani, S.; Priya, J.A.; Rao, P.S.; Abburi, K. Removal of copper and nickel from aqueous solutions using chitosan coated on perlite as biosorbent. *Sep. Sci. Technol.* **2005**, *40*, 1483–1495.
203. Hasan, S.; Krishnaiah, A.; Ghosh, T.K.; Viswanath, D.S.; Boddu, V.M.; Smith, E.D. Adsorption of divalent cadmium (Cd(II)) from aqueous solutions onto chitosan-coated perlite beads. *Ind. Eng. Chem. Res.* **2006**, *45*, 5066–5077.
204. Hasan, S.; Ghosh, T.K.; Viswanath, D.S.; Boddu, V.M. Dispersion of chitosan on perlite for enhancement of copper(II) adsorption capacity. *J. Hazard. Mater.* **2008**, *152*, 826–837.
205. Dinu, M.V.; Dragan, E.S. Evaluation of Cu^{2+}, Co^{2+} and Ni^{2+} ions removal from aqueous solution using anovel chitosan/clinoptilolite composite: Kinetics and isotherms. *Chem. Eng. J.* **2010**, *160*, 157–163.
206. Gandhi, M.R.; Viswanathanb, N.; Meenakshi, S. Preparation and application of alumina/chitosan biocomposite. *Int. J. Biol. Macromol.* **2010**, *47*, 146–154.

207. Boddu, V.M.; Abburi, K.; Talbott, J.L.; Smith, E.D. Removal of hexavalent chromium from wastewater using a new composite chitosan biosorbent. *Environ. Sci. Technol.* **2003**, *37*, 4449–4456.
208. Fan, D.; Zhu, X.; Xu, M.; Yan, J. Adsorption properties of chromium (VI) by chitosan coated montmorillonite. *J. Biol. Sci.* **2006**, *6*, 941–945.
209. Bleiman, N.; Mishael, Y.G. Selenium removal from drinking water by adsorption to chitosan-clay composites and oxides: Batch and columns tests. *J. Hazard. Mater.* **2010**, *183*, 590–595.
210. Vijaya, Y.; Popuri, S.R.; Boddu, V.M.; Krishnaiah, A. Modified chitosan and calcium alginate biopolymer sorbents for removal of nickel (II) through adsorption. *Carbohydr. Polym.* **2008**, *72*, 261–271.
211. Choi, S.; Jeong, Y. The removal of heavy metals in aqueous solution by hydroxyapatite/cellulose composite. *Fibers Polym.* **2008**, *9*, 267–270.
212. Grisdanurak, N.; Akewaranugulsiri, S.; Futalan, C.M.; Tsai, W.C.; Kan, C.C.; Hsu, C.W.; Wan, M.W. The study of copper adsorption from aqueous solution using crosslinked chitosan immobilized on bentonite. *J. Appl. Polym. Sci.* **2012**, *125*, 132–142.
213. Zhang, J.; Jin, Y.; Wang, A. Rapid removal of Pb(II) from aqueous solution by chitosan-g-poly(acrylic acid)/attapulgite/sodium humate composite hydrogels. *Environ. Technol.* **2011**, *32*, 523–531.
214. Wang, X.; Zheng, Y.; Wang, A. Fast removal of copper ions from aqueous solution by chitosan–g–poly(acrylic acid)/attapulgite composites. *J. Hazard. Mater.* **2009**, *168*, 970–977.
215. Wang, X.; Wang, A. Adsorption characteristics of chitosan-g-poly(acrylic acid)/attapulgite hydrogel composite for Hg(II) ions from aqueous solution. *Sep. Sci. Technol.* **2010**, *45*, 2086–2094.
216. Anirudhan, T.S.; Rijith, S. Synthesis and characterization of carboxyl terminated poly(methacrylic acid) grafted chitosan/bentonite composite and its application for the recovery of uranium(VI) from aqueous media. *J. Environ. Radioact.* **2012**, *106*, 8–19.
217. Abdel Khalek, M.A.; Mahmoud, G.A.; El-Kelesh, N.A. Synthesis and caracterization of poly-methacrylic acid grafted chitosan-bentonite composite and its application for heavy metals recovery. *Chem. Mater. Res.* **2012**, *2*, 1–12.
218. Wang, X.; Wang, A. Equilibrium isotherm and mechanism studies of Pb(II) and Cd(II) ions onto hydrogel composite based on vermiculite. *Desalin. Water Treat.* **2012**, *48*, 38–49.
219. Anirudhan, T.S.; Suchithra, P.S. Heavy metals uptake from aqueous solutions and industrial wastewaters by humic acid-immobilized polymer/bentonite composite: Kinetics and equilibrium modeling. *Chem. Eng. J.* **2010**, *156*, 146–156.
220. Larraza, I.; López-Gónzalez, M.; Corrales, T.; Marcelo, G. Hybrid materials: Magnetite-polyethylenimine-montmorillonite, as magnetic adsorbents for Cr(VI) water treatment. *J. Colloid Interface Sci.* **2012**, *385*, 24–33.
221. Bulut, Y.; Akçay, G.; Elma, D.; Serhatli, I.E. Synthesis of clay-based superabsorbent composite and its sorption capability. *J. Hazard. Mater.* **2009**, *171*, 717–723.
222. Urbano, B.F.; Rivas, B.L.; Martinez, F.; Alexandratos, S.D. Equilibrium and kinetic study of arsenic sorption by water-insoluble nanocomposite resin of poly[N-(4-vinylbenzyl)-N-methyl-D-glucamine]-montmorillonite. *Chem. Eng. J.* **2012**, *193–194*, 21–30.

223. Zhao, G.; Zhang, H.; Fan, Q.; Ren, X.; Li, J.; Chen, Y.; Wang, X. Sorption of copper(II) onto super-adsorbent of bentonite-polyacrylamide composites. *J. Hazard. Mater.* **2010**, *173*, 661–668.
224. Ulusoy, U.; Şimşek, S. Lead removal by polyacrylamide-bentonite and zeolite composites: Effect of phytic acid immobilization. *J. Hazard. Mater.* **2005**, *127*, 163–171.
225. Cui, H.; Qian, Y.; Li, Q.; Zhang, Q.; Zhai, J. Adsorption of aqueous Hg(II) by a polyaniline/attapulgite composite. *Chem. Eng. J.* **2012**, *211–212*, 216–223.
226. Zhao, Y.; Chen, Y.; Li, M.; Zhou, S.; Xue, A.; Xing, W. Adsorption of Hg^{2+} from aqueous solution onto polyacrylamide/attapulgite. *J. Hazard. Mater.* **2009**, *171*, 640–646.
227. Yang, L.; Li, Y.; Hu, H.; Jin, X.; Yeb, Z.; Ma, Y.; Zhang, S. Preparation of novel spherical PVA/ATP composites with macroreticular structure and their adsorption behavior for methylene blue and lead in aqueous solution. *Chem. Eng. J.* **2011**, *173*, 446–455.
228. Kaşgöz, H.; Durmus, A.; Kaşgöz, A. Enhanced swelling and adsorption properties of AAm–AMPSNa/clay hydrogel nanocomposites for heavy metal ion removal. *Polym. Adv. Technol.* **2008**, *19*, 213–220.
229. Şölener, M.; Tunali, S.; Özcan, A.S.; Özcan, A.; Gedikbey, T. Adsorption characteristics of lead(II) ions onto the clay/poly(methoxyethyl)acrylamide (PMEA) composite from aqueous solutions. *Desalination* **2008**, *223*, 308–322.
230. Demirbaş, O.; Alkan, M.; Doğan, M.; Turhan, Y.; Namli, H.; Turan, P. Electrokinetic and adsorption properties of sepiolite modified by 3-aminopropyltriethoxysilane. *J. Hazard. Mater.* **2007**, *149*, 650–656.
231. Turhan, Y.; Turan, P.; Doğan, M.; Alkan, M.; Namli, H.; Demirbas, Ö. Characterization and adsorption properties of chemically modified sepiolite. *Ind. Eng. Chem. Res.* **2008**, *47*, 1883–1895.
232. Zhang, A.-C.; Sun, L.-S.; Xiang, J.; Hu, S.; Fu, P.; Su, S.; Zhou, Y.-S. Removal of elemental mercury from coal combustion flue gas by bentonite-chitosan and their modifier. *J. Fuel Chem. Technol.* **2009**, *37*, 489–495.
233. Xu, Q.; Yin, P.; Zhao, G.; Yin, G.; Qu, R. Synthesis and characterization of silica gel microspheres encapsulated by salicyclic acid functionalized polystyrene and its adsorption of transition metal ions from aqueous solutions. *Cent. Eur. J. Chem.* **2010**, *8*, 214–222.
234. Xu, Q.; Yin, P.; Zhao, G.; Sun, Y.; Qu, R. Adsorption selectivity and dynamic adsorption behaviors of Cu(II), Ag(I), and Au(III) on silica gel encapsulated by amino functionalized polystyrene. *J. Appl. Polym. Sci.* **2010**, *117*, 3645–3650.
235. Yin, P.; Xu, Q.; Qu, R.; Zhao, G.; Sun, Y. Adsorption of transition metal ions from aqueous solutions onto a novel silica gel matrix inorganic-organic composite material. *J. Hazard. Mater.* **2010**, *173*, 710–716.
236. Kumar, G.P.; Kumar, P.A.; Chakraborty, S.; Ray, M. Uptake and desorption of copper ion using functionalized polymer coated silica gel in aqueous environment. *Sep. Purif. Technol.* **2007**, *57*, 47–56.
237. Zhang, K.; Wang, Q.; Meng, H.; Wang, M.; Wu, W.; Chen, J. Preparation of polyacrylamide/silica composite capsules by inverse pickering emulsion polymerization. *Particuology* **2013**, in press.

238. Buhani; Suharso; Sembiring, Z. Immobilization of Chetoceros sp microalgae with silica gel through encapsulation technique as adsorbent of Pb metal from solution. *OJC* **2012**, *28*, 271–278.
239. Li, F.; Du, P.; Chen, W.; Zhang, S. Preparation of silica-supported porous sorbent for heavy metal ions removal in wastewater treatment by organic-inorganic hybridization combined with sucrose and polyethylene glycol imprinting. *Anal. Chim. Acta* **2007**, *585*, 211–218.
240. Li, F.; Jiang, H.; Zhang, S. An ion-imprinted silica-supported organic-inorganic hybrid sorbent prepared by a surface imprinting technique combined with a polysaccharide incorporated sol-gel process for selective separation of cadmium(II) from aqueous solution. *Talanta* **2007**, *71*, 1487–1493.
241. Zheng, L.; Jiang, F.-H.; Dong, P.-J.; Zhuang, Q.-F.; Li, F. Preparation of spherical silica-supported biosorbent for copper ions removal in wastewater based on sol-gel reaction and simple treatment with sodium hydroxide. *Chem. Res. Chin. Univ.* **2010**, *26*, 355–359.
242. Singhon, R.; Husson, J.; Knorr, M.; Lakard, B.; Euvrard, M. Adsorption of Ni(II) ions on colloidal hybrid organic-inorganic silica composites. *Colloids Surf. B* **2012**, *93*, 1–7.
243. Shin, S.; Jang, J. Thiol containing polymer encapsulated magnetic nanoparticles as reusable and efficiently separable adsorbent for heavy metal ions. *Chem. Commun.* **2007**, *2007*, 4230–4232.
244. Song, J.; Kong, H.; Jang, J. Adsorption of heavy metal ions from aqueous solution by polyrhodanine-encapsulated magnetic nanoparticles. *J. Colloid Interface Sci.* **2011**, *359*, 505–511.
245. Chang, Y.-C.; Chen, D.-H. Preparation and adsorption properties of monodisperse chitosan-bound Fe_3O_4 magnetic nanoparticles for removal of Cu(II) ions. *J. Colloid Interface Sci.* **2005**, *283*, 446–451.
246. Chang, Y.-C.; Chen, D.-H. Recovery of gold(III) ions by a chitosan-coated magnetic nano-adsorbent. *Gold Bull.* **2006**, *39*, 98–102.
247. Tao, S.; Wang, C.; Ma, W.; Wu, S.; Meng, C. Designed multifunctionalized magnetic mesoporous microsphere for sequential sorption of organic and inorganic pollutants. *Microporous Mesoporous Mater.* **2012**, *147*, 295–301.
248. Gupta, A.; Yunus, M.; Sankararamakrishnan, N. Zerovalent iron encapsulated chitosan nanospheres–A novel adsorbent for the removal of total inorganic Arsenic from aqueous systems. *Chemosphere* **2012**, *86*, 150–155.
249. Jiang, W.; Chen, X.B.; Niu, Y.J.; Pan, B.C. Spherical polystyrene-supported nano-Fe_3O_4 of high capacity and low-field separation for arsenate removal from water. *J. Hazard. Mater.* **2012**, *243*, 319–325.
250. Wan, S.L.; Zhao, X.; Lv, L.; Su, Q.; Gu, H.N.; Pan, B.C.; Zhang, W.M.; Lin, Z.W.; Luan, J.F. Selective adsorption of Cd(II) and Zn(II) ions by nano-hydrous manganese dioxide (HMO)-encapsulated cation exchanger. *Ind. Eng. Chem. Res.* **2010**, *49*, 7574–7579.
251. Zhang, F.; Lan, J.; Zhao, Z.; Yang, Y.; Tan, R.; Song, W. Removal of heavy metal ions from aqueous solution using Fe_3O_4-SiO_2-poly(1,2-diaminobenzene) core-shell sub-micron particles. *J. Colloid Interface Sci.* **2012**, *387*, 205–212.
252. Zhang, M.; Zhang, Z.; Liu, Y.; Yang, X.; Luo, L.; Chen, J.; Yao, S. Preparation of core-shell magnetic ion-imprinted polymer for selective extraction of Pb(II) from environmental samples. *Chem. Eng. J.* **2011**, *178*, 443–450.

253. Zhang, S.; Zeng, M.; Xu, W.; Li, J.; Li, J.; Xu, J.; Wang, X. Polyaniline nanorods dotted on graphene oxide nanosheets as a novel super adsorbent for Cr(VI). *Dalton Trans.* **2013**, *42*, 7854–7858.
254. Wu, Y.-N.; Zhang, B.; Li, F.; Zhu, W.; Xu, D.; Hannam, P.; Li, G. Electrospun fibrous mats as a skeleton for fabricating hierarchically structured materials as sorbents for Cu^{2+}. *J. Mater. Chem.* **2012**, *22*, 5089–5097.
255. Ma, X.; Li, L.; Yang, L.; Su, C.; Wang, K.; Jiang, K. Preparation of hybrid $CaCO_3$–pepsin hemisphere with ordered hierarchical structure and the application for removal of heavy metal ions. *J. Cryst. Growth* **2012**, *338*, 272–279.
256. Ma, X.; Li, L.; Yang, L.; Su, C.; Wang, K.; Yuan, S.; Zhou, J. Adsorption of heavy metal ions using hierarchical $CaCO_3$–maltose meso/macroporous hybrid materials: Adsorption isotherms and kinetic studies. *J. Hazard. Mater.* **2012**, *209–210*, 467–477.

Supporting Information

Figure S1. View of the two types of cages in the MOF structure made by reaction of $Zr_6O_4(OH)_4(OMc)_{12}$ clusters with muconic acid. Reproduced with permission from [104]. Copyright 2010 The Royal Society of Chemistry.

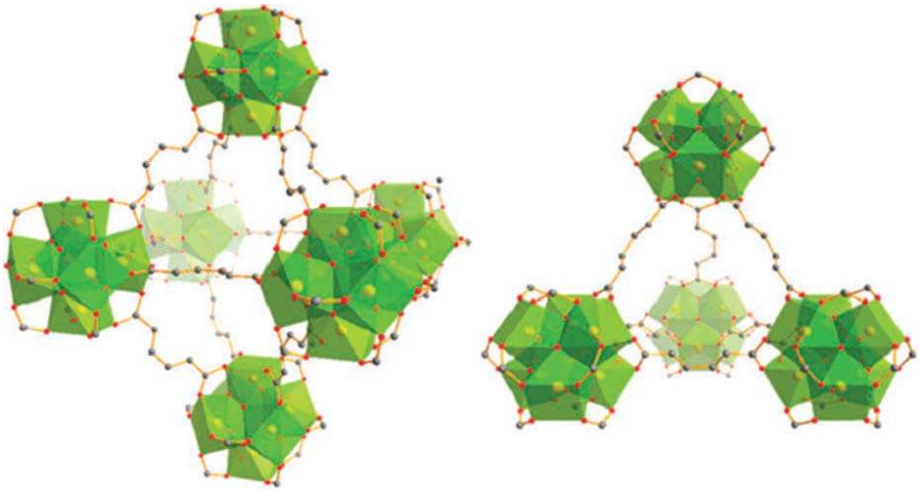

Figure S2. Illustration for the preparation of a macro-mesoporous TiO_2-graphene composite film. Reprinted with permission from [132]. Copyright 2011 American Chemical Society.

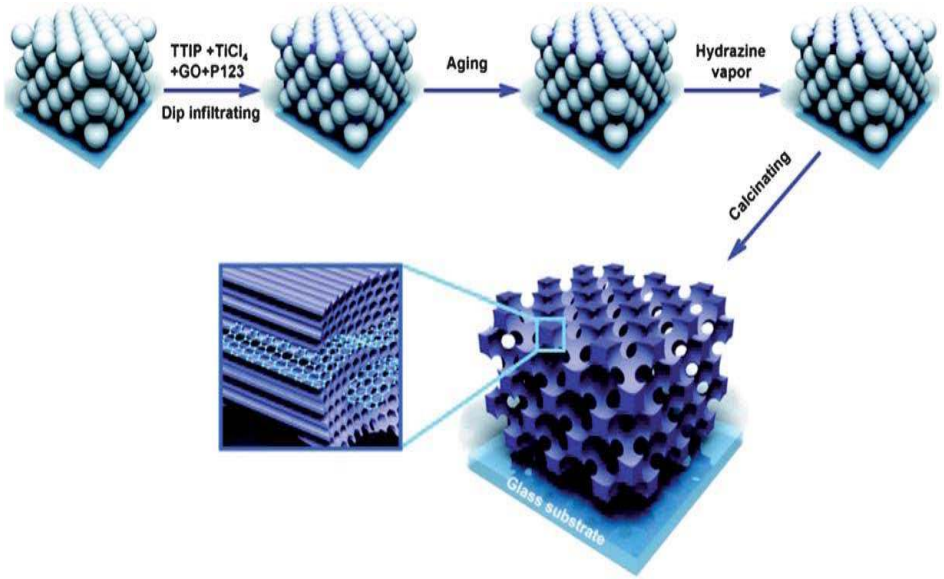

Figure S3. Schematic representation of (**a**) Pen and (**b**) its interacting group. Reprinted with permission from [153]. Copyright 2012 Elsevier.

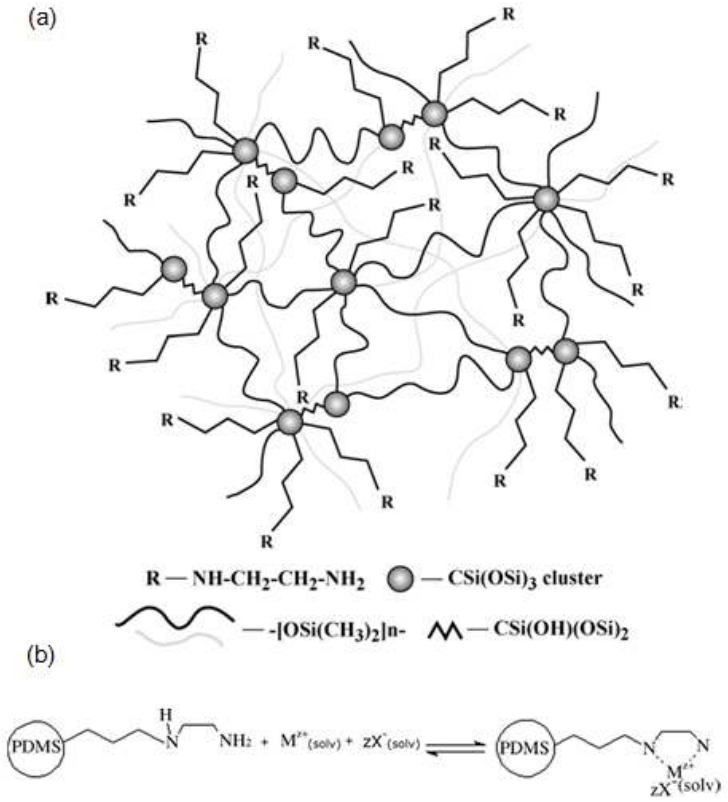

Figure S4. Adsorption of Cd^{2+} (◊) and Ni^{2+} (□) from their binary mixtures at (**a**) pH = 5 and (**b**) pH = 2. Reprinted with permission from [195]. Copyright 2007 American Chemical Society.

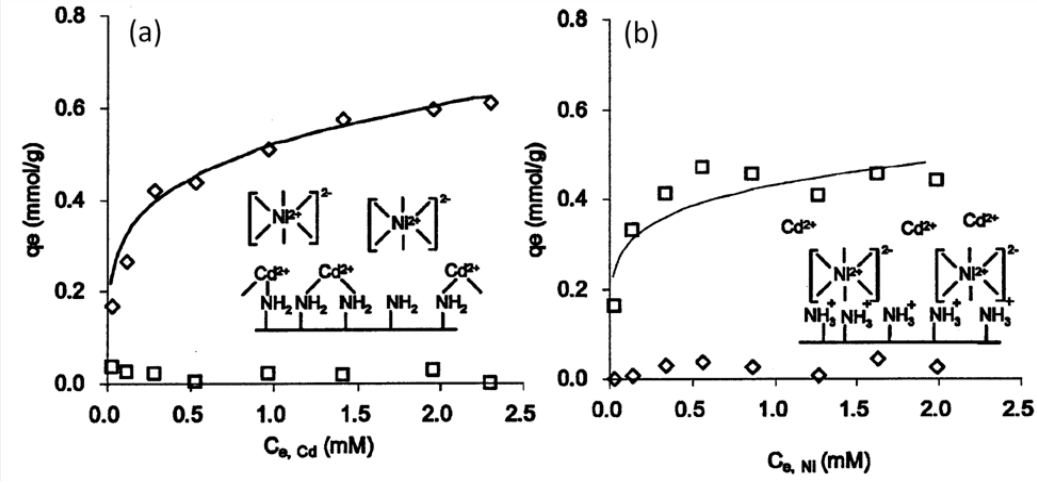

Figure S5. Schematic structure of CTS-*g*-PAA/APT composite. Reprinted with permission from [214]. Copyright 2009 Elsevier.

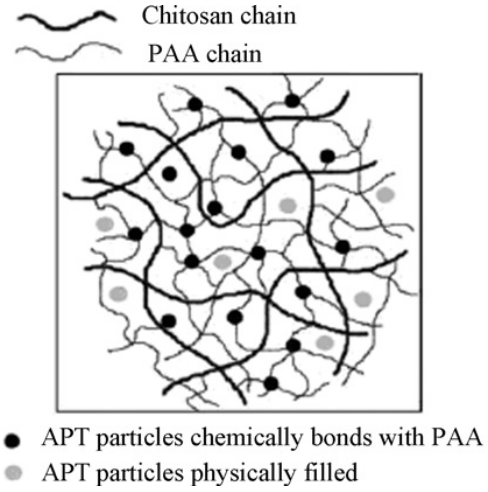

Figure S6. Schematic structure of of CTS-g-PMAA/Bent. Reprinted with permission from [216]. Copyright 2012 Elsevier.

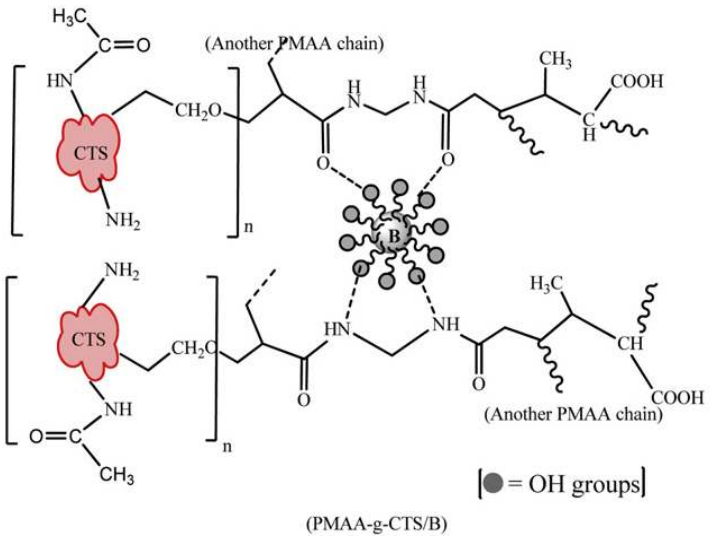

Figure S7. The distribution of different species of Cu(II) at concentration of 6.0×10^{-4} M in 0.01M $NaClO_4$ and CO_2-free solutions at 25 °C. Reprinted with permission from [224]. Copyright 2005 Elsevier.

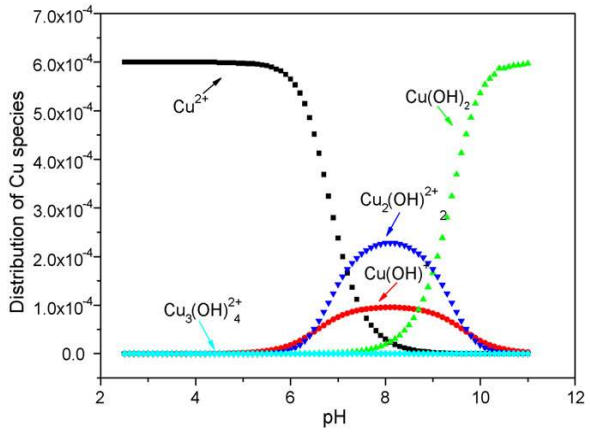

Figure S8. SEM images of (**a**) silica gel; (**b**) SG–PS–NH_2 and (**c**) SG–PS–azo–SA. Reprinted with permission from [233]. Copyright 2010 Springer Science and Business Media.

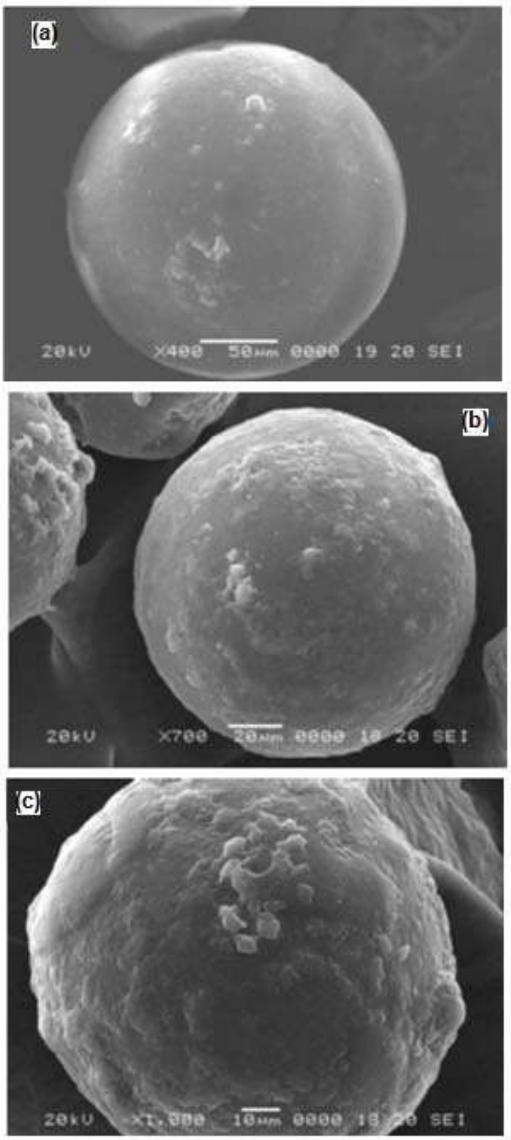

Figure S9. DSC analysis of (**a**) CS; (**b**) silica gel and (**c**) chitosan-grafted silica gel. Reprinted with permission from [239]. Copyright 2007 Elsevier.

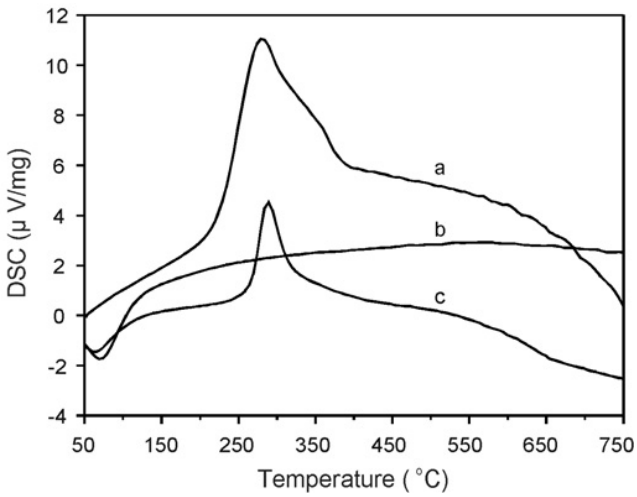

Figure S10. XRD patterns of GO nanosheets, PANI nanorods, PANI/GO nanocomposites. Reproduced with permission from [253]. Copyright 2013 The Royal Society of Chemistry.

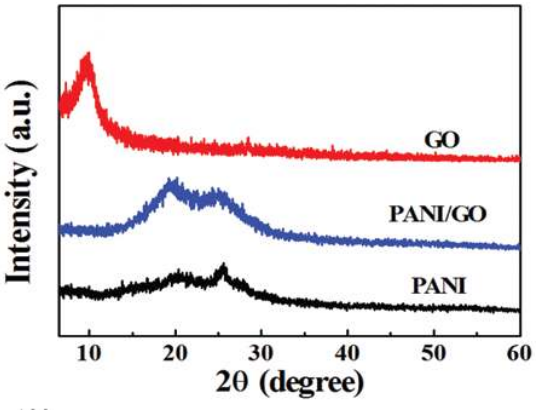

Figure S11. Pore size distributions of prepared membranes with bimodal porous structure. Reproduced with permission from [254]. Copyright 2012 The Royal Society of Chemistry.

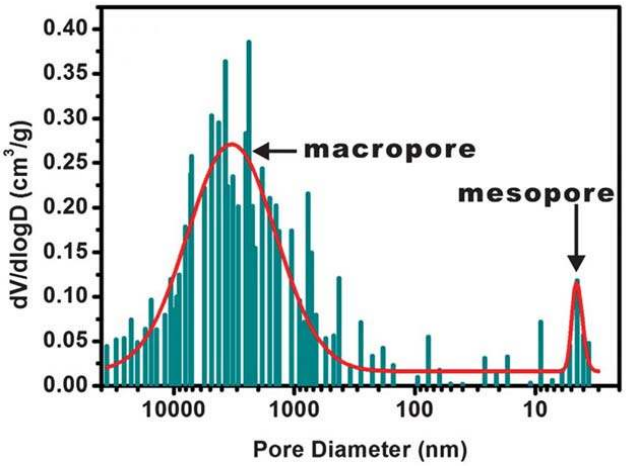

Figure S12. SEM images of $CaCO_3$ crystals in pepsin aqueous solution (**a** and **b**). Reprinted with permission from [255]. Copyright 2012 Elsevier.